ATOMIC WEAPONS ESTABLISHMENT

AWE REPORT No. O 3/96

Amplitude versus offset (AVO) and the Zoeppritz equations for partitioning of seismic waves at an interface: theory, new computer program, examples and review of past errors.

R G Pearce*
J B Young

*Department of Geology and Geophysics, University of Edinburgh, Grant Institute, West Mains Road, Edinburgh, EH9 3JW

Recommended for issue by: A Douglas, Group Leader, Seismic Detection Group

Approved for issue by: G J George, Project Contract Manager

CONTENTS

		Page
	SUMMARY	4
1.	INTRODUCTION	4
2.	PLANE WAVES INCIDENT UPON A PLANE INTERFACE—INITIAL ASSUMPTIONS	6
3.	NOTATION AND INTRODUCTION TO CONCEPTS	8
3.1	Definition of quantities and sign convention	8
3.2	Elliptically polarised *S* waves	10
3.3	Frequency dependence and pulse shape	10
3.4	Combined treatment of *SV* and *SH*	11
4.	THEORY	14
4.1	Displacement potentials for *P* and *S* waves	14
4.2	The plane wave solution; relation between displacement and displacement potential	15
4.3	Plane wave solutions for displacement	19
4.4	Boundary conditions for different cases	20
4.5	The solid-solid interface as a general case	22
4.6	Application of boundary conditions for the solid-solid interface	23
4.7	The Zoeppritz equations in matrix form	25
4.8	A note on super-critical angles of incidence	28
4.9	Energy equations	28
4.10	Motion at the free surface	29
5.	EXAMPLES, INCLUDING IMPORTANT INTERFACES IN THE EARTH	30
5.1	Introduction to graphic display and cases	30
5.2	The solid-solid interface	33
5.2.1	The Mohorovičić (Moho) discontinuity	33
5.2.1.1	Introduction	33
5.2.1.2	*P* incident from above (figure 2)	33
5.2.1.3	*SV* incident from above (figure 3)	34
5.2.1.4	*SH* incident from above (figure 4)	35
5.2.1.5	*P* incident from below (figure 5)	35
5.2.1.6	*SV* incident from below (figure 6)	36
5.2.1.7	*SH* incident from below (figure 7)	37
5.2.2	High wave-speed contrast (figures 8–13)	37
5.2.3	Anomalous Poisson's ratio (figures 14–19)	38
5.3	The solid-fluid interface	38
5.3.1	The sea bed (figures 20–23)	38
5.3.2	The core-mantle boundary (CMB) (figures 24–31)	40
5.3.3	The inner-core boundary (ICB) (figures 32–39)	41

5.3.4	The high wave-speed fluid (figures 40–43)	41
5.4	The fluid-fluid interface (seawater/sediment) (figures 44 and 45)	42
5.5	The solid free surface (Earth's surface) (figures 46–48)	42
5.6	The fluid free surface (sea surface) (figure 49)	44
5.7	Displacement at the solid free surface (figures 50 and 51)	44
6.	NOTATION DIFFERENCES AND ERRORS IN OTHER WORK	45
7.	DEPARTURES FROM THE INITIAL ASSUMPTIONS	48
7.1	The non-monochromatic incident wave	48
7.2	The non-plane incident wave	49
7.3	The curved interface	50
7.4	The irregular interface	50
7.5	The non-abrupt interface	50
7.6	The lubricated solid-solid interface	50
7.7	Non-semi-infinite media: wave-speed gradients and proximity of other interfaces	51
7.8	Imperfectly elastic media	51
7.9	Anisotropic media	52
8.	AVO ANALYSIS AND APPROXIMATIONS TO THE ZOEPPRITZ EQUATIONS	52
9.	ACKNOWLEDGEMENTS	53
	REFERENCES	54
	APPENDIX A: COMPUTER PROGRAM—BRIEF DESCRIPTION	58
	APPENDIX B: COMPUTER PROGRAM—LISTINGS AND DOCUMENTATION	59
	B1 SUBROUTINE ZOMAT AND DEPENDENT SUBPROGRAMS	59
	B2 SUBROUTINES ZOEPP AND SET—EXAMPLE OF A DRIVER FOR ZOMAT	67
	TABLE 1	77
	FIGURES 1–51	78–128

SUMMARY

We present a new computer program to determine the partitioning of seismic plane waves at a plane interface between homogeneous isotropic media (solution of the Zoeppritz equations). This program rationalises the treatment of solid-solid, solid-fluid and fluid-fluid interfaces and the free surface, and considers both sub- and super-critical angles for incident *P* and *S* waves, including *S* waves with arbitrary polarisation direction and incorporating elliptical polarisation. The program can be invoked at different levels. Partitioning into reflected and refracted rays can be calculated for an incident *P* or *S* wave at a specified angle for specified media. Alternatively this partitioning can be calculated for the complete range of incident angles, and presented in a form suitable for graphical display. For each case a series of interfaces may be concatenated to simulate rays passing through a series of layers which may or may not be parallel. We present the theory in detail, and include an extensive review of the literature. We do this in particular because of the proliferation of errors and ambiguities in previous work, and because of confusion regarding different authors' definitions and sign conventions. Errors are reported and other authors' conventions are clarified. Examples are given to show the range of behaviour corresponding to a wide range of circumstances, and the program is applied to important interfaces within the Earth. The assumptions inherent in the Zoeppritz equations, and their consequent limits of applicability are stated, with some consideration of the practical ways in which these limits may become important. The emphasis of the examples and of the discussion is towards global seismology, and in particular towards problems which relate to earthquake/explosion discrimination. However, the theory and program are equally applicable to exploration seismology (in particular they form the basis of amplitude-versus-offset (AVO) analysis), and the literature review includes references in that branch of the subject.

1. INTRODUCTION

Calculation of reflection and refraction coefficients at various types of interface between different propagation media are required frequently in seismology—indeed whenever theoretical absolute or relative amplitudes are sought from a layered structure. Whenever ray theory can be applied to the partitioning of seismic waves at boundaries, a straightforward calculation of the coefficients is invaluable. In global seismology this leads to a prediction of the angular dependence of the amplitudes of seismic phases such as *pP*, *sP* and *PcP*, which has an important effect on teleseismic waveforms. In seismic refraction the very existence of head-wave arrivals is associated with critical refraction at boundaries—behaviour which is embodied in the partitioning of spherical waves at those boundaries. In seismic reflection data the primary cause of the variation of observed amplitude with offset (AVO) is the behaviour of the seismic reflection coefficients at the target interface, and this variation has become a widely-used diagnostic in interpretation.

In all cases the difficulties inherent in the prediction of absolute amplitudes in the real Earth mean that the variation of reflected or refracted amplitude with ray angle is important. Near critical angles of incidence the coefficients vary rapidly with angle, so that knowledge of the expected behaviour is crucial in interpretation, and has a high information content. The behaviour is, however, non-trivial and can be very sensitive to the structure as both longitudinal and shear waves are involved in the process.

In applications such as ray tracing, generation of synthetic seismograms, and inversion by layer stripping, these coefficients may be calculated implicitly within a broader computation.

Nevertheless, there are many situations where the coefficients are required explicitly. The present work arose from the need to estimate the effect of interfaces within the Earth on the amplitudes of seismic phases observed from earthquakes and underground nuclear explosions, to assist with their discrimination. For example, the relative amplitude method of determining earthquake source mechanisms (Pearce [1], [2] and [3]), and its later generalisation to other seismic source types by Pearce and Rogers [4], benefits from a reliable estimate of *pP* and *sP* reflection coefficients at the free surface (and where applicable at the sea bed and sea surface), and this estimate may need to include the effects of other interfaces within the Earth's crust. AVO study of seismic reflection data in hydrocarbon exploration is another example where partitioning coefficients are needed explicitly.

The relevant equations were given in the early work of Knott [5] and Zoeppritz [6]. Many publications have given the theory or results for various media, encouraged by the ease with which these equations can now be solved by computer. But notation varies, many works contain errors, and most do not state their sign convention. Many authors also fail to consider properly the behaviour at super-critical angles of incidence, when one or more of the resulting waves ceases to propagate; behaviour at super-critical angles is nevertheless important in real situations. There is also confusion between the partitioning of seismic energy, particle displacement and displacement potential, all of which are numerically different. There are parallel papers in the literatures of earthquake seismology and seismic exploration which are seldom cross-referenced, yet which deal with exactly the same material, again with different conventions. Another problem is that many authors have paid little attention to the limits of validity of the equations—essentially they apply to plane waves incident upon a plane interface, and their application to, for example, spherical waves, curved interfaces or interfaces which are closely spaced, is at best an approximation. It is essential to be aware of the effects of relaxing each of the initial assumptions, so that the validity or otherwise of the Zoeppritz equations can be established in practical situations.

The origin of the present computer program is in an unpublished note (Blamey [7]), who gave the partitioning equations in particle displacement, for plane waves incident upon a plane solid-solid interface, taken from McCamy, Meyer and Smith [8], and for waves incident at a free surface, taken from Kolsky [9] pages 28–31. An associated FORTRAN computer program was later extended to include incidence either side of a plane solid-fluid interface, taken from the equations of Ergin [10]. A complex version of the program was written to enable waves beyond critical angles of incidence to be treated (Young, ZOEPP subroutine package, standard and complex versions, unpublished). Unfortunately all three references used for these different cases differ in their sign convention, and although some changes of sign were made when implementing the solid-air interface, inconsistencies remained.

In this Report these and many other inconsistencies in the literature are pointed out, and a new computer program is presented. The theory is developed in some detail to allow comparison between this and other work, in particular with regard to the all-important sign conventions, the difference between displacement and displacement potential, and also to give an insight into behaviour at super-critical angles. Information relating to the limits of applicability of the equations is also included. We shall refer particularly to applications in global seismology although, of course, the theory and program can be applied quite generally within the limitations stated. Results computed using this program are presented graphically for a range of examples to indicate the range of behaviour possible, and results are presented for important interfaces in the Earth, providing a reference for the behaviour of seismic body waves at these discontinuities.

The new program gives complete treatment of incident *P*, *SV* and *SH* waves, at both sub-critical and super-critical angles, with combined *SV* and *SH* allowing incident *S* with any polarisation direction relative to the interface. It treats elliptical polarisation, which is necessary to describe fully the behaviour at super-critical angles. All media types are treated as special cases in the same unified matrix formulation based upon the solid-solid interface, and the program is designed for different levels of use, ranging from single calculations as required for ray tracing algorithms, to a full output of coefficients for all resulting waves over the full range of incident angles. A series of interfaces may be

concatenated so that the composite reflection or refraction coefficients can be calculated for a chosen sequence of reflections/refractions within a structure whose interfaces need not be parallel.

Since real interfaces always pose questions concerning the limits of applicability of the equations, a list of the assumptions employed in their derivation is given in section 2. Our notation is given in section 3, with an introduction to wave behaviour as necessary to define appropriate quantities. In section 4 the theory relating to plane interfaces between all combinations of solid and fluid media are brought together using a common formulation, and examples to illustrate behaviour in various circumstances is given in section 5, using important interfaces in global seismology where possible. Differences between the notation of this and other publications are pointed out and explained in section 6, together with a review of errors in past works. In section 7 the effects of relaxing each of the initial assumptions are outlined, with references to relevant work. In Appendix A the program is explained. The program listing, together with its user documentation, is given in Appendix B.

2. PLANE WAVES INCIDENT UPON A PLANE INTERFACE—INITIAL ASSUMPTIONS

In this section attention is confined to plane waves incident upon a plane interface—the corresponding partitioning equations for the amplitude of particle displacement are widely referred to as the Zoeppritz equations, and form the basis of the computer program. We consider a uniform, plane, monochromatic P or S wave incident upon a plane, abrupt interface between two semi-infinite, homogeneous, isotropic, perfectly elastic (and hence non-dispersive) media in welded contact. These assumptions are now listed and explained.

(A) Requirements for the incident wave

(A1) Uniform The incident wave has the same amplitude at every point on any selected wavefront.

(A2) Monochromatic The incident wave has a single frequency component. After establishing the required relations for a monochromatic wave of arbitrary frequency, these will be shown to be independent of frequency for sub-critical angles of incidence, enabling the principle of superposition to be used to extend the applicability to arbitrary waveforms (see section 7.1). However, for super-critical angles it will be shown that the form of the non-propagating or "evanescent" wave is frequency-dependent.

(A3) Plane Any chosen wavefront lies in a plane which extends to infinity. The non-plane incident wave is considered in section 7.2. It must be remembered that waves from a point source (which is usually close to reality) are spherical and not planar. A plane wave is a good local approximation to a spherical wave at very large distances from the source, and is a good local approximation to any wave as long as variations in amplitude along a wavefront are small within a wavelength, and the radius of curvature of the wavefront is large compared with the area of wavefront that is being examined. Moreover, a point source at infinity in a halfspace still generates headwaves and surface waves at the boundary, since the approximation is only locally good. We cannot make the length of a boundary short compared with the distance to a point source if the boundary itself extends to infinity. However, the plane-wave case is more valuable than might be expected since cylindrical or spherical waves can be decomposed into a superposition of plane waves (see section 7.2), for example using the τ–p transform.

(A4) Stationary The incident wave is continuous throughout time. In principle, contravention of this assumption requires relaxation of assumption A2. In practice seismic waves are normally transient; this introduces a departure from the initial assumptions which is important in some circumstances.

(B) Requirements for the interface

(B1) Plane The interface is planar. The curved interface is considered in section 7.3, and the irregular interface in section 7.4. It must be remembered that on a global scale the interfaces of the Earth are spherical and not planar, although this will only become significant at very long periods.

(B2) Abrupt The two media are separated by a perfect discontinuity in the elastic moduli and density (and hence implicitly in the *P*- and *S*- wave speeds) with no transition zone. This condition clearly becomes more difficult to satisfy at higher frequencies. The non-abrupt interface is considered in section 7.5.

(B3) Welded In the case of two solid media in contact, slip does not take place along the interface; this implies continuity of the two components of displacement which are parallel to the interface. If one or both media are fluid, then this condition is not applicable. It is possible for limited slip to occur between two solid media, or in an extreme case for the interface to be perfectly lubricated. These cases are considered briefly in section 7.6, and the differences in boundary conditions implied by perfect lubrication are considered in section 4.4. Additionally we assume that the media remain in contact, implying continuity of the normal component of displacement.

(C) Requirements for the two media

(C1) Semi-infinite Each medium continues to infinity both along and away from the interface—i.e. there are no effects from other interfaces or end effects due to termination of the interface. The effect of other interfaces nearby may be important if closer than several wavelengths from the interface, and this effect will in general be frequency-dependent (see section 7.7).

(C2) Homogeneous In each medium the elastic constants and the density (and hence, implicitly, the *P*- and *S*- wave speeds) are independent of position. Relaxation of this condition implies wave-speed and/or density gradients, and hence non-plane waves (see section 7.2).

(C3) Isotropic The *P*- and *S*- wave speeds are independent of particle motion direction in the medium. This normally implies that the medium is described by two elastic constants, but this does not have to be the case. A Poisson solid comprising masses held together with identical springs has only one elastic constant and is isotropic. By changing the stiffness of some of the springs, the medium becomes anisotropic with only two elastic constants. Treatment of anisotropic media requires appropriate generalisation of the equations and is not considered in this report. There are situations in which anisotropy may become important, in particular when the degree of anisotropy is sufficient to affect significantly the shear-wave signals; the reader is referred to Crampin [11]. Violation of the assumption of isotropy is considered in section 7.9.

(C4) Perfectly elastic Both media are elastic with stress proportional to strain and can be described by two scalar elastic parameters, in addition to density. It is assumed that there are no viscous or other anelastic effects, and that the wave motions are of small amplitude so that finite strain effects can be neglected. Relaxation of these assumptions would invalidate the wave equation which we solve; this is considered in section 7.8.

(C5) Non-dispersive The elastic constants (and hence, implicitly, the *P* and *S* wave speeds) are independent of wavelength. Deviations from this would result in angular dispersion of refracted waves derived from a non-monochromatic incident wave (as happens

to light passing through a glass prism). The assumption of perfectly elastic media in assumption C4 implies no dispersion; if there is dispersion there must be energy loss, and anelasticity in the earth must, in principle, be associated with a small amount of dispersion to maintain causality.

3. NOTATION AND INTRODUCTION TO CONCEPTS

3.1 Definition of quantities and sign convention

A summary of the notation used is given in figure 1. Let the interface lie in the plane $x_3=0$ in the Cartesian system (X_1,X_2,X_3). Without loss of generality let waves be incident from positive X_3 in the plane $x_2=0$, which we define as the "ray plane", and which is sometimes referred to as the "sagittal plane". Particle displacement from equilibrium at the point $\mathbf{x}=(x_1,x_2,x_3)$ on a ray is defined as $\mathbf{u}=(u_1,u_2,u_3)$, measured in the same coordinate system. Let A, B, C, D, E, F, G, H, and I be the displacements of incident P, incident SV, reflected P, reflected SV, refracted P, refracted SV, incident SH, reflected SH and refracted SH respectively where, by definition, each S wave is resolved into two orthogonal components, both of which are normal to the ray—one in the ray plane (SV) and the other parallel to the interface (SH). Any polarisation of incident S can thus be treated by first resolving it into these two components. Of course, only if the interface is horizontal do SV and SH correspond to the true vertical and horizontal components respectively, though we follow the usual convention of still referring to these components as SV and SH.

Further, let a, b, a, b, e, f, b, b and f be the respective angles between the ray paths of each wave and the normal to the interface. Here we have assumed the law of reflection in order to eliminate the separate angles c and d, and without loss of generality we have set the angles describing incident, reflected and refracted SH equal to the corresponding angles for SV. The waves are incident and reflected in layer i and refracted in layer ii—small Roman suffixes i and ii being used here to avoid confusion with the Cartesian directions 1, 2 and 3. The angles a, b, d and f are all positive when real (i.e. whenever they correspond to propagating waves) and lie between 0 and $\pi/2$; the propagation direction of each wave has a component along positive X_1. The P-wave speed, S-wave speed, density and two Lamé elastic parameters in each of the layers i and ii respectively are denoted by U_i, V_i, ρ_i, λ_i, μ_i, U_{ii}, V_{ii}, ρ_{ii}, λ_{ii}, and μ_{ii}. In contexts not specific to either layer the suffix is omitted.

In addition to the above definitions, a sign convention for the measurement of each displacement A to I must be defined with respect to the ray direction and the interface, in order to be able to compare fully the incident and resulting waves. This convention is defined by the direction of arrows adjacent to each ray in figure 1, and requires some comment. Each of the displacements A to I represents an harmonic wave, which may be fully described by a displacement amplitude or "modulus" (which is always positive), and a phase angle defined in $[0,2\pi]$. We therefore need to define for each wave the direction of displacement which corresponds to a chosen phase, say zero-phase. This is shown for each of A to I in figure 1. These directions might loosely be referred to as the "direction of positive displacement" but since we are defining displacement amplitude as a modulus, positive only, they are more accurately described as "directions of zero-phase". If we were instead to allow the displacement to be positive or negative, with the phase defined in $[0,\pi]$, then the directions shown would become directions of positive displacement.

Our convention can be applied equally to transient waves. For example, if we consider an impulse in displacement, a direction of zero-phase defined in figure 1 can be thought of as the direction of this displacement if its phase is zero; if its phase is π, then the impulse is in the opposite direction.

An harmonic wave may alternatively be fully described using a real and imaginary part of a complex number by making each of A to I complex; this is done in our computations. The modulus of the complex number is then equivalent to the modulus of our displacement, and the argument of the

complex number is its phase. In figure 1 we use the same symbols A to I to label the directions of zero-phase for convenience.

The definitions used here for the directions of zero-phase displacements of A to I have been chosen so that those for the P waves A, C and E are all in the direction of propagation, while the zero-phase directions of the SH displacements G, H and I all lie along positive X_2. The directions of zero-phase for SV displacements B, D and F then follow if a right-handed Cartesian system is demanded for the coordinate system [SV,SH,propagation direction] for each S wave. This same demand for all these rays is essential to ensure that all rays are described with a self-consistent convention. Our choice of convention for the P waves A, C and E means that if an incident compressive impulse results in compressive reflected and refracted impulses, then A, C and E are all zero-phase. Further, an incident SH pulse, with disturbance towards positive X_2, and which yields reflected and refracted pulses also towards positive X_2, corresponds to G, H and I all zero-phase. Our definitions for SV are such that zero-phase B, D and F all have a component towards negative X_3. Although these choices are intuitive and are required to maintain self-consistency for the passage of waves through a succession of interfaces, most authors use a variety of other conventions (see section 6).

Following the above convention, the displacement amplitude will always be expressed as a positive value; any "change of polarity" at the interface will be expressed in the phase. Thus a polarity change will be expressed as a π phase change, not a change of sign in the amplitude. This convention corresponds to the standard modulus/argument form of a complex number.

In the theory which follows we refer to the complex displacements as A, B etc.; the displacement modulus of each wave is strictly $|A|$, $|B|$ etc. Except where there may be confusion we omit the modulus signs. Where the phase is 0 or π, the displacement is real.

Taking the incident P wave as an example, the modulus $|A|$ and the phase ϕ_A are given by

$$|A| = \sqrt{(\mathrm{Re}(A))^2 + (\mathrm{Im}(A))^2} \tag{1a}$$

and

$$\cos\phi_A = \frac{\mathrm{Re}(A)}{|A|}, \qquad \sin\phi_A = \frac{\mathrm{Im}(A)}{|A|}, \qquad 0 \le \phi < 2\pi\,. \tag{1b}$$

Here we preserve the separate signs of $\cos\phi_A$ and $\sin\phi_A$ when using arctangent to find ϕ_A explicitly, since we define ϕ_A to range from 0 to 2π. Similar relations hold for the other waves B to I.

If any of the reflected or refracted waves emerge at angles larger than the angle of incidence, then it is possible to increase the angle of incidence to a value at which the reflected or refracted wave emerges parallel to the interface. Such an angle is termed the "critical angle" of incidence for the appropriate reflected or refracted wave, and larger angles of incidence are "super-critical". In particular, an incident P or S wave may have a critical angle for the refracted P wave (and in extreme cases the refracted S wave), and an incident S wave will always have a critical angle for reflected P. Thus an incident S wave may have up to three critical angles. Super-critical angles of incidence result in non-propagating "evanescent" waves along the boundary, and non-trivial phase changes in the remaining propagating waves; our complex algebra will include these cases implicitly as shown later. At incident angles for which all waves exist as propagating waves, the only phase change which can occur upon reflection or refraction is 180° (π radians), corresponding merely to a change of polarity. We refer to this as a "trivial" phase change, as distinct from intermediate phase changes which we term "non-trivial". Since for a phase of π the displacement is real, it is only at super-critical angles that we shall need to be concerned with complex algebra.

Differences in the notation used by other authors and their consequences, together with an account of the errors of other work are given in section 6.

3.2 Elliptically polarised *S* waves

We have pointed out that any *S*-wave polarisation can be represented by resolving it into *SV* and *SH* components, each with an appropriate displacement modulus and phase. Provided the *SV* and *SH* amplitudes (i.e. their displacement moduli) are coincident on the ray at a given time, the wave is plane-polarised. However, this need not be the case. If the maximum displacements of the two components are not coincident along the ray, the resultant displacement vector will rotate as the point of observation moves along the ray (and as time passes at any fixed point on the ray). This gives elliptical, or helical, polarisation, and the term "polarisation angle" can no longer refer to a plane of polarisation. In general an incident *S* wave may be of this form.

It will be shown that the behaviour of *SH* at the interface is independent of the *P-SV* system of waves, so it follows from the above discussion that an incident plane polarised *S* wave with an intermediate polarisation angle (i.e. which is neither wholly *SV* nor wholly *SH*) will in general produce reflected and refracted *S* waves with different polarisation angles from that of the incident wave, on account of the different partitioning coefficients of the *SV* and *SH* components. Moreover, if an *S* wave with an intermediate polarisation angle is incident at an angle which is super-critical in respect of either reflected or refracted *P*, then the reflected and refracted *S* waves will acquire elliptical polarisation as a result of the non-trivial phase change suffered by the *SV* component but not by the *SH* component. If an intermediately polarised *S* wave is incident at an angle which is super-critical in respect of refracted *S*, then both the reflected *SV* and *SH* components will suffer (in general different) non-trivial phase changes. This is a practical way in which elliptically polarised *S* waves can be generated. Similar behaviour is observed in electromagnetic waves, as noted by, e.g., Stratton [12] page 500, (although in that case there is no analogue of the *P* waves). This behaviour was used by Fresnel to produce circularly polarised light by total reflection.

It is clear that we must include the most general form of *S*-wave polarisation for all the wave motions in our formulation, in order to ensure correct treatment not only of the relative phase (i.e. "polarity") of each travelling wave, but also the nature of the evanescent waves resulting from super-critical angles of incidence. After resolving each of the *S* waves into an *SV* and *SH* component as we have done, we ensure that the formulation is general by specifying a separate displacement modulus and phase for each *P*, *SV* and *SH* wave. We emphasise, though, that for the *S* waves, the quantities still refer to the *SV* and *SH* components separately.

3.3 Frequency dependence and pulse shape

The set of complex displacements and angles introduced in section 3.1 define the (monochromatic) wave motions fully. Since we shall see that according to the Zoeppritz equations the partitioning is frequency-independent for the propagating waves, it follows that these amplitudes can be used as a scaling factor for the reflection and refraction of any chosen incident waveform, provided the monochromatic wave has not suffered a non-trivial phase change.

We are concerned strictly with continuous monochromatic plane waves, but our results can be extended to transient waveforms with certain limitations. At sub-critical angles of incidence all phase changes are either 0 or π, so a transient waveform retains its shape but is possibly inverted after reflection or refraction. At super-critical angles of incidence, the non-propagating (evanescent) reflected or refracted waves, whose resulting angles have "passed beyond" 90° have a complex angle of reflection or refraction; evanescent waves have a frequency-dependent behaviour because, as we shall see, they are associated with the interface itself and represent particle motion decaying away from the interface towards either side over a distance which depends upon wavelength. The behaviour of these evanescent waves is fully described by our formulation but results in a frequency-dependent expression for the decay (section 4.8). Moreover, since the remaining propagating waves associated with super-critical angles of incidence undergo non-trivial phase changes, any non-monochromatic incident wave, whether transient or stationary, has a different shape after reflection or refraction if the incident angle is

super-critical. Indeed, the P wave may then have a different shape from the S wave in the same medium. In this situation it is not possible to regard the pulses simply as scaled by our amplitudes $|A|$ to $|I|$.

3.4 Combined treatment of *SV* and *SH*

In cases where S waves have polarisation directions intermediate between SV and SH, we may wish to describe the wave using parameters which make explicit its amplitude, angle of polarisation and eccentricity, rather than expressing the wave in terms of its separate SV and SH components. This is particularly so if the wave is elliptically polarised. The computer program does not currently have an option to express S-wave motion in this way, but appropriate quantities are defined here to allow for such an extension in the computation.

The term "polarisation angle" is normally applied only to plane-polarised waves where it describes the angle between the direction of shear-wave particle motion and some reference direction in the plane normal to the ray direction. In the case of an elliptically polarised S wave, we extend the definition of polarisation angle to describe the angle at which the amplitude vector is a maximum as it rotates describing an ellipse. We adopt the convention (see inset in figure 1) that the polarisation angle is measured clockwise when viewed along the ray in the direction of propagation, with zero lying in the plane x_2=0 (the ray plane) and towards negative X_3. It follows that a zero-phase SV wave (i.e. B or D or F zero-phase with G or H or I zero amplitude respectively) always has a polarisation angle, defined as j, k or l respectively, equal to zero. If SV and SH both exist and are in phase, the shear wave is plane polarised with an amplitude, defined here as J, K or L respectively, that depends upon the SV and SH amplitudes, and a polarisation angle which depends upon their ratio. If SV and SH are out of phase, the resultant amplitude depends additionally upon their phase difference; in this case the polarisation angle depends upon the amplitude ratio of SV and SH, and upon their phase difference if their ratio is not unity. The eccentricity of the ellipse is determined by the phase difference only; we denote the eccentricities by ε_J, ε_K and ε_L for the incident, reflected and refracted waves respectively.

The displacement vector derived from the orthogonal SV and SH waves describes an elliptical Lissajous' figure according to standard theory (see e.g. Braddick [13] page 10). We define the polarisation angle in $[-\pi,\pi]$, negative and positive phases corresponding to opposite senses of rotation of the displacement vector. With our definitions of the directions of positive SV and SH, the amplitude vector describes a right-handed ellipse when viewed along the propagation direction if SH leads SV by between 0 and π, and a left-handed ellipse if SH lags SV by between 0 and π.

Considering first the incident S wave, let the Lissajous' figure be described in the coordinate system X', where X'_1 lies along G (the zero-phase direction of SH), and X'_2 lies along B (the zero-phase direction of SV) (see inset in figure 1). In this plane we may write the SH and SV components respectively as

$$x'_1 = |G|\cos\omega t\,, \qquad x'_2 = |B|\cos(\omega t - (\phi_B - \phi_G)) \tag{2a, b}$$

where ϕ_B and ϕ_G are the phases of the SV and SH components respectively, and for convenience we have chosen zero time so that there is zero phase lag in the X'_1 component. Eliminating ωt from equations (2a) and (2b) we obtain the equation of the ellipse:

$$\frac{x'_1{}^2}{|G|^2} - \frac{2x'_1x'_2}{|G||B|}\cos(\phi_B - \phi_G) + \frac{x'_2{}^2}{|B|^2} = \sin^2(\phi_B - \phi_G). \tag{3}$$

In this equation we have lost information on whether G lags or leads B.

In order to find the polarisation angle j, the S-wave amplitude J and the eccentricity ε_J, we can rotate the X' coordinate system by an angle j into a system X'' in which the major axis lies along X''_2 (see inset in figure 1). We then have

$$\frac{x''_1{}^2}{J^2(1-\varepsilon_J{}^2)}+\frac{x''_2{}^2}{J^2}=1. \tag{4}$$

The required rotation follows from, for example, Jones and Jordan [14] page 55

$$\tan\left(2j-\frac{\pi}{4}+\frac{\pi}{4}\text{sign}(|B|-|G|)\right)=\frac{2|B||G|\cos(\phi_B-\phi_G)}{(|B|+|G|)(|B|-|G|)},$$
$$\text{with } 0\le j\le \pi/2 \text{ for } \cos(\phi_B-\phi_G)\ge 0, \quad \text{and } \pi/2<j\le\pi \text{ for } \cos(\phi_B-\phi_G)<0 \tag{5a}$$

where the angle on the left hand side has been chosen to ensure that j is always measured to the major axis irrespective of the relative sizes of $|B|$ and $|G|$. (This result can alternatively be obtained by converting equation (3) into polar coordinates (R,θ), and setting $dR/d\theta = 0$ to find the orientation of the major and minor axes.) In equation (5a) j is only defined in $[0,\pi/2]$ because of the arctangent operation on $2j$. We require j to be defined in $[0,\pi]$, so the condition on $\phi_B-\phi_G$ to achieve this is given.

The relationship between the coefficients in equations (3) and (4) provides explicit expressions for J and ε_J in terms of B, G and $\phi_B-\phi_G$ (see for example Jones and Jordan [14] pages 55 and 56). For J we obtain

$$\frac{1}{J^2}=\frac{P+Q}{2\sin^2(\phi_B-\phi_G)} \quad \text{for } \phi\ne n\pi; \qquad \frac{1}{J^2}=P \quad \text{for } \phi=n\pi;$$
$$\text{where} \quad P=\frac{1}{|G|^2}+\frac{1}{|B|^2}; \quad Q=\sqrt{\left(\frac{1}{|G|^2}-\frac{1}{|B|^2}\right)^2+\left(\frac{2\cos(\phi_B-\phi_G)}{|G||B|}\right)^2} \tag{5b}$$

and for ε_J we obtain

$$\varepsilon_J{}^2=1-\left(\frac{P-Q}{P+Q}\right) \tag{5c}$$

with P and Q defined as in equation (5b). To complete these relations we point out that the phase difference $\phi_B-\phi_G$ can be expressed in terms of the complex amplitudes B and G. From equivalents to equation (1b) we obtain

$$\cos(\phi_B-\phi_G)=\frac{\text{Re}(B)}{|B|}\cdot\frac{\text{Re}(G)}{|G|}+\frac{\text{Im}(B)}{|B|}\cdot\frac{\text{Im}(G)}{|G|};$$
$$\sin(\phi_B-\phi_G)=\frac{\text{Im}(B)}{|B|}\cdot\frac{\text{Re}(G)}{|G|}-\frac{\text{Re}(B)}{|B|}\cdot\frac{\text{Im}(G)}{|G|}. \tag{5d}$$

Since $\phi_B-\phi_G$ must be defined in $[-\pi,\pi]$ to provide information on the sense of rotation of the S particle motion vector, we have stated the sine and cosine explicitly.

Similar equations to (5a–d) follow for the reflected S wave. For its polarisation angle k we obtain

$$\tan\left(2k-\frac{\pi}{4}+\frac{\pi}{4}\text{sign}(|D|-|H|)\right)=\frac{2|D||H|\cos(\phi_D-\phi_H)}{(|D|+|H|)(|D|-|H|)}$$
$$\text{with } 0\le k\le \pi/2 \text{ for } \cos(\phi_D-\phi_H)\ge 0, \quad \text{and } \pi/2<k\le\pi \text{ for } \cos(\phi_D-\phi_H)<0\,. \tag{6a}$$

For its amplitude K we obtain

$$\frac{1}{K^2} = \frac{P+Q}{2\sin^2(\phi_D - \phi_H)} \quad \text{for } \phi \neq n\pi; \qquad \frac{1}{K^2} = P \quad \text{for } \phi = n\pi;$$

$$\text{where} \quad P = \frac{1}{|H|^2} + \frac{1}{|D|^2}; \qquad Q = \sqrt{\left(\frac{1}{|H|^2} - \frac{1}{|D|^2}\right)^2 + \left(\frac{2\cos(\phi_D - \phi_H)}{|H||D|}\right)^2}\,. \tag{6b}$$

For the eccentricity ε_K we obtain

$$\varepsilon_K{}^2 = 1 - \left(\frac{P-Q}{P+Q}\right) \tag{6c}$$

with P and Q defined as in equation (6b). The phase difference $\phi_D - \phi_H$ is given by

$$\cos(\phi_D - \phi_H) = \frac{\mathrm{Re}(D)}{|D|}\cdot\frac{\mathrm{Re}(H)}{|H|} + \frac{\mathrm{Im}(D)}{|D|}\cdot\frac{\mathrm{Im}(H)}{|H|};$$

$$\sin(\phi_D - \phi_H) = \frac{\mathrm{Im}(D)}{|D|}\cdot\frac{\mathrm{Re}(H)}{|H|} - \frac{\mathrm{Re}(D)}{|D|}\cdot\frac{\mathrm{Im}(H)}{|H|}\,. \tag{6d}$$

Similarly, for the refracted S wave, the polarisation angle l is given by

$$\tan\left(2l - \frac{\pi}{4} + \frac{\pi}{4}\mathrm{sign}(|F| - |I|)\right) = \frac{2|F||I|\cos(\phi_F - \phi_I)}{(|F| + |I|)(|F| - |I|)},$$

$$\text{with } 0 \le l \le \pi/2 \text{ for } \cos(\phi_F - \phi_I) \ge 0, \quad \text{and } \pi/2 < l \le \pi \text{ for } \cos(\phi_F - \phi_I) < 0\,. \tag{7a}$$

The amplitude L is given by

$$\frac{1}{L^2} = \frac{P+Q}{2\sin^2(\phi_F - \phi_I)} \quad \text{for } \phi \neq n\pi; \qquad \frac{1}{L^2} = P \quad \text{for } \phi = n\pi;$$

$$\text{where} \quad P = \frac{1}{|I|^2} + \frac{1}{|F|^2}; \qquad Q = \sqrt{\left(\frac{1}{|I|^2} - \frac{1}{|F|^2}\right)^2 + \left(\frac{2\cos(\phi_F - \phi_I)}{|I||F|}\right)^2} \tag{7b}$$

and the eccentricity ε_L is

$$\varepsilon_L{}^2 = 1 - \left(\frac{P-Q}{P+Q}\right) \tag{7c}$$

with P and Q defined as in equation (7b). The phase difference $\phi_F - \phi_I$ is given by

$$\cos(\phi_F - \phi_I) = \frac{\mathrm{Re}(F)}{|F|}\cdot\frac{\mathrm{Re}(I)}{|I|} + \frac{\mathrm{Im}(F)}{|F|}\cdot\frac{\mathrm{Im}(I)}{|I|};$$

$$\sin(\phi_F - \phi_I) = \frac{\mathrm{Im}(F)}{|F|}\cdot\frac{\mathrm{Re}(I)}{|I|} - \frac{\mathrm{Re}(F)}{|F|}\cdot\frac{\mathrm{Im}(I)}{|I|}\,. \tag{7d}$$

Although the above treatment has to some extent anticipated the theory to be given in the next section, it has been presented here to provide definitions of a full set of quantities for describing the vector motion of an arbitrary S wave.

4. THEORY

4.1 Displacement potentials for *P* and *S* waves

The equations governing the reflection and refraction of elastic waves under the assumptions given in section 2 are most easily derived by formulating appropriate travelling wave expressions which are solutions of the *P* and *S* wave equations for the two media, and then imposing appropriate boundary conditions of displacement and stress at the interface. These boundary conditions provide the necessary relations between the displacement amplitudes and the phases of the six waves, which give an unique solution for any particular case. The relations between the six angles *a* to *f* also follow, constituting the familiar laws of reflection and refraction.

We begin with the relation between the components of stress, p_{ij} and strain e_{ij} which, for an isotropic and perfectly elastic medium, reduces to Hooke's law in three dimensions—see for example Bullen [15] pages 29–30:

$$p_{ij} = \lambda \delta_{ij} \operatorname{div} \mathbf{u} + 2\mu e_{ij} \qquad i = 1, 2, 3, \quad j = 1, 2, 3 \tag{8a}$$

where

$$e_{ij} = \frac{1}{2}\left(\frac{\partial u_j}{\partial x_i} + \frac{\partial u_i}{\partial x_j}\right). \tag{8b}$$

Application of Gauss's law gives force per unit volume, and the application of Newton's second law yields the equation of motion (see for example Ewing, Jardetsky and Press [16] page 6, Jeffreys [17] page 31, Bullen and Bolt [18] page 88):

$$(\lambda + \mu) \operatorname{grad}(\operatorname{div} \mathbf{u}) + \mu \nabla^2 \mathbf{u} = \rho \frac{\partial^2 \mathbf{u}}{\partial t^2}. \tag{9}$$

The separate application of the div and curl operators to this equation yields two forms of the wave equation, indicating that it is possible to propagate either dilatational (*P*) or rotational (*S*) disturbances. For propagating plane waves in isotropic media the particle motions of *P* and *S* waves are purely longitudinal and transverse respectively.

For *P* waves, remembering that div(grad) $\equiv \nabla^2$ we obtain

$$\left(\frac{\lambda + 2\mu}{\rho}\right) \nabla^2(\operatorname{div} \mathbf{u}) = \frac{\partial^2}{\partial t^2}(\operatorname{div} \mathbf{u}) \qquad (P \text{ waves}). \tag{10}$$

For *S* waves, remembering that curl(grad) $\equiv 0$ we obtain

$$\left(\frac{\mu}{\rho}\right) \nabla^2(\operatorname{curl} \mathbf{u}) = \frac{\partial^2}{\partial t^2}(\operatorname{curl} \mathbf{u}) \qquad (S \text{ waves}). \tag{11}$$

The propagation speeds *U* and *V*, of *P* and *S* waves respectively, follow from equations (10) and (11):

$$U = \left(\frac{\lambda + 2\mu}{\rho}\right)^{1/2} \qquad V = \left(\frac{\mu}{\rho}\right)^{1/2}. \tag{12a,b}$$

In the present problem the particle displacement $\mathbf{u}(\mathbf{x},t)$ at the point $\mathbf{x}$ at time t is, in general, the sum of displacements resulting from more than one disturbance, including both *P* and *S* waves. These two wave types may be distinguished by their different particle motions with respect to the ray.

The particle motion of a P wave may be expressed as the spatial derivative of a scalar potential, and that of an S wave by the vector spatial derivative of a vector potential. We define scalar and vector potentials ϕ and $\boldsymbol{\psi}$ such that

$$\mathbf{u}(\mathbf{x},t) = \text{grad}\ \phi(\mathbf{x},t) + \text{curl}\ \boldsymbol{\psi}(\mathbf{x},t) \tag{13}$$

(following, e.g., Ewing, Jardetsky and Press [16] equation 1.20'), (We have also used the symbol ϕ for the phase of a signal, but it will always be clear from the context which meaning is intended.)

We can verify that these potentials do indeed describe the P and S motions by substitution of this definition into equations (10) and (11). (Here we simply substitute the second derivatives of the potentials, so that we demonstrate a necessary but not sufficient condition for verification. For a rigorous treatment see for example chapter 2 of Hudson [19].)

Remembering that div(curl) ≡ 0, substitution into equation (10) yields:

$$\left(\frac{\lambda+2\mu}{\rho}\right)\nabla^2(\text{div}(\text{grad}\ \phi)) = \frac{\partial^2}{\partial t^2}(\text{div}(\text{grad}\ \phi)). \tag{14}$$

Using equation (12a), and remembering that div(grad) ≡ ∇^2, this reduces to

$$\nabla^2\phi = \frac{1}{U^2}\frac{\partial^2\phi}{\partial t^2}. \tag{15}$$

We now substitute equation (13) into equation (11) for S waves. Remembering again that curl(grad) ≡ 0, we obtain

$$\left(\frac{\mu}{\rho}\right)\nabla^2(\text{curl}(\text{curl}\ \mathbf{u})) = \frac{\partial^2}{\partial t^2}(\text{curl}(\text{curl}\ \mathbf{u})). \tag{16}$$

Using the identity ∇^2 ≡ grad(div) – curl(curl), and remembering again that div(curl) ≡ 0, this becomes

$$\nabla^2\boldsymbol{\psi} = \frac{1}{V^2}\frac{\partial^2\boldsymbol{\psi}}{\partial t^2}. \tag{17}$$

The scalar and vector potentials both separately satisfy the wave equation; ϕ is a field which describes P waves only and $\boldsymbol{\psi}$ is a field which describes S waves only. The scalar and vector potentials are not physical quantities, but they enable that part of the displacement $\mathbf{u}_P(x_1,x_2,x_3)$ which results from P waves, and that part $\mathbf{u}_S(x_1,x_2,x_3)$ which results from S waves to be separated, and solved independently. If the total displacement at the point $\mathbf{u}$ is required it is given simply by $\mathbf{u} = \mathbf{u}_P+\mathbf{u}_S$ (or $\mathbf{u} = \mathbf{u}_P+\mathbf{u}_{SV}+\mathbf{u}_{SH}$ if we resolve the S wave into SV and SH components). Of course, any number of P and S waves may be added in this way.

4.2 The plane wave solution; relation between displacement and displacement potential

For plane waves we can proceed by attempting a trial substitution of a propagating monochromatic wave into equations (15) and (17) for P and S waves respectively. We know that any P wave contributions to the displacement at a certain time and place travel with one speed, and any S wave contributions travel at a different speed. It follows that plane-wave solutions to the wave equation will have a different form for the P and S waves, so it is sensible to solve for them separately using appropriate trial solutions.

We first verify that the P-wave part of the displacement, $\mathbf{u}_P$, and the S wave part $\mathbf{u}_S$, also separately satisfy the wave equation. Application of grad to equation (15) gives

$$\text{grad}(\text{div}(\text{grad}\ \phi)) = \frac{1}{U^2}\frac{\partial^2}{\partial t^2}(\text{grad}\ \phi)\ . \tag{18}$$

Use of the vector identity curl(curl) ≡ grad(div) – ∇^2, and substitution of $\mathbf{u}_P$ = grad ϕ gives

$$\text{curl}(\text{curl}\ \mathbf{u}_P) + \nabla^2\mathbf{u}_P = \frac{1}{U^2}\frac{\partial^2\mathbf{u}_P}{\partial t^2}\ . \tag{19}$$

By definition we know that curl $\mathbf{u}_P$ = 0, so we obtain

$$\nabla^2\mathbf{u}_P = \frac{1}{U^2}\frac{\partial^2\mathbf{u}_P}{\partial t^2}\ . \tag{20}$$

Application of curl to equation (17) and use of the vector identity curl(curl) ≡ grad(div) – ∇^2, yields

$$\text{curl}(\text{grad}(\text{div}\ \boldsymbol{\psi}) - \text{curl}(\text{curl}\ \boldsymbol{\psi})) = \frac{1}{V^2}\frac{\partial^2}{\partial t^2}\text{curl}\ \boldsymbol{\psi}\ . \tag{21}$$

Substitution of $\mathbf{u}_S$ = curl $\boldsymbol{\psi}$ and remembering that the operator curl(grad) ≡ 0, we obtain

$$\text{curl}(\text{curl}\ \mathbf{u}_S) = \frac{1}{V^2}\frac{\partial^2\mathbf{u}_S}{\partial t^2}\ . \tag{22}$$

Using the above vector identity again, and remembering that div $\mathbf{u}_S$ = 0, this becomes

$$\nabla^2\mathbf{u}_S = \frac{1}{V^2}\frac{\partial^2\mathbf{u}_S}{\partial t^2}\ . \tag{23}$$

We have therefore shown that separate *P*- and *S*-wave solutions can be sought either in displacement (equations (20) and (23) respectively) or in displacement potential (equations (15) and (17) respectively). These sets of equations are similar and we expect their solutions to have a similar form. We first consider the general plane wave solution to equations (15) and (17), which we solve for the displacement potentials. Again we use the incident *P* and the incident *S* wave of figure 1 respectively as examples; as this is a general form we omit the medium suffix i for clarity. We specify trial solutions of the form

$$\phi = A_\phi \exp\left[\frac{i\omega}{U}(x_1\sin a - x_3\cos a) - i\omega t\right] \tag{24a}$$

and

$$\boldsymbol{\psi} = \left(B_{\psi 1}, B_{\psi 2}, B_{\psi 3}\right)\exp\left[\frac{i\omega}{V}(x_1\sin b - x_3\cos b) - i\omega t\right] \tag{24b}$$

respectively. Because we are substituting into the wave equation for the displacement potentials rather than for the displacements, we have defined different amplitudes from those of figure 1. For the scalar potential we introduce a scalar amplitude A_ϕ (which will relate to the displacement amplitude *A*), and for the vector potential we introduce a vector amplitude ($B_{\psi 1}$,$B_{\psi 2}$,$B_{\psi 3}$) (which will relate to both the displacement amplitudes *B* and *G*).

For each wave the exponent defines the spatial and temporal variation of the wave motion. The first two terms give the spatial variation of the particle motion in the X_1 and X_3 directions respectively (there is no variation in X_2), and for the P wave we can identify the horizontal wave slowness as $(\sin a)/U$ and the vertical slowness as $(\cos a)/U$. The horizontal and vertical wavenumbers are $(\omega \sin a)/U$ and $(\omega \cos a)/U$ respectively. Provided a is real, these represent travelling waves resolved along the two directions. (The X_3 component is specified as negative because the wave motion proceeds with a component in the negative X_3 direction.) The third term in the exponent, $-i\omega t$, gives the time dependence of the particle motion; the sign of the exponent gives waves travelling in the same sense as the slowness components, i.e. towards positive X_1 and negative X_3. Similar relations apply for the S wave with U replaced by V.

If the whole exponent is imaginary we have uniform travelling waves; this is the normal case. If the whole exponent becomes complex then its real component corresponds to decaying motion, and this can happen in various ways. For example, if a becomes complex, this introduces a real part into the spatial terms in the exponent, and we have a wave decaying spatially; this occurs for evanescent waves (section 4.8). If U is complex then again this introduces a real part into the exponent, so that anelastic attenuation can be represented by a complex wave speed (section 7.8).

There are important differences in numerical value and scaling between the displacement amplitudes and the displacement potential amplitudes, and in previous work it is not always clear which has been used. This is a major source of confusion and error in a number of works, an account of which is given in section 6. Before proceeding we therefore establish the relations between these two sets of amplitudes; again we choose the incident P and S waves as examples.

We can evaluate $\mathbf{u}_P$ in terms of the displacement <u>potential</u> amplitude by taking the grad of equation (24a) to obtain

$$\mathbf{u}_P = \frac{i\omega}{U}\left(A_\phi \sin a,\ 0,\ -A_\phi \cos a\right) \exp\left[\frac{i\omega}{U}\left(x_1 \sin a - x_3 \cos a\right) - i\omega t\right]. \tag{25}$$

This gives us the three components of the displacement amplitude expressed in terms of the scalar potential amplitude defined in equation (24a). If we express equation (25) in terms of the displacement amplitude as defined in figure 1, we obtain

$$\mathbf{u}_P = (\,A \sin a,\ 0,\ -A \cos a) \exp\left[\frac{i\omega}{U}\left(x_1 \sin a - x_3 \cos a\right) - i\omega t\right] \tag{26}$$

where we have used our definition of A in figure 1 to resolve the displacement amplitude into the required Cartesian components. From equations (25) and (26) the relation between the displacement and potential amplitudes for this wave is therefore

$$A = \frac{i\omega A_\phi}{U}. \tag{27}$$

The form of the factor $i\omega/U$ is generally applicable. The i shows that the displacement and the displacement potential are $\pi/2$ out of phase, which we expect since the displacement is the gradient of the potential. The ω shows that the relationship is proportional to frequency, and this arises from the gradient being steeper at higher frequencies. The $1/U$ shows that the relationship depends upon the relevant seismic wave speed in the medium, and this is an important reason for us to be clear which amplitudes we are considering. When taking the ratios between the amplitudes of different waves, the $i\omega$ cancels out, so these quantities do not affect the Zoeppritz coefficients if we change between displacement and displacement potential. However, the wave speeds will in general be different for each wave, so this <u>does</u> mean the Zoeppritz coefficients are different depending upon whether we use displacement or displacement potential.

A further point concerns the signs of A and A_ϕ. In equation (27) we see that A and A_ϕ have the same sign. If we consider waves travelling in different directions, or if we change the definition of the coordinate axes in figure 1, the signs of the X_1 and X_3 exponents of equation (24a) may also change, changing the signs of the displacement components when equation (24a) is differentiated to obtain equation (25). The signs of the components in equation (26) will also change, following the definition of A. However, it turns out that irrespective of the propagation direction of the wave with respect to the coordinate axes, A and A_ϕ have the same sign. Because we have defined the amplitudes of all three P waves to be in the direction of propagation, it follows that the equivalent relations to equation (27) for the reflected and refracted waves also have the same sign. However, if we were to redefine positive P-wave amplitude to point against the direction of propagation, then only the amplitude components in equation (26) would change sign, so that the displacement and displacement potential would always have the opposite signs. Of course, the displacement potential amplitude could be defined negative in equation (24a) to give both amplitudes the same sign, but this assumes that all waves are defined with displacement amplitude opposite to the propagation direction. In conventions (e.g. some of those referred to in section 6) which do not define positive P-wave displacement amplitude along the direction of ray propagation for all waves, the relation between displacement and displacement potential changes sign depending upon the wave considered (section 6). This is a further reason for defining displacement amplitude positive in the direction of propagation for all P waves.

Proceeding in a similar way for the S wave we take the curl of equation (24b) to obtain

$$\mathbf{u}_S = \frac{i\omega}{V}\left(B_{\psi 2}\cos b,\ -B_{\psi 1}\cos b - B_{\psi 3}\sin b,\ B_{\psi 2}\sin b\right)\exp\left[\frac{i\omega}{V}\left(x_1\sin b - x_3\cos b\right) - i\omega t\right]. \qquad (28)$$

This gives us the displacement amplitude expressed in terms of our displacement potential amplitudes and is equivalent to equation (25) for the P wave. In our definition of the S wave in terms of an SV and an SH component in figure 1, the SV component lies in the ray plane and so defines the X_1 and X_3 Cartesian components, and the SH component lies parallel to the interface and so defines the X_2 Cartesian component. If we express equation (28) in terms of the displacement amplitudes defined in figure 1 we obtain the following relation for the S-wave particle displacement

$$\mathbf{u}_S = (-B\cos b,\ G,\ -B\sin b)\exp\left[\frac{i\omega}{V}\left(x_1\sin b - x_3\cos b\right) - i\omega t\right] \qquad (29)$$

where again we have resolved the amplitudes B and G into their Cartesian components. Comparing coefficients in equations (28) and (29), we obtain three relations between the three components of the S wave displacement potential amplitudes and the two components of the displacement amplitude B and G. We have

$$-B\cos b = \frac{i\omega}{V}\cos b\ .\ B_{\psi 2} \qquad (30a)$$

$$G = -\frac{i\omega}{V}\left(\cos b\ .\ B_{\psi 1} + \sin b\ .\ B_{\psi 3}\right) \qquad (30b)$$

$$-B\sin b = \frac{i\omega}{V}\sin b\ .\ B_{\psi 2}\ . \qquad (30c)$$

We see that one of equations (30a) and (30c) is redundant. We require an additional relation to eliminate one of the three displacement potential coefficients and this comes from the imposition of div $\boldsymbol{\psi} = 0$ without loss of generality (see Hudson [19] equation (2.39)). From equation (24b) we have

$$\text{div}\ \boldsymbol{\psi} = \frac{i\omega}{V}\left(\sin b\ .\ B_{\psi 1} - \cos b\ .\ B_{\psi 3}\right) = 0\ . \qquad (31)$$

From equations (30a), (30b) and (31) we obtain

$$B = -\frac{i\omega}{V} B_{\psi 2} \tag{32a}$$

$$G = -\frac{i\omega}{V\sin b} B_{\psi 3} = -\frac{i\omega}{V\cos b} B_{\psi 1} \,. \tag{32b}$$

In this case we see that the displacement amplitudes have opposite signs to the displacement potential amplitudes. With the coordinate system and amplitude definitions as in figure 1, the equivalent equations to (32a) and (32b) for the refracted S wave (involving F and I) are similar, but for the reflected S wave (D and H) there is a change of sign in the last term of equation (32b).

In equation (32b) the relation between G and the displacement potential amplitudes depends upon the incident angle b. This is because the vector displacement potential of any component of an S wave lies along the normal to the plane containing the ray and the particle displacement direction. In the case of B, D and F the potential amplitude lies along the X_2 axis, whereas for G, H and I it lies at different angles in the ray plane. Thus the above change of sign for the reflected S wave is associated with the difference in ray direction rather than the particle motion direction. Moreover, our choice of convention in figure 1 has ensured that the terms in equation (32) do not change sign for different waves except to allow for different propagation directions. E.g. if the sense of D were reversed (defined towards positive X_3) the sign of the right-hand side of equation (32a) would change for the reflected wave. Such inconsistency has been avoided by our choice of a right-handed coordinate system in [SV,SH,propagation direction] for all rays (section 3.1).

The above discussion highlights the importance of defining whether the amplitude of the displacement, or of the displacement potential, is plotted. We see that as well as a $\pi/2$ phase change between the two amplitudes, the potential amplitude is scaled by the wavenumber, ω/U or ω/V for P waves and S waves respectively. This implies a different scaling factor at different frequencies. In the case of an arbitrary plane wave the frequency does not appear in the ratio of the potential amplitudes of the different waves at the interface, but the wave speeds do. It is invariably the displacement amplitude which has physical meaning and which is the key factor in determining, for example, the validity of the ray approximation or the effect of neighbouring interfaces; we shall use the displacement amplitudes throughout. Comparisons with other work are made in section 6.

4.3 Plane wave solutions for displacement

We now require expressions for the total displacement $(u_1,u_2,u_3) = \mathbf{u}(x_1,x_2,x_3)$ at any point $\mathbf{x}(x_1,x_2,x_3)$ in both media i and ii, and these can be defined by summing expressions for each wave motion as defined in figure 1. This will take account of the amplitudes and directions of each wave motion. For medium i ($x_3>0$) we have four wave motions—the incident P and S waves, and the reflected P and S waves. We have

$$\begin{aligned}
\mathbf{u}_{\mathrm{i}}(x_1,x_2,x_3) = {} & (A\sin a,\, 0,\, -A\cos a) \exp\left[\frac{i\omega}{U_{\mathrm{i}}}(x_1\sin a - x_3\cos a) - i\omega t\right] \\
& + (-B\cos b,\, G,\, -B\sin b) \exp\left[\frac{i\omega}{V_{\mathrm{i}}}(x_1\sin b - x_3\cos b) - i\omega t\right] \\
& + (C\sin a,\, 0,\, C\cos a) \exp\left[\frac{i\omega}{U_{\mathrm{i}}}(x_1\sin a + x_3\cos a) - i\omega t\right] \\
& + (D\cos b,\, H,\, -D\sin b) \exp\left[\frac{i\omega}{V_{\mathrm{i}}}(x_1\sin b + x_3\cos b) - i\omega t\right] .
\end{aligned} \tag{33}$$

For medium ii ($x_3<0$) we have only two wave motions—the refracted P and S waves:

$$\mathbf{u}_{ii}(x_1,x_2,x_3) = (E\sin e,\ 0,\ -E\cos e)\exp\left[\frac{i\omega}{U_{ii}}(x_1\sin e - x_3\cos e) - i\omega t\right]$$
$$+ (-F\cos f,\ I,\ -F\sin f)\exp\left[\frac{i\omega}{V_{ii}}(x_1\sin f - x_3\cos f) - i\omega t\right]. \qquad (34)$$

Thus each of equations (33) and (34) comprise three equations, one for each of the X_1, X_2, and X_3 Cartesian components of displacement.

We recall from the discussion in section 3.1 that each of the amplitudes A to I is specified complex to allow for possible phase differences between the waves, which may result from the application of boundary conditions. As already stated, these phase differences are non-trivial at super-critical angles of incidence. Normally either A, or both B and G are zero (depending upon whether we have incident P or S), and it is normally convenient to set the phase of the incident wave to zero, or perhaps π to simulate opposite polarity. Treatment of the arbitrarily polarised S wave is ensured by the specification of separate complex amplitudes for SV and SH, again as required for super-critical angles of incidence.

4.4 Boundary conditions for different cases

We now state the boundary conditions which must be satisfied and applied to equations (33) and (34) in order to determine the required relations between the wave motions at opposing sides of the interface. Each boundary condition to be satisfied relates one component of particle displacement or one of the components of stress (two tangential and one normal) on the two sides of the interface. Thus there are, in general, six conditions governing u_1, u_2, u_3, p_{31}, p_{32} and p_{33} which depend upon the types of media comprising layers i and ii, and the nature of the contact at the interface. Various cases are discussed by many authors, for example Ewing, Jardetsky and Press [16] pages 7 and 74 et seq, Officer [20] page 190 et seq, Jeffreys [17] pages 31 and 35, and Bullen and Bolt [18] page 140 et seq.

In fact only two types of medium need to be defined explicitly, and these are the solid, which can sustain both dilatational and shear stresses, and the fluid (i.e. either liquid or gas) which can sustain only dilatational stress (and hence cannot support S waves). It will be shown that all cases of practical interest can be treated using the four possible combinations of these two media types, whose boundary conditions are given below. It will further be shown that the fluid can be treated as a special case of the solid, enabling one matrix equation to describe all possible cases. Where fewer than six boundary conditions need to be fulfilled, this is associated with a corresponding reduction in the number of unknowns in equations (33) and (34), since certain of the waves will not exist for the reasons stated.

Medium i solid, Medium ii solid

If both media are solid they are assumed to be in welded contact. This means that all three components of displacement and all three components of stress are continuous across the boundary:

$$(u_1)_i = (u_1)_{ii} \qquad (u_2)_i = (u_2)_{ii} \qquad (u_3)_i = (u_3)_{ii} \qquad (35a\text{–}c)$$

$$(p_{31})_i = (p_{31})_{ii} \qquad (p_{32})_i = (p_{32})_{ii} \qquad (p_{33})_i = (p_{33})_{ii}\ . \qquad (35d\text{–}f)$$

Medium i solid, Medium ii fluid

If one of the media—say medium ii—is a fluid, the inability of a fluid to sustain shear means that both tangential components of shear stress in the solid must tend to zero at the boundary.

Further, slippage can now occur along the boundary, so that equations (35a) and (35b) are relaxed. The continuity of normal displacement and stress is, however, retained. We have

$$(u_3)_i = (u_3)_{ii} \tag{36c}$$

$$(p_{31})_i = 0 \qquad (p_{32})_i = 0 \qquad (p_{33})_i = (p_{33})_{ii} \,. \tag{36d–f}$$

Medium i fluid, Medium ii solid

If, instead, medium i is a fluid, then similar boundary conditions to equations (36) apply, with the media reversed:

$$(u_3)_i = (u_3)_{ii} \tag{37c}$$

$$(p_{31})_{ii} = 0 \qquad (p_{32})_{ii} = 0 \qquad (p_{33})_i = (p_{33})_{ii} \,. \tag{37d–f}$$

Medium i fluid, Medium ii fluid

If both layers are fluid, there is still the possibility of slippage along the boundary, so that no conditions can be placed upon u_1 or u_2. The knowledge that the two tangential components of stress are zero across the boundary provides no useful information, since shear motion can never be generated anywhere in either fluid. We have:

$$(u_3)_i = (u_3)_{ii} \tag{38c}$$

$$(p_{33})_i = (p_{33})_{ii} \,. \tag{38f}$$

The solid free surface

An interface is described as a free surface if medium ii is a vacuum. In this case no conditions can be placed upon the displacement of the solid at the boundary, but all three stress components must vanish there:

$$(p_{31})_i = 0 \qquad (p_{32})_i = 0 \qquad (p_{33})_i = 0 \,. \tag{39d–f}$$

The fluid free surface

If, instead, medium i is a fluid, then only equation (39f) is required; equations (39d) and (39e) contain no useful information because shear stresses are not present anywhere in the fluid. We have

$$(p_{33})_i = 0 \,. \tag{40f}$$

The solid rigid boundary

Another special case is the rigid boundary (Ewing, Jardetsky and Press [16] page 74), where all motion at the boundary is suppressed. If the medium is solid, this requires that all three components of displacement are zero. We have:

$$(u_1)_i = 0 \qquad (u_2)_i = 0 \qquad (u_3)_i = 0 \,. \tag{41a–c}$$

The fluid rigid boundary

If, instead, the medium is a fluid, then it is not possible to constrain $(u_1)_i$ or $(u_2)_i$, and only the normal component of displacement can be constrained to zero. Thus we have

$$(u_3)_i = 0 \qquad (42c)$$

The perfectly lubricated solid-solid interface

If two solid media are in contact at a perfectly lubricated interface, so that slippage can occur along the boundary, then the tangential components of shear in both media must tend to zero at the boundary. However, the requirement that the two media must remain in contact implies that continuity of normal displacement and stress are still required. We have

$$(u_3)_i = (u_3)_{ii} \qquad (43c)$$

$$(p_{31})_i = (p_{31})_{ii} = 0 \quad (p_{32})_i = (p_{32})_{ii} = 0 \quad (p_{33})_i = (p_{33})_{ii} \,. \qquad (43d\text{–}f)$$

This case is not considered further except in section 7.6.

4.5 The solid-solid interface as a general case

With a view to rationalising the code for programming the Zoeppritz equations, we introduce a unified procedure for computation rather than treating all cases separately, even though this may introduce some unnecessary calculations for the simplest cases (e.g. fluid-fluid boundary). It is now shown that all the cases discussed above, with the exception of the lubricated solid-solid interface, can be treated as special cases of the (welded) solid-solid interface. This can be seen most simply by inferring the required values of the Lamé coefficients λ and μ, and the density ρ, for each medium, and then using equations (12a) and (12b) to calculate the corresponding values required of their dependent variables which are used in the equations, namely the *P*- and *S*- wave speeds U and V respectively. Also of relevance is the incompressibility k, and the relative size of the compressional and shear moduli, which is normally expressed using Poisson's ratio σ. From equations (12a) and (12b), and the definitions of incompressibility and Poisson's ratio, we have respectively

$$U\sqrt{\rho} = \sqrt{(\lambda + 2\mu)}\,; \qquad V\sqrt{\rho} = \sqrt{\mu}\,; \qquad k = \lambda + \frac{2}{3}\mu\,; \qquad \sigma = \frac{\lambda}{2(\lambda+\mu)}\,. \qquad (44a\text{–}d)$$

A solid medium, by definition, can sustain both compression and shear. Thus we require $\lambda+(2/3)\mu>0$ and $\mu>0$. Also we require $\rho>0$. (Note that $\lambda>0$ is not explicitly required, although a negative λ implies that when an element of material is extended along one axis, it also extends along the other axes.) The above requirements will be satisfied if we have $U>0$, $V>0$ for both media, and this is the most general form. If the two Lamé parameters are equal, then $\sigma=0.25$, $U=\sqrt{3}V$ and the medium is referred to as a "Poisson solid". In any case it follows from equations (44a) and (44b) that we must have $U>V$.

A fluid medium, by definition, can sustain compression but not shear. Thus we require $\lambda>0$ and $\mu=0$. Again we must have $\rho>0$. These conditions will be satisfied if $U>0$, and from equation (44b) we require that $V=0$ as expected. Thus if medium i is a fluid, we set $V_i=0$, and if medium ii is a fluid we set $V_{ii}=0$. Both of these conditions are applied if two fluid media are in contact. We see from equation (44d) that any fluid, whether liquid or gas, has $\sigma=1/2$, since λ cancels whenever $\mu=0$. However, a liquid is hardly compressible, so that k (and hence λ) is very large, whereas a gas is highly compressible, with consequently much smaller values of k and μ. Nevertheless, gases have much lower densities than liquids, so from equation (44a) we conclude that these numerical contrasts compensate, and consequently the *P*-wave speeds of liquids and gases are of the same order.

For a solid or fluid free surface medium ii must be a void. This implies that medium ii has zero density, so we set $\rho_{ii}=0$. This is the only condition which is required to define a void for medium ii. From equations (84a) and (84d) we see that if Lamé's parameters and density all tend to zero, the wave speeds become indeterminate, not zero. For a void, the values of U_{ii} and V_{ii} have no effect on the results for medium i. We may set $V_{ii}=0$, in which case medium ii will behave as the limiting case of a

zero-density fluid, so that the transmitted S-wave displacement is zero. However, we shall see in section 4.7 that although the transmitted P-wave energy tends to zero as ρ_{ii} tends to zero, its displacement amplitude still has to satisfy the free surface continuity of displacement, so the calculated P-wave displacement in the void is in general non-zero, and depends upon the angle of the notional transmitted P-wave as determined by Snell's law according to the value assigned to U_{ii}. If we set $U_{ii}=0$, the angle e will always be zero, and the value calculated for E will be equal to the normal surface displacement (see section 4.10). Although these points are academic for a true free surface, the behaviour in medium ii as ρ_{ii} tends to zero is important when considering waves transmitted into the atmosphere at the Earth's free surface, for which ρ_{ii} is indeed non-zero, allowing atmospheric sound waves. This is discussed in section 5.5.

For a solid rigid boundary we require that any compression or shear results in no strain in the second medium. This means that medium ii must have infinite density, so that $\rho_{ii}=\infty$. We shall show in section 4.7 that the behaviour of medium i is then independent of the values of U_{ii} and V_{ii}, as in the case of the free surface.

For a fluid rigid boundary we again require $\rho_{ii}=\infty$, this time with $\mu=0$. A practical example which approximates to the fluid rigid boundary is when medium i is the Earth's atmosphere and medium ii the solid Earth. Then $\rho_{ii}>>\rho_i$, and for acoustic waves incident in the atmosphere the condition $\rho_{ii}=\infty$ is a good approximation—i.e. there is negligible coupling of acoustic waves from the atmosphere to the Earth.

It can be seen from the above that, while the free surface and the rigid boundary both have the characteristic that no energy is transmitted into medium ii, their different boundary conditions result in different reflection coefficients—they represent an infinitely rarefied, or an infinitely dense, medium ii respectively. Here we have contrived a rigid boundary by giving medium ii infinite inertia. This is not the same as giving medium ii infinite rigidity. From equations (44) infinite rigidity implies infinite wave speed, which is a different condition. We emphasise this point to avoid a possible confusion in our terminology.

The perfectly lubricated (or indeed a partially lubricated) solid-solid interface cannot be incorporated into this scheme as its boundary conditions are conflicting with those of the normal solid-solid interface. Continuity of the tangential components of displacement and stress must be relaxed, and this results in different relations from the general case considered here.

Finally we note that we must always have $0<\rho_i<\infty$, so that medium i can sustain the waves which may be incident in it.

4.6 Application of boundary conditions for the solid-solid interface

We now apply the six boundary conditions of displacement and stress given in equations (35a–f), to the equations for the total wavefields given in equations (33) and (34) for the two media respectively. We first apply the boundary conditions separately for each component of particle displacement, u_1, u_2 and u_3, equating equations (33) and (34) separately for the three displacement components. It is clear that equality of amplitudes and exponents both have to be satisfied; we consider first the amplitudes. For the u_1, u_2 and u_3 components respectively we obtain

$$A\sin a - B\cos b + C\sin a + D\cos b = E\sin e - F\cos f \tag{45}$$

$$G + H = I \tag{46}$$

$$-A\cos a - B\sin b + C\cos a - D\sin b = -E\cos e - F\sin f\,. \tag{47}$$

For the boundary conditions in stress we refer to equations (8a) and (8b), which give the stress components p_{ij} in terms of the spatial derivatives of the particle displacements. We are concerned

with the three components of stress across the interface, which correspond to i=3 with j=1, 2 and 3, which from equations (8a) and (8b) are

$$p_{31} = \mu\left(\frac{\partial u_1}{\partial x_3} + \frac{\partial u_3}{\partial x_1}\right) \tag{48a}$$

$$p_{32} = \mu\left(\frac{\partial u_2}{\partial x_3} + \frac{\partial u_3}{\partial x_2}\right) \tag{48b}$$

$$p_{33} = \lambda\left(\frac{\partial u_1}{\partial x_1} + \frac{\partial u_2}{\partial x_2} + \frac{\partial u_3}{\partial x_3}\right) + 2\mu\frac{\partial u_3}{\partial x_3}. \tag{48c}$$

Taking the appropriate derivatives of equations (33) and (34), substituting them into two expressions similar to equation (48a) for the two media, and equating them, we get for p_{31}

$$\begin{aligned}\mu_i\left\{\left[A\sin a.\left(\frac{-\cos a}{U_i}\right) - B\cos b\,.\left(\frac{-\cos b}{V_i}\right) + C\sin a\,.\left(\frac{\cos a}{U_i}\right) + D\cos b\,.\left(\frac{\cos b}{V_i}\right)\right]\right.\\ \left.+\left[-A\cos a\,.\left(\frac{\sin a}{U_i}\right) - B\sin b\,.\left(\frac{\sin b}{V_i}\right) + C\cos a\,.\left(\frac{\sin a}{U_i}\right) - D\sin b\,.\left(\frac{\sin b}{V_i}\right)\right]\right\}\\ = \mu_{ii}\left\{\left[E\sin e\,.\left(\frac{-\cos e}{U_{ii}}\right) - F\cos f\,.\left(\frac{-\cos f}{V_{ii}}\right)\right] + \left[-E\cos e\,.\left(\frac{\sin e}{U_{ii}}\right) - F\sin f\,.\left(\frac{\sin f}{U_{ii}}\right)\right]\right\}.\end{aligned} \tag{49}$$

Rearranging, we obtain

$$\begin{aligned}C\sin 2a + D\left(\frac{U_i}{V_i}\right)\cos 2b + E\left(\frac{V_{ii}}{V_i}\right)^2\left(\frac{U_i}{U_{ii}}\right)\left(\frac{\rho_{ii}}{\rho_i}\right)\sin 2e - F\left(\frac{V_{ii}}{V_i}\right)\left(\frac{U_i}{V_i}\right)\left(\frac{\rho_{ii}}{\rho_i}\right)\cos 2f\\ = A\sin 2a - B\left(\frac{U_i}{V_i}\right)\cos 2b\end{aligned} \tag{50}$$

where we have eliminated μ_i and μ_{ii} using equation (12b).

Similarly, by substituting the appropriate derivatives from equations (33) and (34) into equation (48b) for the two media, we obtain for p_{32},

$$\mu_i\left\{G\left(\frac{-\cos b}{V_i}\right) + H\left(\frac{\cos b}{V_i}\right)\right\} = \mu_{ii}\left\{I\left(\frac{-\cos f}{V_{ii}}\right)\right\} \tag{51}$$

which, rearranging, becomes

$$H\cos b + I\left(\frac{V_{ii}}{V_i}\right)\left(\frac{\rho_{ii}}{\rho_i}\right)\cos f = G\cos b\,. \tag{52}$$

For the normal component of stress p_{33} we utilise equation (48c) similarly and obtain

$$\lambda_i \left\{ A \frac{\sin^2 a}{U_i} - B \frac{\sin b \cos b}{V_i} + C \frac{\sin^2 a}{U_i} + D \frac{\sin b \cos b}{V_i} \right.$$

$$\left. + 0 + A \frac{\cos^2 a}{U_i} + B \frac{\sin b \cos b}{V_i} + C \frac{\cos^2 a}{U_i} - D \frac{\sin b \cos b}{V_i} \right\}$$

$$+ 2\mu_i \left\{ A \frac{\cos^2 a}{U_i} + B \frac{\sin b \cos b}{V_i} + C \frac{\cos^2 a}{U_i} - D \frac{\sin b \cos b}{V_i} \right\}$$

$$= \lambda_{ii} \left\{ E \frac{\sin^2 e}{U_{ii}} - F \frac{\sin f \cos f}{V_{ii}} + 0 + E \frac{\cos^2 e}{U_{ii}} + F \frac{\sin f \cos f}{V_{ii}} \right\} \tag{53}$$

$$+ 2\mu_{ii} \left\{ E \frac{\cos^2 e}{U_{ii}} + F \frac{\sin f \cos f}{V_{ii}} \right\}.$$

Rearranging, and eliminating the Lamé parameters using equations (12a) and (12b), we obtain

$$C\cos 2b - D\left(\frac{V_i}{U_i}\right)\sin 2b - E\left(\frac{U_{ii}}{U_i}\right)\left(\frac{\rho_{ii}}{\rho_i}\right)\cos 2f - F\left(\frac{V_{ii}}{U_i}\right)\left(\frac{\rho_{ii}}{\rho_i}\right)\sin 2f$$

$$= -A\cos 2b - B\left(\frac{V_i}{U_i}\right)\sin 2b \,. \tag{54}$$

Equations (45), (46), (47), (50), (52) and (54) result respectively from application of the six boundary conditions equations (35a–f) to the amplitudes of the wave motions of equations (33) and (34). This corresponds to satisfying the boundary conditions at a chosen instant at one point on the interface. We further require to satisfy the boundary conditions at all times at all points on the interface, and to do this the exponents in equations (33) and (34) also have to be equated. Examination of equations (33) and (34) reveals that, for the continuity of displacement to be satisfied at all points on the interface at all times, the horizontal slowness of all the waves must be identical. We have

$$\frac{\sin a}{U_i} = \frac{\sin b}{V_i} = \frac{\sin e}{U_{ii}} = \frac{\sin f}{V_{ii}} \,. \tag{55}$$

This is of course simply a generalised form of Snell's law, and provides the relations necessary to eliminate the angles (apart from the appropriate incident angle) from the simultaneous equations. (In section 3.1 we assumed the law of reflection to avoid unnecessary additional variables, in particular the angles of reflection c and d, but a similar argument could be used to prove these equations also.)

4.7 The Zoeppritz equations in matrix form

Equations (45), (46), (47), (50), (52) and (54) represent six simultaneous equations in the six (complex) unknowns C, D, E, F, H and I, which are the unknown displacement amplitudes, where the modulus of the complex value denotes the wave amplitude, and the argument its phase. We see that the equations derived from the boundary conditions in the X_2 direction are independent of the others and give two equations relating G to H and I, while the remaining equations can be used to solve for the remaining four unknowns. This separation corresponds to the well-known decoupling of SH partitioning at the interface from that of P and SV together.

We shall normally not be considering incident P and S together, in which case either A, or both B and G will be zero. Since P and S waves would approach the interface at different speeds, it is usually inappropriate to combine the effects of both P and S incident waves. We might, however, have an incident S wave which is polarised in a direction neither parallel to nor perpendicular to the interface, or indeed an incident S wave which is elliptically polarised (see section 3.2). In all cases the S wave is

resolved into its SV and SH components B and G respectively. The separate P-SV and SH sets of equations are then solved, and the resulting components recombined for the reflected and refracted waves in order to find the resulting polarisation directions, which will in general be different.

The angles a, b, d and f also appear in the six equations, and we use equation (55) to calculate the unknown angles d and f from the known angle (a or b for incident P or S waves respectively).

We can express the two systems of simultaneous equations most conveniently as matrix equations, and they can be solved in this way by computer. From equations (45), (47), (50) and (54) we obtain, for incident P or SV (by setting either B=0 or A=0 respectively):

$$\begin{pmatrix} \sin a & \cos b & -\sin e & \cos f \\ \cos a & -\sin b & \cos e & \sin f \\ \sin 2a & \left(\frac{U_i}{V_i}\right)\cos 2b & \left(\frac{V_{ii}}{V_i}\right)^2\left(\frac{U_i}{U_{ii}}\right)\left(\frac{\rho_{ii}}{\rho_i}\right)\sin 2e & -\left(\frac{V_{ii}}{V_i}\right)^2\left(\frac{U_i}{V_{ii}}\right)\left(\frac{\rho_{ii}}{\rho_i}\right)\cos 2f \\ -\cos 2b & \left(\frac{V_i}{U_i}\right)\sin 2b & \left(\frac{U_{ii}}{U_i}\right)\left(\frac{\rho_{ii}}{\rho_i}\right)\cos 2f & \left(\frac{V_{ii}}{U_i}\right)\left(\frac{\rho_{ii}}{\rho_i}\right)\sin 2f \end{pmatrix}\begin{pmatrix} C \\ D \\ E \\ F \end{pmatrix}$$

$$= A\begin{pmatrix} -\sin a \\ \cos a \\ \sin 2a \\ \cos 2b \end{pmatrix} + B\begin{pmatrix} \cos b \\ \sin b \\ -\left(\frac{U_i}{V_i}\right)\cos 2b \\ \left(\frac{V_i}{U_i}\right)\sin 2b \end{pmatrix} \qquad (56a)$$

and from equations (46) and (52), for incident SH we obtain

$$\begin{pmatrix} 1 & -1 \\ \cos b & \left(\frac{V_{ii}}{V_i}\right)\left(\frac{\rho_{ii}}{\rho_i}\right)\cos f \end{pmatrix}\begin{pmatrix} H \\ I \end{pmatrix} = G\begin{pmatrix} -1 \\ \cos b \end{pmatrix}. \qquad (56b)$$

In the computational procedure we must be certain to avoid zero divides when densities or wave-speeds are set to zero. We must also remove any common factors in rows of the matrices which may remain if some elements become zero, otherwise equations will be lost and the problem will become under-determined. We recall from section 4.5 that each or all of the quantities V_i, U_{ii} V_{ii} and ρ_{ii} may be zero under certain circumstances, and that ρ_{ii} will tend to infinity in the case of a rigid boundary. U_i and ρ_i cannot be zero since the minimum requirement is that medium i—as the incident medium—must support P waves. We first ensure that V_i, U_{ii}, V_{ii} and ρ_{ii} do not appear in the denominator of any term in equations (56a) or (56b). This requires reformulation of the third row of the matrix equation (56a), to obtain

$$C\ V_i^2 U_{ii}\ \sin 2a + D\ U_i V_i U_{ii} \cos 2b + E\ U_i V_{ii}^2 \left(\frac{\rho_{ii}}{\rho_i}\right) \sin 2e - F\ U_i U_{ii} V_{ii} \left(\frac{\rho_{ii}}{\rho_i}\right) \cos 2f$$

$$= A\ V_i^2 U_{ii} \sin 2a - B\ U_i V_i U_{ii} \cos 2b\ . \tag{57}$$

It is not necessary to change row 2 of equation (56b) since *SH* waves cannot be incident in medium i if it is a fluid (i.e. if V_i=0).

Equation (57) will be in a suitable form if either or both media are solid or fluid, except in some special cases, which are now considered with reference to section 4.5. For a solid or fluid free surface the third and fourth terms in equation (57) become zero since ρ_{ii}=0; the same happens to terms (4,3) and (4,4) of equation (56a). There is then a common factor of $V_i U_{ii}$ in equation (57) which must be removed before computation, to avoid the third row of equation (56) becoming null if either of V_i or U_{ii} is zero. Once this is done, we see that matrix equations (56) are no longer dependent upon the values of U_{ii} or V_{ii}, which is what we expect from section 4.5 in the case of a free surface (ρ_{ii}=0). The angles of refraction e and f still enter the first and second rows of equation (56a), and these are obtained from Snell's law, equation (55), which does require values for U_{ii} and V_{ii}. Although the values of U_{ii} and V_{ii} do not affect the behaviour in medium i if ρ_{ii}=0, they determine the angles e and f of the refracted rays from which amplitudes E and F are computed to satisfy the boundary conditions at the interface. Thus for a free surface it is sensible (though not necessary) to set U_{ii}=V_{ii}=0. In this case the transmitted S wave will have zero amplitude by analogy with a fluid, so F will be zero. The transmitted P wave will be at normal incidence for all incident angles (e=0), so its displacement amplitude E will equal the normal surface displacement (see section 4.10) since this is continuous across the interface. We reset E=0 after computation.

The above discussion illustrates the fact that the free-surface displacement boundary condition requires that the refracted amplitudes do not in general tend to zero as the density in medium ii tends to zero. This is discussed in connection with the Earth's surface in section 5.5.

For a rigid boundary (section 4.5) ρ_{ii}=∞. For the *P-SV* system we must then divide equation (57) and the fourth row of equation (56a) through by ρ_{ii}, and elements (3,1), (3,2), (3,5), (3,6), (4,1), (4,2), (4,5) and (4,6) all become zero. A common factor of V_{ii} must then be removed from row 3 (equation (57)). A common factor of U_i also appears in both rows 3 and 4, but this can remain as U_i can never become zero. In the resulting matrix equation rows 3 and 4 can only be satisfied if E=F=0, which means that there is zero displacement amplitude for refracted P and SV. This is expected; if these amplitudes were not zero, then infinite energy would be transmitted into medium ii because of its infinite density (see section 4.9).

For *SH* incident at a rigid boundary, we divide the second row of equation (56b) by ρ_{ii}, and retain one non-zero term, giving I=0 (unless f=π/2). This corresponds to zero displacement for refracted *SH* as expected. The first row then gives G=–H, which is also expected since there can be no resultant horizontal displacement at the rigid boundary.

We make no special provision in the computer program for the rigid boundary; this would require a rigid-boundary flag to be specified. It is not possible to test for a rigid boundary in the input data simply on the basis of large ρ_{ii}/ρ_i, since a genuine solid/gas interface also has a large density ratio, but is not rigid because of the compensating large ratio of the two Lamé parameters λ_i and λ_{ii} (see section 4.5).

In some of the above cases, one or more of the leading diagonal terms of the matrices in equations (56) become zero, so the method used to solve the matrix equations must be able to pivot the matrix to compute its roots.

4.8 A note on super-critical angles of incidence

Depending upon the values of U_i, U_{ii}, V_i and V_{ii} we may find that one or more of the sine terms in equation (55) becomes greater than 1.0, and it is straightforward to show that the associated angle then becomes complex. The sine of a complex angle may be expressed in terms of its real and imaginary parts as

$$\sin(x + iy) = \sin x \cosh y + i \cos x \sinh y \,. \tag{58}$$

From equation (55) we see that the sine of the resulting angle remains real (but with an absolute value greater than unity) when super-critical. It follows from equation (58) that $\cos x \sinh y$ must be zero, which requires either $y=0$ or $x=\pi/2$. Clearly the former condition indicates a real angle, so we must have $x=\pi/2$. The angle is therefore complex, with the real part equal to $\pi/2$. Moreover, since $\sin(\pi/2)=1.0$, it follows that the imaginary part is equal to the arccosh of the sine value.

As already pointed out, this complex angle gives rise to non-propagating (evanescent) waves at the interface. This also results in non-trivial phase changes for the remaining propagating waves. Our complex implementation of the computer program allows for this possibility, by specifying the angles a to f and the amplitudes A to I to be complex. From the general form of the exponent in equation (33), it can be seen that when the resulting angle ceases to be real, the spatial term in the exponent has a real part, so that there is a non-propagating wave confined to the vicinity of the boundary, which decays exponentially with distance away from it. For the infinite plane waves we are considering, an evanescent wave effectively propagates along the boundary as it has the same slowness as the other waves, but since it does not propagate away from the boundary it does not contribute to the energy budget in section 4.9. We shall show the amplitude and phase of the evanescent waves in the results which follow, but their particle motions will not be discussed in detail except to calculate the motion at the free surface in sections 4.10 and 5.7.

4.9 Energy equations

It follows from the energy equations originally formulated by Knott [5], that the contribution of each wave to the energy flux across the interface is proportional to the density, to the square of the displacement amplitude and to the wave speed, and is inversely proportional to the tangent of the incident or resulting angle (see for example Costain, Cook and Algermissen [21]). The energy budget at the interface can therefore be expressed as

$$\frac{\rho_i U_i^2 A^2}{\tan a} + \frac{\rho_i V_i^2 B^2}{\tan b} = \frac{\rho_i U_i^2 C^2}{\tan a} + \frac{\rho_i V_i^2 D^2}{\tan b} + \frac{\rho_{ii} U_{ii}^2 E^2}{\tan e} + \frac{\rho_{ii} U_{ii}^2 F^2}{\tan f} \,; \tag{59a}$$

$$\frac{\rho_i V_i^2 G^2}{\tan b} = \frac{\rho_i V_i^2 H^2}{\tan b} + \frac{\rho_{ii} V_{ii}^2 I^2}{\tan f} \,, \quad a, b, e, f \neq 0 \,. \tag{59b}$$

These equations do not hold for normal incidence, for which $a=b=e=f=0$; the tangents then cancel and can be omitted. If any of a, b, d, f are complex, the corresponding terms are omitted; for complex incident or resulting angles (evanescent waves) there is no contribution to the energy density. Although evanescent waves can transport energy along the boundary, they cannot transport energy away from it.

In the case of P and SV waves, either A or B will normally be zero. For incident, reflected or refracted waves approaching glancing angle ($\pi/2$) the denominator becomes infinite, so the contribution to the energy budget approaches zero. This is because no energy can approach or emerge from the interface along travelling rays which are parallel to it. It follows that at glancing incidence the amplitude may become infinite without violating energy conservation. In particular, we shall see in section 5 that the amplitude of a reflected or refracted ray may become infinite as the corresponding critical angle of incidence is reached.

It is also clear from equations (59) that one or more of the reflected or refracted wave amplitudes may be greater than that of the incident wave without violating energy conservation. In general, amplitudes become higher in media with lower density and wave-speeds, because the energy density corresponding to unit displacement amplitude is then lower, and because the energy is transported more slowly across the interface. Also, higher amplitudes may occur at larger angles because the width of the ray packet associated with unit length of interface is then narrower (the case of glancing angle discussed above is an extreme case of this). These points provide some physical insight to the form of equations (59).

The difference between displacement amplitude partitioning at an interface (described by the Zoeppritz equations) and energy partitioning becomes especially important when one medium is a gas, so that there is a large density contrast. The energy in the gaseous medium will then usually be negligible for practical purposes compared with that in the solid or liquid medium. However, the amplitudes will, in general, still be comparable in the two media. This paradoxical behaviour is considered in section 5.5 in connection with the Earth's free surface.

The principle of energy conservation expressed in equations (59) provides a convenient means of checking any computational scheme for determining reflected and refracted amplitudes. Such a check was one method used to verify the computer program described here.

4.10 Motion at the free surface

A seismometer at the Earth's surface records not the incident wave but the vector sum of the particle motions associated with the incident wave and the resulting reflected waves (and evanescent waves if they exist). This gives rise to important differences between the particle motions we observe and those of the incident wave. In the simple case of the normally-incident P wave, the addition of the reflected P wave of opposite polarity gives rise to a surface amplitude double that of the incident wave. In general the scaling is not the same for the horizontal and vertical components, so that the particle motion directions at the surface are also different from that of the incident wave. This gives rise to the concept of "apparent angle of emergence" (see e.g. Bullen and Bolt [18] page 189) and affects the ratio of observed amplitudes on a three-component set of seismometers.

It is possible to solve equations (56a, b) for the special case of the free surface, and hence to find expressions for the vertical and horizontal displacement components associated with an incident P wave or SV wave, and the horizontal amplitude of an SH wave. However, these equations are complicated and it is more convenient to create expressions for the surface displacements in terms of the incident and resulting wave amplitudes A to I, and the incident angles a and b, and to substitute the results from the Zoeppritz calculations to compute the surface motion.

Referring to figure 1, and assuming that we may have incident P, SV, and SH incident waves, the three components of surface displacement u_1, u_2 and u_3 are given by

$$u_1 = A\sin a - B\cos b + C\sin a + D\cos b$$

$$u_2 = G + H \qquad (60a,b,c)$$

$$u_3 = -A\cos a - B\sin b + C\cos a - D\sin b\ .$$

Here u_1 is the horizontal component in the ray plane, u_2 is the horizontal component associated with SH particle motion, and u_3 is the vertical component (figure 1). It is convenient to determine the ratio r of the surface amplitude to the incident amplitude for each component for each incident wave type. For the incident P wave we have

$$r_{1P} = \frac{A\sin a + C\sin a + D\cos b}{A\sin a}$$

$$r_{2P} = 0 \qquad (61a,b,c)$$

$$r_{3P} = \frac{A\cos a - C\cos a + D\sin b}{A\cos a}$$

and for the incident *SV* wave we have

$$r_{1SV} = \frac{-B\cos b + C\sin a + D\cos b}{-B\cos b}$$

$$r_{2SV} = 0 \qquad (62a,b,c)$$

$$r_{3SV} = \frac{B\sin b - C\cos a + D\sin b}{B\sin b}.$$

The result for the incident *SH* wave is trivial:

$$r_{1SH} = 0$$

$$r_{2SH} = \frac{G+H}{G} \qquad (63a,b,c)$$

$$r_{3SH} = 0\,.$$

Because $G=H$ for all angles of incidence at the free surface, r_{2SH} is always 2.0.

We recall from section 3.1 that each of A to I are complex, to allow for phase differences between the waves. Thus complex algebra is required to compute the ratios r_{1P} etc., and each ratio has an amplitude and a phase. We must also remember that a, b, d and f were defined complex in section 3.1, to allow for the complex angles of incidence for evanescent waves. This is essential in order to obtain the correct displacement values at super-critical angles. As in the case of the reflection and refraction coefficients, the ratio is real with a phase of either 0 or π unless any of the waves are super-critical. We shall present numerical results in section 5.7.

As pointed out in section 4.5, the replacement of the void in the second medium with a medium of very low density (i.e. a gas) has no significant effect on displacements at the interface. It follows from continuity of displacement that the displacement amplitudes in the gaseous medium must be similar to those in medium i; they do not tend to zero as ρ_{ii} tends to zero. This behaviour is implicit in the Zoeppritz equations but is stated explicitly as it is easily overlooked. It is of practical importance when the Earth's surface is considered in section 5.5.

5. EXAMPLES, INCLUDING IMPORTANT INTERFACES IN THE EARTH

5.1 Introduction to graphic display and cases

We now present a range of examples to show the partitioning of displacement amplitude for *P* and *S* waves incident at a wide range of interfaces. For each case we show the complete range of real incident angles a or b from 0° (normal incidence) to $\pi/2$ (glancing incidence), and we present the results graphically. The program can produce tables of results for a succession of incident angles (see Appendix A), but the graphical display used here is not included as part of the program. For each case three graphs are presented, each with incident angle (of either of *P* or *S*) along the abscissa. The top graph shows the resulting angle of each reflected and refracted wave, the middle graph shows their displacement amplitudes and the bottom one their phase. The amplitude and phase values shown

depend upon the amplitude and phase of the incident wave, which is also shown. Normally, for a single interface the amplitude would be set to (say) 1.0 with a phase of zero for all incident angles. If results were to be shown for an intermediate interface in a succession of interfaces, then the incident wave amplitude and phase may take any values, with dependence upon incident angle.

It follows that each graph giving results for either incident *P* or *SV* may be an overlay of up to six curves, corresponding to each of the incident, reflected and refracted waves. For incident *SH* there will in general be an overlay of three curves. For an intermediately-polarised *S* wave there would be an overlay of up to eight curves (all except incident *P*). Each curve is identified by its corresponding amplitude identifier *A* to *I* (see figure 1). In the top graph (resulting angles) the real part of the angles *a*, *b*, *a*, *b*, *e*, and *f* is plotted as appropriate for incident *P* and *S*, reflected *P* and *S*, and refracted *P* and *S* respectively; (each angle is real unless the wave is evanescent, in which case the angle is not shown). In the middle graph the moduli of complex amplitudes *A* to *I* are plotted as appropriate, and the bottom graph shows the arguments of these amplitudes (i.e. the relative phase of each signal). This follows the convention established in section 3.1 (figure 1). (In section 3.1 we have defined the phase in $[0,2\pi]$, but in the graphs we show the phase in $[-\pi,\pi]$; this difference is unimportant.) Although we have defined phase over a range of 2π with amplitude (modulus) always positive, in what follows the terms "polarity change" and "π phase change" are used interchangeably.

For each curve, values are computed at intervals of 0.5° in incident angle, and the results are interpolated linearly to show a continuous curve on the graphs. This gives an adequate resolution to show the important features of each plot, but in a few cases minor artefacts occur. Examples are when the amplitude approaches a singularity (at a critical angle), or zero (where there is a discontinuity in gradient as the phase changes by π). If such a point is not sampled exactly, then the linear interpolation "misses" the extreme value. This results in short line segments with anomalous gradient in a few cases which are readily identifiable. Also on the bottom graph, the phase returns to zero at normal or glancing incidence if the amplitude becomes zero; again this has no significance since phase is undefined at zero amplitude.

It should be remembered that if we were showing graphs for a series of interfaces during the passage of the ray, the incident angles sampled at any intermediate interface (and its corresponding graphs) would not be equally spaced and would not in general cover the complete range of angles unless the wave speed were the same as that in the first medium of the sequence. We emphasise that the graphs are plotted against the angle of incidence of the wave chosen, rather than against horizontal slowness (i.e. ray parameter). This means that the range of slownesses plotted is different for incident *P* and *S* waves, because in each case we plot against angle of incidence from 0° to 90°. This is important to note when comparing graphs for incident *P* and *S* waves, or graphs of rays passing in opposite directions through the same interface.

It is not normally appropriate to consider incident *P* and *S* waves together; their wave speeds are in any case different in each medium so in practice this would only be sensible for continuous stationary waves. Hence normally either *A*, or both *B* and *G* will be non-existent, i.e. zero. In the case of an *S* wave plane-polarised either in the plane perpendicular to or parallel to the interface (*SV* or *SH* respectively) *G* or *B* will also be zero respectively. If the wave is polarised in any other direction, or is elliptically polarised, then both *B* and *G* will be non-zero. We do not present such cases here. Since the *SH* system of waves behaves independently of the *P-SV* system of waves, appropriate proportions of incident *SV* and *SH* can always be added to simulate any polarisation, and the resulting amplitudes and phases resolved to obtain the resulting polarisations.

Certain waves which do not exist are omitted from the graphs. These are any incident waves which are set to zero, the nonexistent *SV* and *SH* waves in a fluid medium, and resulting waves which cannot exist because the appropriate incident wave is zero (e.g. resulting *SH* waves when incident *SH* is zero). Waves which are evanescent for a range of incident angles are shown with a dotted line on the plots to emphasise that they are not propagating waves. They do not appear on the top graph since only real angles are shown there, but their amplitude and phase appear on the middle and bottom

graphs respectively. However, the curves do not fully describe evanescent waves because their spatial dependence with distance is not shown.

In all cases the numerical values of wave speeds and density in each layer are shown on the plots, and an incident wave displacement amplitude of 1.0 and a phase of 0° are specified for all angles of incidence. It should be remembered that there is no significant relationship between the resulting amplitudes from an incident *P* wave and an incident *S* wave of the same amplitude—these incident waves do not, of course, have the same energy and if comparison of wave energies is required then equations (59a) and (59b) must be used.

The relationship between the incident and resulting angles (and hence the values of critical angles) is determined only by the ratio of wave speeds across the interface through Snell's law (equation 55). The size of these ratios (in particular whether they are greater or less than 1.0) is therefore crucial to the behaviour. The ratio of the amplitudes of each wave is determined also by the density, and it is therefore useful to say that the amplitude depends upon the "impedance", which is the product of density and wave speed.

We attempt to show all classes of behaviour for different types of media and incident wave. Where possible we use the important interfaces of the Earth, as examples of the application of the program to known real situations of relevance to global seismology. We emphasise, however that the results are quite general, within the assumptions made in section 2, and so are equally applicable to reflectors and refractors encountered in exploration seismology. Additional cases are included to show special features of behaviour which are not represented by the major interfaces of the Earth. We consider the solid-solid interface, followed by the solid-fluid interface, then the fluid-fluid interface and finally the solid free surface and the fluid free surface. We show waves incident in both the higher wave-speed and the lower wave-speed medium. Higher wave speed usually implies higher impedance, but higher wave speed may be associated with lower density and such cases are also considered. For the solid-fluid interface we show waves incident in both the solid and the fluid. The fluid normally has the lower impedance but this does not have to be the case, and the higher wave-speed fluid is also considered.

Table 1 gives a list of the cases considered, together with the relevant figure numbers. The figures and discussion consider one pair of media at a time, while the table gives examples in an order determined only by the parameters of the media, making it useful for reference.

For each case we present one set of graphs showing the behaviour of the incident *P* wave; in the case of waves incident in a solid this is followed by two further sets of graphs for the incident *SV* wave and the incident *SH* wave. We recall that there is nothing special about *SV* or *SH*, since an *S* wave may have any plane or elliptical polarisation. Although we do not show such examples, the consequences of reflection and refraction of shear waves of intermediate and elliptical polarisation are implicit in our formulation.

It is possible for an evanescent wave which results from super-critical incidence at one interface to be "incident" on a second interface, and for this to result in propagating waves; this might occur if we consider passage of a ray through a series of interfaces. However, the amplitude of any propagating waves which result in these circumstances depends upon the separation of the interfaces, since the evanescent wave decays in amplitude away from the first interface (section 4.8). We do not consider such cases here, though they can become important in the case of multiple media with different wave speeds, as met in seismic reflection sections. It would be straightforward to extend the program to treat them if the separation between interfaces were specified as input, although in real situations it is likely that other assumptions in section 2 would be violated in such circumstances.

We shall describe the first solid-solid case, exemplified by the Mohorovičić (Moho) discontinuity, in particular detail to highlight those features of the graphs which are common to many or all of the succeeding cases. We shall also discuss the sea bed in more detail as the first example of

the solid-fluid interface. The sections on these two interfaces should therefore be consulted when referring to other sections.

5.2 The solid-solid interface

5.2.1 The Mohorovičić (Moho) discontinuity

5.2.1.1 Introduction

The wave-speed and density contrast between the lower crust and upper mantle varies widely throughout the Earth. Here we consider "classical" values for the continental Moho. We specify U=6.5 km/sec and ρ=2.9 g/cc above the interface and U= 8.1 km/sec, ρ=3.3 g/cc below. These wave speeds are taken from Mueller and Landisman [22]) and the density contrast from Woollard [23]. In both cases V is derived assuming a Poisson solid (i.e. $\lambda=\mu$ or $U=\sqrt{3}V$; see equations (44)). Similar values would be reasonable for the Moho beneath oceanic crust (see for example Ewing [24]).

5.2.1.2 *P* incident from above (figure 2)

Figure 2 shows results for a P wave incident from above (that is, in the low wave-speed medium). At normal incidence the reflected and refracted S waves have zero amplitude. It is not possible for conversion between P and S waves to take place at normal incidence since the particle motions of the incident and resulting waves are in that case orthogonal. (We refer to a conversion from P to S or S to P as a "mode conversion".) It follows that the fractional change in the amplitude of a mode-converted wave as we move away from normal incidence changes very rapidly, since it is increasing from zero. Thus if we can measure such a wave, its amplitude is much more indicative of the wave-speed and density contrast than that of a reflection or refraction which is not a mode conversion. Alternatively, if we know the wave-speed and density contrasts, then the amplitude is very indicative of the angle; an example of this is the phase sP (see section 5.5).

At normal incidence the amplitude is partitioned between the reflected and refracted P waves in a ratio which depends upon the impedance contrast; we expect more to be reflected for a higher contrast. In this case the reflected P is about one fifth of the amplitude of the incident wave.

We see that at normal incidence the incident, reflected and refracted P waves are all of the same polarity; in particular, there is not a polarity reversal upon reflection when the wave is incident in the lower wave-speed medium. We see that the refracted SV wave has the opposite polarity to that of the reflected SV wave. This means that, for the positive incident P wave, the reflected and refracted SV waves are both polarised away from the interface (figure 1). Of course, there is no reflected SH since this cannot be generated from incident P.

As the angle of incidence is increased the refracted P wave remains the dominant wave; indeed its amplitude increases until at 45° incident angle it becomes of higher amplitude than the incident wave. (This does not violate energy conservation because energy flux depends also on the moduli and density—section 4.9.) At about 52° incident angle the amplitude of the reflected SV wave passes through zero and its polarity changes; this means that its polarisation is now towards the interface when the incident P wave is positive (figure 1). The amplitude of the reflected P wave varies little over near-normal angles of incidence. This is an important principle in the stacking of different offset traces in common-depth-point processing of seismic reflection data. Nevertheless, amplitude-versus-offset (AVO) analysis of pre-stack reflection data depends upon the observation of such differences in the presence of favourable wave-speed contrasts (section 8).

There are many circumstances in which a resulting wave changes polarity upon passing through zero amplitude as the angle of incidence is changed. The angle at which this occurs can be an important diagnostic of the wave-speed contrast across the interface, and in seismic reflection surveying

it is sensible to avoid stacking offset ranges which contain signals of opposite polarity. These issues are discussed by Levin [25].

The amplitude of the refracted *P* wave continues to increase until at about 54° incident angle the critical angle is reached and the refracted *P* wave emerges at 90° (along the interface). This corresponds to the angle at which a Moho-refracted head wave would leave the Moho. The refracted *P*-wave amplitude becomes infinite but this does not violate energy conservation for the reasons given in section 4.9. Beyond the critical angle the refracted *P* wave becomes evanescent, and we see non-trivial phase changes for the remaining propagating waves as expected (section 4.8). Beyond the critical angle for the refracted *P* wave, the amplitude of the reflected *P* wave is high, and approaches that of the incident wave. This corresponds to the high-amplitude "wide-angle reflections" often recorded on seismic refraction lines from interfaces at the top of a higher wave-speed medium. Less easy to detect is the change of phase with reflection angle, which is predicted in figure 2 for the super-critical range.

As the angle of incidence approaches 90° the *S* waves drop to zero amplitude as does the evanescent wave, and the incident wave is simply converted to a reflected *P* wave of equal amplitude; this corresponds to a wave travelling horizontally in the first medium, with the interface having minimal effect. At glancing angle of incidence, as for normal incidence, mode conversion is not possible because the *P* and *S* waves have only orthogonal components when resolved normal to and parallel to the interface.

The resulting angle of refracted *P* changes rapidly as the critical angle of incidence is approached. By contrast, the reflected and refracted *SV*, which do not become critical, have resulting angles which change less rapidly as glancing incidence is approached. This behaviour applies generally; the angle of reflection or refraction changes rapidly as a function of incident angle as the respective critical angle of incidence is approached, while the rate of change of the reflection or refraction angles of all other waves with respect to incident angle tends to zero as glancing incidence is approached.

The qualitative form of these graphs would remain similar if the wave-speed and/or density contrasts were changed, but the numerical values of the key amplitudes and angles would change. This is generally the case; if there is significantly different behaviour an additional case will be presented (see for example section 5.2.2).

5.2.1.3 *SV* incident from above (figure 3)

Figure 3 shows results for an *S* wave polarised in the ray plane (*SV*), incident from above on the Moho; this yields very different results from the *P* wave. The form of the graphs is generally more complicated because there are generally more critical angles for an incident *S* wave than for a *P* wave. This results from the fact that *S* waves travel slower than *P* waves.

At normal incidence the *P* waves have zero amplitude because mode conversion is not possible. As in the case of the *P* wave, most of the energy is refracted because the impedance contrast across the interface is not large. We see that all three *SV* waves have the same polarity (i.e. the same phase) and reference to figure 1 shows that the incident and reflected *SV* waves have opposing particle motion directions, and that the refracted *SV* polarisation is similar to that of the incident *SV*.

At about 23° incident angle the reflected *SV* passes through zero amplitude with a change of polarity (π change in phase). At about 27° incident angle the same happens to the reflected *P* wave, though the amplitude of the refracted *SV* wave still dominates. At 28° incident angle refracted *P* is critical, though this hardly affects the amplitude or the phase of refracted *SV*. At about 35° incident angle reflected *P* becomes critical, again without significant effect on refracted *SV*. At about 54° refracted *SV* becomes critical. We see that the approach of this third critical angle has associated with it a strong increase in refracted *SV* amplitude (it exceeds that of incident *SV* beyond about 47° incident

angle). This is by contrast with the first two (*P*-wave) critical angles, which do not have an infinite singularity.

Beyond the third critical angle all the resulting waves are evanescent except for the reflected *S* wave. Thus all the incident energy must pass to reflected *S*. Since the law of reflection requires these two waves to have the same angle, their wavefronts must have the same energy density, so conservation of energy requires that they have the same amplitude, which we observe on the graphs. This is somewhat analogous to "total internal reflection" in optics. In the seismic case (solid-solid interface) it can only happen for an incident *S* wave because an incident *P* wave can never have a critical angle for reflected *S*.

At glancing incidence, when the evanescent wave disappears, the incident and reflected *S* waves are seen to have opposite polarity. Reference to figure 1 reveals that the particle motion is in the opposite direction for the glancing incident and reflected *S* waves.

The order in which the three critical angles occur depends upon the wave-speed ratios, so that there can be a much larger range of behaviour as a function of incident angle than is typical for *P* waves. This highlights the importance of having the ability to run cases with any chosen parameter values.

5.2.1.4 *SH* incident from above (figure 4)

Figure 4 shows results from an incident *S* wave as above, but polarised parallel to the interface (*SH*). As for all cases of *SH* the behaviour is relatively simple. Only the three *SH* waves exist. At normal incidence we see that the same percentage of *SH* is refracted as for the *SV* wave in figure 3. This has to be so, because *SV* and *SH* are indistinguishable at normal incidence as they both have particle motions parallel to the interface. Away from normal incidence the percentage is different because some of the *SV* (but none of the *SH*) may be converted to *P*.

At normal incidence the reflected *SH* has opposite polarity to incident *SH*, and the refracted *SH* has the same polarity. Reference to figure 1 shows that this implies that the incident and reflected particle motions oppose, and that of refracted *SH* is the same as incident *SH*. This is similar behaviour to that observed for *SV* above. (In the case of a normally-incident SV wave, the convention of figure 1 requires the reflected SV to have the same polarity if the incident and reflected particle motions to add destructively, whereas for SH waves destructive interference is achieved if the normal and reflected particle displacements have opposite polarity; this is a consequence only of our choice of sign convention.)

At 43° incident angle the reflected *SH* passes through zero amplitude and changes polarity, and the amplitude of refracted *SH* then exceeds that of incident *SH*. This is not a significant angle in *SV*, but for *SH* it is important. At this angle (whose numerical value depends upon the wave-speed ratio) there is no partitioning of energy; the only effect on the travelling *SH* wave is a change in its direction of propagation.

The critical angle for refracted *SH* is reached at 54°, which must be the same as for *SV* since this angle depends only upon the wave-speed ratios. As for *SV*, beyond this angle there is total internal reflection and the incident and reflected *SH* have the same amplitude. At glancing incidence the phase of reflected *SH* is π different from that of incident *SH*. Reference to figure 1 shows that the particle motion directions of these two waves are opposed at the interface; this is the same behaviour as observed for *SV* in figure 3.

5.2.1.5 *P* incident from below (figure 5)

We next consider waves incident in the high wave-speed medium; that is, incident on the Moho from below. Figure 5 shows an incident *P* wave for this situation. A *P* wave incident in the

higher wave-speed medium has the highest wave speed of all four wave speeds. Therefore there can be no critical angles and the behaviour is simpler than for the *P* wave incident from the lower wave-speed medium. At normal incidence we see that no *S* waves are generated (as expected), and that most of the incident *P* wave is transmitted, as it is when the *P* wave is incident in the lower wave-speed medium (figure 2); this depends upon the impedance contrast. The amplitude of the refracted *P* wave is higher than that of the incident wave. (This does not contravene conservation of energy because the energy corresponding to a given amplitude is lower in a lower impedance medium—see section 4.9.) We also see that the reflected *P* wave undergoes a π phase change (i.e. its polarity is opposite to that of the incident wave). Reference to the sign convention in figure 1 confirms that this means a positive incident *P* wave generates a negative reflected *P* wave. This is a difference from the behaviour in figure 2, where there is no polarity change. It is generally true that a near-normally incident *P* wave reflects with opposite polarity off a lower wave-speed medium; light behaves similarly. In seismology an important case is the phase *pP* reflected from the Earth's surface (see section 5.5).

As the angle of incidence increases there is little change in the resulting *P* amplitudes until about 60°, when there is rapid change up to glancing incidence, when all resulting energy must be in the reflected *P* wave. As previously pointed out, the fractional change in resulting *SV* amplitudes near normal incidence is large because they are zero at normal incidence; this means that the resulting *S* waves are much more indicative of incident angle than the *P* waves are. For this case, there are no changes in polarity of any resulting waves from normal incidence to glancing incidence.

In section 5.2.1.2 the existence of high-amplitude wide-angle *P*-wave reflections was pointed out. By contrast with figure 2, figure 5 shows that there is no high-amplitude wide-angle reflection if the incident medium has the higher wave speed. This means that such reflections are not observed when there is a "wave-speed inversion", where the wave-speed is decreasing with depth.

5.2.1.6 *SV* incident from below (figure 6)

Figure 6 shows an *SV* wave incident at the Moho from below. At normal incidence the refracted *SV* wave dominates because of the low impedance contrast, as for the *P* wave in figure 5. The reflected (but not the refracted) *SV* has opposite polarity to the incident *SV*, and reference to the convention in figure 1 shows that the particle motion of all three waves is in the same direction. This is different from the behaviour at near-normal incidence when the *SV* wave is incident in the lower impedance medium (figure 3), in which incident and reflected *SV* have the same polarity (i.e. opposing particle motions). This is analogous to the different behaviour of reflected *P* according to whether it is reflected off the higher or lower wave-speed medium.

Away from normal incidence, the reflected *SV* wave passes through zero amplitude with a π phase change (change of polarity) at 26° incident angle. Because the incident *S* wave has a lower wave speed than either the reflected or refracted *P* waves, there are two critical angles. At 36° the critical angle for reflected *P* is reached, and at 46° that for refracted *P*. These angles are associated with discontinuities, but not singularities, in amplitude. There is no third critical angle, and hence no total internal reflection, because the refracted *S* wave is in the lower wave-speed medium. If the wave-speed contrast were greater, so that the refracted *P* wave had a lower wave-speed than the incident *S* wave, then there would only be one critical angle—for the reflected *P* wave; this situation is considered in section 5.2.2.

At glancing incidence the reflected *SV* wave, which then contains all the resulting energy, has opposite polarity to the incident wave, which from figure 1 implies opposing particle motion directions for the two waves. This is similar to the behaviour of incident *SV* in a low wave-speed medium at glancing angle of incidence (figure 3). (Whether the phase difference is shown as $+\pi$ or $-\pi$ is, of course, immaterial.)

5.2.1.7 *SH* incident from below (figure 7)

Figure 7 shows results for an incident *SH* wave in the same situation. At normal incidence all three waves have the same polarity, so that the incident and reflected *SH* particle motions are in the same direction; this is the same behaviour as for the incident *SV* wave (figure 6). Indeed, we conclude that *P*, *SV* and *SH* all behave similarly at normal incidence in that their incident and reflected particle-motion directions oppose when the incident medium has the lower wave speed (figures 2, 3 and 4 respectively), and they reinforce otherwise (figures 5, 6 and 7 respectively).

As in the case of *SH* incident in the lower wave-speed medium (figure 4) there is an angle at which there is no partitioning and all energy is transmitted. This occurs at 59° and comparison with figure 4 shows that this is equal to the refraction angle of zero partitioning in that case, so this represents the same slowness, as we would expect from reciprocity. Beyond this angle, reflected *SH* changes polarity, but since *SH* is incident in the higher wave-speed medium, there is no critical angle.

At glancing incidence the incident and reflected *SH* particle motions are opposed. Indeed, we conclude that, at glancing incidence, the particle-motion directions of the incident and reflected waves are opposed in the case of incident *P*, *SV* and *SH*, and irrespective of whether the incident medium has the lower wave speed (figures 2, 3 and 4 respectively) or the higher wave speed (figures 5, 6 and 7 respectively). Although implicit in the boundary conditions, this behaviour can be understood more straightforwardly from energy conservation requirements, especially for incident *S* waves. Incident and reflected waves at glancing angle cannot contribute to the energy flux across the interface. For *S* waves at glancing incidence there is no reflected *P* wave to contribute to this budget either, so displacement at the interface must be zero to avoid refracted waves generating an energy flux in medium ii.

5.2.2 High wave-speed contrast (figures 8–13)

At the Moho discontinuity considered above, the *S*-wave speed in the high wave-speed medium is less than the *P*-wave speed in the low wave-speed medium. If the wave-speed contrast between the two media is greater, then both wave speeds in one medium become less than both wave speeds in the other, and this has a significant effect on the behaviour of the curves. Figures 8–13 show results for an interface of this type, and these figures may be compared directly with figures 2–7 respectively.

For a *P* wave incident in the low wave-speed medium (figure 8) there are two critical angles, rather than one for the Moho (figure 2) because refracted *SV* can now become super-critical (in this example the critical angles occur near 29° and 64° incident angle). Otherwise the behaviour is similar except that the non-trivial phase changes at super-critical angles of incidence are different. Behaviour at glancing incidence is the same as in figure 2.

For incident *SV* in the lower wave-speed medium (figure 9) all three resulting waves become super-critical as in the case of the Moho (figure 3), but reflected *P* and refracted *SV* become super-critical in the opposite order because of their different relative wave speeds. As in the case of the Moho, there is a large singularity at the critical angle of incidence corresponding to *SV*. In this example the critical angles occur near 17°, 30° and 36°, and there is total reflection beyond this angle; this does not occur at any angle for the Moho case. An abrupt change in the phase of reflected *P* can be seen at 31° incident angle.

Incident *SH* in the lower wave-speed medium (figure 10) is similar to that for the Moho (figure 4) except for its critical angle of incidence.

For waves incident in the higher wave-speed medium there is very little difference in the case of an incident *P* wave (figure 11 compared with figure 5). For incident *SV* (figure 12 compared

with figure 6) refracted *P* does not become super-critical, so that there is only one critical angle. An interesting feature is that there is one super-critical angle (at about 43°) at which the phases of all the resulting waves becomes zero; at this angle the polarisation of reflected *S* resulting from incident *S* of an intermediate polarisation direction will (exceptionally) not be elliptically polarised. The same effect occurs in figure 6 at about 39° incident angle but is less noticeable there on account of its proximity to the critical angle. Incident *SH* (figure 13) behaves in a similar way to that in figure 7 for the Moho.

5.2.3 Anomalous Poisson's ratio (figures 14–19)

An alternative ordering of the wave speeds at a solid-solid interface can occur if the Poisson's ratios are very different for the two media. In this case it is possible for the higher *S*-wave speed to be in one medium and the higher *P*-wave speed to be in the other medium (which we still refer to as the "higher wave-speed medium"). Results for such a case are shown in figures 14–19; comparison can be made directly with figures 2–7 respectively for the Moho. As expected, there is some change in the order at which critical angles are reached, and there are also some differences in the polarities of some resulting waves.

For waves incident in the lower wave-speed medium, incident *P* (figure 14) results in only refracted *P* becoming super-critical. Because of the *S* wave-speed differences, reflected *SV* now has no polarity change at normal incidence whereas refracted *SV* does. The behaviour is opposite in this respect to the Moho (figure 2). However, the polarity of reflected *SV* still switches over before the critical angle. For incident *SV* (figure 15) refracted *SV* does not become super-critical, therefore there is no singularity in its amplitude. Again, the change in relative wave speeds results in polarity differences compared with the Moho case (figure 3), so that reflected *P*, rather than refracted *P* now has a phase of π at normal incidence. Incident *SH* (figure 16) does not become super-critical for this case, unlike in the case of the Moho (figure 4).

For waves incident in the higher wave-speed medium, incident *P* (figure 17) results in reflected and refracted *S* with polarities opposite to those for the Moho case (figure 5). This difference arises from the difference in ratios of the two *S*-wave speeds in the two cases. For incident *SV* (figure 18) all three resulting waves go super-critical even though the wave is incident in the medium with the higher *P*-wave speed. There is in this case a singularity at the critical angle of incidence for refracted *SV*, and all three resulting waves have different polarities from those for the Moho case (figure 6) at near-normal incidence. Incident *SH* (figure 19) becomes super-critical, and at normal incidence reflected *SH* has a polarity change, since it is reflected off a medium with a higher *S*-wave speed. This does not occur for the Moho case (figure 7), for which *SH* is reflected off a medium with lower *S*-wave speed. This circumstance of polarity change is opposite to the behaviour of reflected *P* waves, which typically have a polarity change when reflected off a medium with lower *P*-wave speed. It is important to remember that the significance of a polarity change is different for *P* and *S* waves in view of their different particle motions, and the effect that this difference has when the boundary conditions are imposed.

5.3 The solid-fluid interface

5.3.1 The sea bed (figures 20–23)

This interface gives rise to *pP* and *sP* beneath the oceans. It is also an important interface in marine seismic reflection surveying. Often there are sediments with low wave speed beneath the sea bed, but these may be thin, and may be much less than a wavelength in thickness depending upon the recorded frequency range, in which case they will not be "seen" by the incident wave. We choose a *P*-wave speed of 6.0 km/sec in the solid layer. This is likely to be a realistic wave speed as "seen" by seismic waves with frequency 1 Hz or lower in global seismology; the speed may be too high for the higher frequencies in seismic reflection data, where the incident wave may spend several wavelengths in a low-wave speed topmost solid layer. For the sea layer we use 1.5 km/sec.

We first consider a *P* wave incident from below in the solid (figure 20). This case is similar to that of figure 5 (solid-solid interface with *P* wave incident in the higher wave-speed medium) except that medium ii cannot sustain *S* waves because it is a fluid. The results are similar. The absence of any refracted *SV* wave does not make a significant difference to the remaining waves, except that the reflected *P* wave passes through zero amplitude with a change of polarity at 55° incident angle, and back again at 79°. We shall see below, when considering the core-mantle boundary, that this effect results from the higher wave-speed contrast rather than because the refractive medium is a fluid. A second difference is in the amplitude ratios near to normal incidence. At the sea bed a larger proportion of the upward-going incident *P* wave is reflected than for the Moho, because the wave-speed contrast is much greater. However, the amplitude of the refracted *P* wave is very much higher than for the Moho (figure 5), because medium ii has a much lower wave-speed. This results in a higher displacement amplitude for a given energy (section 4.9).

We next show an *SV* wave incident from below the sea bed (figure 21). This case can be compared with figure 6. Because the *S* wave cannot be transmitted into the fluid, all the *S* wave energy is reflected at normal incidence, so the incident and reflected *S* waves have the same amplitude. Away from normal incidence reflected and refracted *P* waves can also be generated, so the amplitude of the reflected *S* wave is less; it passes through zero amplitude, with a change of polarity, at an angle of incidence of about 33°. This behaviour is similar to that in figure 6 except that the angle is different on account of the different wave-speed contrast.

The critical angle of incidence for reflected *P* is reached at 35°. The reflected *P* amplitude approaches infinity at this angle; this is not the case in figure 6. There is no second critical angle because the refracted *P* wave (in the sea layer) travels slower than the *S* wave in the incident layer. This situation occurs only for an interface with very high wave-speed contrast, the sea bed being a rare example.

At glancing incidence all energy is transferred to the reflected *S* wave, with particle motions in opposing directions at the reflection point, as for the solid-solid case (figure 6).

Figure 22 shows an *SH* wave incident at the sea bed. This case is trivial since all energy has to be transferred to reflected *SH* at all angles. The absence of a refracted *SH* results in no change of polarity as the angle of incidence is increased, so that at glancing incidence the incident and reflected particle motions reinforce at the interface; this is a difference from the solid-solid interface behaviour (figure 7).

Figure 23 shows results for a *P* wave incident in the fluid. This corresponds to a downward travelling *P* wave in the sea and so is important in marine seismic reflection surveying, and in the consideration of sea reverberations (*pwP* etc.) in teleseismic observations. Because of the high impedance contrast most energy is reflected, so that at near-normal incidence the reflected *P* wave has a much higher amplitude than the refracted *P* wave. This ratio remains almost constant, with only a small conversion to refracted *SV*, as the angle of incidence is increased. However, because of the high impedance contrast, the critical angle of incidence for refracted *P* is reached rapidly, at only 14°. At 26° the second critical angle is reached, corresponding to the refracted *SV* wave, and so for all larger incident angles there is total internal reflection as observed in figure 3 for the solid-solid case (section 5.2.1.3), with the incident and reflected *P* waves having the same amplitude. This means that only near-vertical *P* waves in the sea give rise to propagating waves beneath, and that seismic sources in the sea layer will typically give rise to high-amplitude evanescent waves.

This case may be compared with the similar solid-solid case in figure 2 (the Moho), though its impedance contrast is much higher. At glancing incidence the *P*-wave particle motions oppose at the point of reflection, as in the case of the solid-solid interface (figure 2).

5.3.2 The core-mantle boundary (CMB) (figures 24–31)

This interface is unusual in the Earth because it represents an interface with a large inversion of *P*-wave speed, while there is still an increase in density. We take first the speeds and densities from the Jeffreys-Bullen (JB) model (see Jeffreys [17]), which gives U=13.64 km/sec, V=7.304 km/sec and ρ=5.68 g/cc above the interface, and U=8.1 km/sec, ρ=9.43 g/cc below (the outer core is taken to be fluid). There has been some uncertainty in the values for wave speeds and densities in the outer and inner core. The more recent Preliminary Reference Earth Model (PREM) of Dziewonski and Anderson [26] gives U, V and ρ above the boundary as 13.72 km/s, 7.26 km/s and 5.6 g/cc respectively, with U and ρ below the boundary as 8.06 km/s and 9.9 g/cc respectively. We show results for both sets of values; this will give an idea of the range of behaviour associated with the acknowledged uncertainty in medium parameters, and some significant differences will be highlighted.

The assumption that this interface is abrupt may be unsound for short-period waves. When calculating the phases of waves that have traversed the outer core it must be remembered that, apart from possible polarity changes at interfaces, some core phases pass through a cusp within the outer core on account of the high rate of wave-speed increase beneath the core-mantle boundary; such a cusp has a $\pi/2$ phase change associated with it.

Figures 24, 25 and 26 show respectively the curves for *P*, *SV* and *SH*, incident from above, computed using the values of Jeffreys; figure 27 gives those for a *P* wave incident from below. These may be compared with the corresponding figures 20, 21, 22 and 23 respectively for the sea bed solid-fluid interface discussed above, and here we note only the main differences. We note that these are the first curves for which Poisson's ratio in a solid is not assumed to be 0.25, and instead the *S*-wave speed is given explicitly.

Although the forms of the curves for the sea bed and the core-mantle boundary are similar, the contrast in wave speeds across the interface is much less for the core-mantle boundary. For waves incident in the solid, this results in differences in the key angles of incidence. In particular, for the incident *P* wave there is a large difference in the angles at which the reflected *P* wave passes through zero and changes polarity. A major difference from the sea bed for the incident *P* wave occurs at normal incidence, where the amplitude of the reflected *P* wave is almost zero. This may be unexpected in view of the lower impedance contrast compared with the sea bed, but arises because of the inverse density contrast, which results in a very low impedance contrast for *P* waves. This has an important effect on the observed amplitude of the phase *PcP*. We might expect to see a reversed-polarity *PcP* at near-normal incidence in view of the outer core being a lower-impedance medium. However, figure 24 predicts no significant *PcP* at normal incidence, and when its amplitude becomes significant above about 15° angle of incidence, its polarity is no longer reversed with respect to the incident wave.

For incident *SV* a difference arises from the fact that at the sea bed the *P*-wave speed in the fluid is lower than the *S*-wave speed in the solid, whereas at the core mantle boundary it is not. Therefore in figure 25 there are two critical angles of incidence rather than one; for near-normal angles of incidence the *SV* wave behaves similarly. The phase of refracted *P* beyond the critical angle of incidence for reflected *P* is close to zero between incident angles of 40° and 65° incident angles. This is an important result which shows that *SKP* does not suffer significant changes in pulse shape at larger epicentral distances due to super-critical angles of incidence. Again the behaviour of *SH* (figure 26) is simple with total reflection at all incident angles.

The *P* wave incident from below (figure 27) exhibits one critical angle of incidence (for refracted *P*), but none for refracted *SV* as its speed is lower. The critical angle is reached at a higher incident angle than for the sea bed case (about 37°) because of the lower wave-speed contrast.

Figures 28, 29 30 and 31 show equivalents to figures 24, 25 26 and 27 respectively, computed using the PREM model. For incident *P* from above (figure 28) there is no zero in the

reflected P amplitude near to normal incidence, and no associated polarity change. This is important since it means that PcP is predicted to have no polarity change at normal incidence when using the PREM model, whereas a polarity change is predicted for the Jeffreys-Bullen model. This behaviour is determined by the ratio of the P-wave impedances in the two media (product of density and wave speed). The ratio of the P-wave impedances of the incident and refractive media is greater than unity (1.01) for the Jeffreys-Bullen model and less than unity (0.96) for the PREM model. The high sensitivity of the behaviour to the model arises because the wave-speed and density contrasts are opposite, making the impedance contrast very close to unity.

For incident SV from above (figure 29) reflected SV (as well as refracted P) has a trivial phase change between angles of incidence of 40° and 65° despite being super-critical to reflected P. This means that ScS with intermediate polarisation angles at these larger angles of incidence will appear plane-polarised; this is not so for the Jeffreys-Bullen model (figure 25). Incident SH from above (figure 30) behaves essentially the same as for the Jeffreys-Bullen model (figure 26).

For P waves incident from below (figure 31) there is a polarity change at normal incidence, rather than no polarity change until an angle of incidence of 10° as in the Jeffreys-Bullen model (figure 27). This difference in behaviour is associated with the difference in behaviour for P waves incident from above, already pointed out. However, in this case it is unlikely to be of practical importance since near-normal reflection from the underside of the core will only occur for phases such as $PKIKKIKP$ at very small epicentral distances.

5.3.3 The inner-core boundary (ICB) (figures 32–39)

The wave-speed and density contrasts across this boundary are not well known, though the inner core is known to be solid. Again we present results using the both the JB parameters given in Jeffreys [17], and those from PREM [26]. Jeffreys gives U=9.4 km/sec and ρ=14.2 g/cc above the interface and U=11.16 km/sec, ρ=16.8 g/cc below, where a Poisson solid is assumed. PREM gives U=10.36 km/sec and ρ=12.2 g/cc above the interface and U=11.02 km/sec, V=3.50 km/s and ρ=12.8 g/cc below; here the S-wave speed is given explicitly. There have been many proposals for a transition zone spanning this boundary, over a depth range up to 300km (see e.g. Bolt [27]) so the abrupt interface may not be valid, at least for short period waves. Moreover, many seismic waves approach this interface at large incident angles, when its behaviour will be particularly sensitive to the nature of the interface and to the angle of incidence itself. At longer periods the curvature of the interface will become significant, leading to a violation of assumption B1 in section 2.

Figures 32, 33 and 34 show results for incident P, SV and SH waves respectively incident from below, and figure 35 shows the curves for a P wave incident from above, all using the Jeffreys parameters. We can see that the behaviour is in general intermediate between that of the sea bed and the core-mantle boundary, as expected.

Figures 36, 37, 38 and 39 show equivalent results to those of figures 32, 33, 34 and 35 respectively, using the PREM parameters. An important difference in parameters results from the S-wave speed in the inner core, which is given explicitly in the PREM model and which indicates a highly anomalous Poisson's ratio. The S-wave speeds used for the inner-core are therefore very different for the two models. This has a major effect only on incident SV from below (figure 37), which has the two critical angles of incidence (for reflected and refracted P) much closer together, and at 28° and 30° rather than at 35° and 43° in the case of the Jeffreys-Bullen model (figure 33). Incident SH from below (figure 38) is totally reflected at all angles of incidence, and is therefore identical for both models.

5.3.4 The high wave-speed fluid (figures 40–43)

The three examples of the solid-fluid interface so far considered all have a lower P-wave speed in the fluid, though the core-mantle boundary has a higher density in the fluid. We now show

results for an example in which both the P-wave speed and the density of the fluid medium are higher than in the solid. These are shown in figures 40–43. It is sensible to compare waves incident in the solid with those incident in the lower wave-speed solid in the case of a solid-solid interface, so that we compare figures 40, 41 and 42 with 2, 3 and 4 respectively. For the incident P wave (figure 40) the behaviour is similar to that in figure 2 except that the absence of a refracted SV wave results in a different polarity for reflected SV. If we compare with a solid-fluid interface with a low wave-speed fluid (say the sea bed, figure 20) we see that reflected P has no polarity change in the present case, unlike in the case of the sea bed. This is in agreement with the usual behaviour of reflected P which has no polarity change when reflected off a higher wave-speed medium.

For incident SV (figure 41) refracted P becomes super-critical so that there is total reflection beyond about 36° since there is no refracted S wave. This behaviour is rather different from both the solid-solid case (figure 3) and the sea bed (figure 21).

Because there is no refracted S, SH is totally reflected at all angles of incidence as for the sea bed (figure 22), and as for the sea bed there is no polarity change. It is different for the solid-solid case (figure 4) where a critical angle of incidence for refracted SH is reached.

5.4 The fluid-fluid interface (seawater/sediment) (figures 44 and 45)

The fluid-fluid interface is unusual in practice since a plane interface is unlikely to be sustained between two fluids except in special cases. One example of interest arises from the existence of deep marine sediments with a high water content. Wood [28] considered the acoustic properties of an aqueous suspension under the assumption of no rigidity. Although it is now generally thought that most marine sediments have non-zero rigidity, experimental data presented by Hamilton and Bachman [29] show that for porosities of the order of 80%, P-wave speeds and densities indicate very low rigidity. A consequence of this is that the elastic moduli have little effect on the wave speed, which is lower than that of water on account of the higher density (see equation (12a)). At a porosity of 80% wave speeds as low as 1.490 km/s are observed (figure 7 of [29]), corresponding to a density of 1.4 gm/cc (figure 14 of [29]). By comparison, the wave speed and density of sea water are about 1.53 km/s and 1.02 gm/cc respectively.

This example is shown in figures 44 and 45, for P waves incident from below and above respectively. Since only P waves can exist in either medium the behaviour is simple in principle. The core-mantle boundary is the only other example here which has a density contrast opposite to the wave-speed contrast. This has an effect upon the amplitudes and positions of zeros in amplitudes, which are governed by impedance ratios (section 5.1), but does not affect the positions of critical angles, which are determined by wave-speed ratios only. In figure 44 there is a polarity change in reflected P at 71°, before the critical angle is reached at about 76°; beyond this there is total reflection with a non-trivial phase change. In figure 45 there is also a polarity change in reflected P, at about 76°. These polarity changes arise because the impedance (product of wave speed and density) contrast is opposite to the wave-speed contrast. When the impedance contrast is "normal", the P wave reflected in the lower wave-speed medium has zero phase change at all angles of incidence including normal incidence, and P wave reflected in the higher wave-speed medium have a π phase change at all angles of incidence.

5.5 The solid free surface (Earth's surface) (figures 46–48)

We use the Earth's surface as an example of an interface in which the second medium is a void. Of course, the Earth's atmosphere differs from this in one important respect—its density is non-zero, giving rise to atmospheric sound waves. Because the density contrast is large, the energy transmission from the Earth to the atmosphere has a negligible effect on the behaviour in the solid layer, so that the atmosphere may be taken as a void, provided we are not concerned with that small part of the energy which is transmitted. If we are, then the atmosphere must be specified as a fluid medium ii with appropriate P-wave speed and density; some consequences of taking account of the atmosphere are mentioned at the end of this section.

Because, for a void, layer ii is assumed to have zero density the amplitudes of reflected waves at the free surface do not depend explicitly upon the near-surface wave speeds U_i and V_i, or density ρ_i, but only upon the ratio of the two wave speeds. The presence of near-surface sediments usually produces thin lower wave-speed surface layers, whose importance in the amplitude partitioning will depend upon whether the layer thicknesses are a significant fraction of the seismic wavelength of interest. For short period (1 second) signals the wavelength in the crust is around 10 km, but for those of long period (20 seconds), wavelengths are about 150 km. We set U_i=6.0 km/sec, representing an average of near-surface wave speeds neglecting sediments (see, e.g. Mueller and Landisman [22]), and we set ρ_i=2.9 g/cc (an average value following Woollard [23]). A Poisson solid is assumed.

The free surface is an important interface both in global seismology and in local and exploration seismology. In global seismology the reflected amplitudes of the phases *pP* and *sP* are important in the analysis of seismic sources, in particular where teleseismic observations of the seismic source using these phases is used to constrain source mechanisms, as for example with the relative amplitude method [4]. At the station the behaviour of incoming *S* waves at larger incident angles is also important. In seismic reflection surveying, multiple reflections involving the solid free surface can be important, but deviations from plane waves mean that the results presented here are not valid for reflections above shallow buried sources.

Figures 46, 47 and 48 show respectively the curves for an incident *P*, *SV* and *SH* wave. We first consider the incident *P* wave. The reflected *P*-wave amplitude passes through zero at an incident angle of 60° (this angle is exact for a Poisson solid) and again at about 77°. A change of polarity occurs at both of these angles, so that the reflected *P* wave has a polarity opposite to incident *P* except for a small range of intermediate angles near to glancing incidence. It is interesting to note that the opposing polarities of the incident and reflected waves at near-normal incidence corresponds to a reinforcement of their particle motions at the interface. As pointed out in section 4.10 it is the sum of these motions which is recorded by a surface seismometer, and in section 5.7 this surface motion is considered for all angles of incidence.

Considering the incident *SV* wave, at near-normal incidence the incident and reflected *SV* waves have opposing particle-motion directions at the interface. The amplitude of reflected *SV* passes through zero at an angle of incidence of 30° (this angle is exact for a Poisson solid). The critical incident angle for reflected *S* occurs at approximately 35° (for a Poisson solid as assumed in this example) and this has important implications for *S* waves arriving at a seismic station at greater angles of incidence. The evanescent wave, being associated with the interface, will contribute to the particle motion at the surface, so that the particle motion recorded will not have a simple relationship to the incident *S* wave. The angle of incidence of direct *S* may be greater than the critical angle in the case of closer teleseismic distances (say less than 40°) depending upon the near-surface wave speed. Beyond the critical angle the *SV* is totally reflected.

The incident *SH* wave, figure 48, is always totally reflected, so that a reflected *S* wave of any intermediate polarisation direction will be elliptically polarised beyond the critical angle for reflected *P*.

If the void were replaced by an appropriate fluid layer to yield results for waves in the atmosphere, the effect on the incident and reflected wave amplitudes in the subsurface would be negligible because the transmitted energy is small. However, as noted in sections 4.5 and 4.9, the displacement amplitudes of the waves refracted into the atmosphere are comparable with those in the subsurface; indeed continuity of displacement at the interface gives rise to an atmospheric *P*-wave whose amplitude is exactly twice that of a normally-incident *P* wave. This paradoxical result is important when considering reports of "earthquake sounds". Although the transmitted energy is small because the density is low (section 4.9), local microearthquake signals may be sufficiently high frequency to be perceived by the ear, but not felt. This results in "true" earthquake sounds, as distinct from secondary audible effects resulting from the shaking of objects in the presence of high seismic intensity.

5.6 The fluid free surface (sea surface) (figure 49)

The sea surface is important in global seismology because of the sea reverberations *pwP*, *pwwP* etc. associated with the surface reflection *pP*. These were first identified by Mendiguren in 1972 [30]; see also Pearce [31]. The sea surface is also important in marine seismic surveying where similar multiples are prominent on recorded data. Figure 49 shows a *P* wave incident at the sea surface; this is a simple case since the wave is always totally reflected, with a change of polarity at all incident angles.

Of special interest is the composite effect of the sea layer on the passage of a *P* wave, compared with the true *pP* reflection from the sea bed. The amplitude of this "first sea reverberation", usually referred to as *pwP*, can be found by multiplying the coefficients of the upward transmitted *P* wave at the sea bed (figure 20), the reflection at the sea surface (figure 49) and the downward transmitted wave at the sea bed (figure 23). The new computer program described in Appendices A and B can provide such cumulative coefficients if successive interfaces along a raypath are concatenated.

If we wish to consider seismic waves transmitted from the sea into the atmosphere, then medium ii must be changed from a void to a fluid with suitable wave-speed and density, as described for the solid free surface in section 5.5. Similar arguments apply, though it may not be valid to regard the sea surface as planar at wavelengths corresponding to audio-frequencies.

5.7 Displacement at the solid free surface (figures 50–51)

In section 4.10 a formulation was given for computing the total displacement at the free surface by adding the displacements of the incident and resulting waves. A seismometer at the free surface records one component of this displacement. Normally we are concerned with the displacement of the incident wave rather than that of the free surface, and the differences may become important if we are taking relative amplitudes of the different components of this displacement. Following equations (61) to (63) we express this difference as the ratio of the surface displacement to the incident wave displacement, computed separately for each of the three components, and separately for incident *P*, *SV* and *SH*. It follows that if this ratio is the same, and in phase, for any two components, then the ratio of the incident wave displacements for the two components will be the same as the ratio of the surface displacements, so that relative amplitude observations of those components may be used without a correction. In these circumstances the particle motion of the incident wave and the free surface are in the same direction. In other circumstances a correction must be made before the observed relative amplitudes of the two components can be used as if they represent the particle motion of the incident wave. As pointed out in section 4.10, the ratios are complex to allow for phase differences, and for an *S* wave incident at a super-critical angle the evanescent waves must be included in the computation. In general this results in elliptical particle motion at the free surface for super-critical angles, even if the incident *S* wave is plane-polarised.

In figure 50 we show the ratio of surface displacement to incident wave displacement for the vertical, radial and transverse components as a function of incident angle in the case of the incident *P* wave, for a Poisson solid. (The radial component is the horizontal component in the ray plane, and the transverse component is the horizontal component normal to the ray plane.) As before, the "horizontal" is defined as parallel to the surface. Figure 50a shows the modulus of the ratio and figure 50b shows the phase of the ratio. The vertical and radial components are not equal in amplitude but have a ratio of about 0.85 at normal incidence, increasing to unity at an angle of incidence of 60°. Beyond 70° the ratio deviates considerably from unity, and approaches infinity at glancing incidence. The transverse component is, of course, zero. Figure 50b shows that there is no phase difference between the surface displacement and the incident wave displacement at any angle of incidence.

It is not immediately apparent how the curves in figure 50 arise from equations (61a–c) since the displacements *A*, *C* and *D* which appear in those equations are themselves variables which

depend upon the angle of incidence. Of course, at normal incidence the amplitude of the radial component of the incident P wave is zero, as is the radial component of the surface displacement, but it is seen from figure 50 that the ratio remains finite. To confirm figure 50 analytically we may consider the "apparent angle of emergence" (Bullen and Bolt [18] page 189), which is the angle of emergence of the P wave as deduced from the particle motion at the free surface. If we denote this by $\hat{a}$, then equation 8.18 of reference [18] gives the relation between the apparent and actual angles of emergence for a Poisson solid:

$$2\sin^2 a = 3(1 - \cos\hat{a}) \tag{64}$$

remembering that reference [18] expresses angles with respect to the boundary rather than the normal. The ratio of the vertical and radial amplitude curves in figure 50 is given by

$$\frac{|r_{3P}|}{|r_{1P}|} = \frac{\tan a}{\tan\hat{a}} . \tag{65}$$

Eliminating $\hat{a}$ from equations (64) and (65) we obtain

$$\frac{|r_{3P}|}{|r_{1P}|} = \frac{3 - 2\sin^2 a}{2\cos a \sqrt{(3 - \sin^2 a)}} . \tag{66}$$

From this it can be seen that the ratio is equal to $\sqrt{3}/2$ for a=0, 1.0 for $a=\pi/3$ and is infinite for $a=\pi/2$; this is the behaviour of figure 50a.

Figure 51 shows results for an incident S wave. Since an incident SV wave relates only to the vertical and radial components, and an incident SH wave relates only to the transverse component, both are shown on the same figure. As mentioned in section 4.10 the behaviour of SH is trivial; the surface displacement is twice that of the incident wave at all angles of incidence, with no phase change. At near-normal incidence the curves corresponding to the vertical and radial components are the same as for the P wave at near-normal incidence, but their ratio passes through unity at about 30° and grows larger towards the critical angle at about 35°, where it becomes infinite. Beyond the critical angle of incidence there is a phase difference between the incident wave and the surface displacement (figure 51b), and this is different for the vertical and radial components. This results in an elliptical particle motion at the surface even when the incident S wave is plane-polarised. It follows that to recover the amplitude and polarisation direction of the incident S wave, each component of the observed surface motion must first be phase-shifted to correct for this difference. In practice, the presence of multiple layering usually makes the surface motion even more complex, so that incident S waves are not normally used for waveform studies at post-critical angles of incidence. It is important to remember, though, that even from about 5° before the critical angle of incidence, the surface displacement behaves very differently from the incident wave (figure 51).

The curves shown in figures 50 and 51 are similar to those presented by Evans [32]. If the medium is not a Poisson solid (i.e. $U/V \neq \sqrt{3}$), the curves have a similar form, but features may occur at different incident angles. We emphasise that all these results are valid for plane waves only. In particular, the behaviour of waves impinging on the surface from a buried point source are in some circumstances quite different; this is discussed in section 7.2.

6. NOTATION DIFFERENCES AND ERRORS IN OTHER WORK

In his paper on the reflection and refraction of plane waves in 1946, Fu [33] began: "Even though the literature on this problem is enormous, there seems to be still room for further discussions". The increase in this literature has not diminished during the succeeding fifty years, and it is unfortunate that many of these publications have contained or reported on errors and inconsistencies. These include errors and omissions in the definition of notation, in the equations, and in the computed curves.

We describe and explain specific cases, together with a comparison of different authors' methods of presentation, in order to minimise the likelihood of the present work adding to the confusion.

We shall refer to the convention defined in section 3 and illustrated in figure 1. As explained in section 3.1, figure 1 shows directions of zero-phase corresponding to the displacements of the six waves A to I; this is because we choose to define displacement in terms of a modulus and a phase. When comparing with other work in which the displacement amplitude is allowed to be positive or negative (so that phase only needs to be introduced at super-critical angles) our directions of zero-phase may be regarded as equivalent to the positive (as opposed to negative) sense of displacement.

Most authors who have considered the solid-solid interface have used a convention which differs from ours only in that the sense of C is reversed. These include Richter [34], McCamy, Meyer and Smith [8], Costain et al [21] and [35], Singh et al [36] and previous versions of the program ZOEPP (solid-solid section). A common source of confusion under that convention is that if incident and reflected P are both in the same sense (for example compressive) then the two amplitudes are nevertheless of the opposite sign. Although of the above authors only Singh et al. actually define their sign convention, a further source of confusion is that their defining diagram contains two errors, as noted by Hales and Roberts [37]. First, it shows the reflected P amplitude, C, along rather than opposed to the direction of propagation (i.e. it is shown as in our figure 1), and secondly it shows the reflected SV amplitude, D, towards negative rather than positive X_1.

The above confusion would have been revealed for the simple case of a P wave incident at near-normal incidence at the free surface or against a lower wave-speed medium. However, there are specific circumstances which served to obscure it. Singh et al. present no computed results; McCamy et al. plot only the modulus of the displacement (although they do not make this clear), and Costain et al. do not consider incident P. For incident S, Costain et al. annotate their curves for reflected and refracted waves with 180° phase changes, which occur as a function of angle on each curve; they do not relate these phases to the phases of the incident wave, although non-trivial phase changes are given for super-critical angles. Of course, the polarities of resulting waves with respect to the incident waves at pre-critical angles (which we represent as the presence or absence of a π phase change), are of fundamental importance.

For SH, Richter duplicates the use of B, D and F for his SH waves rather than using G, H and I respectively, but his senses correspond to our figure 1.

Still further confusion arises because most authors who consider the solid-fluid and fluid-solid interfaces (for example Ergin [10]), and previous versions of the program ZOEPP (solid-fluid and fluid-solid sections) use another alternative convention. Although not stated, it agrees with our notation (figure 1) except that the incident SV amplitude (or zero-phase direction), B, is in the opposite sense—i.e. towards positive X_1. Ergin also duplicates the use of B and D for incident and reflected SH respectively, and since his (unstated) convention agrees with ours for SH, this means that the Cartesian system formed by [SV,SH,propagation direction] represents a left-handed rather than a right-handed system for the incident S wave. This is not self-consistent because it means that the incident and reflected S wave conventions are oppositely handed; it causes particular confusion if interfaces are to be concatenated in successive computations.

Aki and Richards [38] page 139 et seq. derive scattering matrices, to account simultaneously for incident P and S waves in both media. Their sign convention differs from ours in the senses of the incident and refracted SV. Their upward propagating waves are defined as being in the direction of their negative Z, which is in the same direction as our incident waves. The upward travelling incident waves in their tables 5.3 therefore correspond to our geometry and have the same signs in their exponents. The signs for both the X and Z components of the premultipliers for the incident and refracted SV are of opposite sign to those in our equation (33) on account of this difference in the sense of their amplitude definitions. Surprisingly, the definition of their SH sign convention (their figure 5.7) does not show the sense of these waves, but from their table 5.2 it follows

that all three *SH* waves are in the same sense, as in our convention. As in publications previously referred to, it follows that the incident, reflected and refracted *S* waves do not all form a system of the same handedness in [*SV*,*SH*,propagation direction].

The convention used by Aki and Richards is used by Young and Braile [39], who take their equations from Macelwane [40]. Young and Braile do not consider *SH*, and present only energy ratios in their results. Gubbins [41] (page 62) defines *SV* in the opposite sense to us, but fails to give a convention for refracted *P* or *SV*. He defines all three *SH* waves in the opposite sense to us.

In addition to the papers published in the journals and books on earthquake seismology as referred to above, there has been a similar history of papers in the exploration seismology literature, during the same time period, but usually with no cross references and again with generally different conventions of notation (e.g. Muskat and Meres [42], Muskat [43], Bortfeld [44], Koefoed [45], Daley and Hron [46], Tooley et al [47]). Most of these references do not define their conventions explicitly, except for Bortfeld and Koefoed. Koefoed uses the same convention as ours, although he does not consider incident *S*. Bortfeld uses the opposite sense to us for the incident and refracted *SV* waves. Daley and Hron [46] state (p 129) that coefficients differ "slightly" depending upon whether potentials or amplitudes are used, and they say that there is no difference for *SH* waves; this fails to illuminate the fundamental difference in behaviour of displacement and displacement potential (section 4.2). Also, their figure 2.1 is upside down. Miles [48] gives the Zoeppritz equations for incident *P* in her figure 4. The convention differs from ours only in the sense of refracted *P*. She gives a diagram defining this convention which has the wrong sense for reflected *S*. She also states erroneously, with the aid of a misleading vector diagram, that the displacement is zero at the interface, rather than continuous.

Because amplitude-versus-offset (AVO) analysis is a topic in seismic reflection surveying, its literature also tends to refer only to the earlier work published in the journals of exploration geophysics. This application of the Zoeppritz equations is discussed separately in section 8.

Waters [49] pages 39–40 uses the convention that we adopt here, and defines this convention in a diagram (his figure 2.8). He also warns that many papers contain errors of sign or use different sign conventions. Unfortunately his equation 2A.6, which gives the Zoeppritz equations in matrix form, contains two elements with incorrect sign. These are the elements (3,3) and (3,4) of his $\underline{P}$ matrix. The diagram defining his convention is, however, correct. The equations used by Waters were taken from Sheriff ([50] pages 248–249) as corrected by Sheriff [51]. Sheriff states that the Zoeppritz equations describe the partitioning of energy, and that it is energy which is plotted in his graphs, although he refers to the graphs as displaying amplitude; he refers to the equations in terms of potential as "Knott's equations". In fact, the Zoeppritz equations [6] are those which relate displacements, and those of Knott [5] relate the energy (section 4.9).

Additional problems of sign convention and definitions arise at super-critical angles. Many authors (e.g. McCamy, Meyer and Smith [8] page 924, Singh, Ben-Menahem and Shimshoni [36] page 278, and Officer [20] page 196) state that at super-critical angles of incidence the resulting angle of the corresponding wave becomes imaginary. We have shown in section 4.8 that the angle becomes complex rather than imaginary, with its real part equal to $\pi/2$.

The non-propagating evanescent waves associated with super-critical reflection or refraction represent a disturbance decaying in amplitude away from the interface, and with a wavelength along the interface equivalent to the apparent horizontal velocity of the travelling waves (which is the same for all the waves). If the incorrect sign is used for computing the complex square root associated with the exponent in the super-critical case, the evanescent wave amplitude instead becomes infinite away from the interface and, more subtly, the phase shifts associated with the remaining propagating waves will be in error. It was pointed out by Singh, Ben-Menahem and Shimshoni [36] that Jeffreys [52] made this error, and that since McCamy, Meyer and Smith [8] used this convention, some of their curves are in error beyond the critical angles. Moreover, Costain, Cook and Algermissen [21], who used the correct sign for the complex square root, later published a Corrigendum [35], prompted by the incorrect

equation of Jeffreys [52], in which their correct curves were replaced by erroneous ones. This confusion is discussed in more detail (correctly) by Singh, Ben-Menahem and Shimshoni [36].

Many authors develop their theory in terms of scalar and vector potentials for the *P* and *S* waves respectively, rather than in terms of displacement. Some of these authors, e.g. Ewing, Jardetsky and Press [16] and Officer [20] give final expressions for potential amplitudes rather than for displacement amplitudes, and these may be of opposite sign. We have explained in section 4.2 that these two alternative amplitudes are different, and some authors do not make this fact explicit. It must be remembered that the potential amplitudes are scaled by the appropriate seismic wave speed (equations (27) and (32)), and that the physical quantity normally required is the displacement, or perhaps the energy, but not the potential since this has no physical significance.

Many authors plot the square root of the energy ratio: this loses information on particle-motion direction, and its numerical values must not be confused with displacement, energy, or displacement potential. Ewing et al. plot the displacement potential ratio for the fluid-fluid interface, and they give expressions in terms of potentials, except for the case of *SH*.

Achenbach ([53] page 182 et seq.) does not state his convention; he uses the same convention as ours but does not include incident *SV* in his matrix formulation.

Finally we note that some authors, (e.g. Costain, Cook and Algermissen [21] and [35], Gubbins [41]), have the waves incident in layer 2 rather than in layer 1, and that some authors, (e.g. Ewing, Jardetsky and Press [16] chapter 3, Bullen and Bolt [18] page 141, Officer [20] page 191) specify angles relative to the interface rather than relative to the normal.

Because of the mutual inconsistencies between the conventions of McCamy, Meyer and Smith [8], Kolsky [9] and Ergin [10], the previous versions of the computer program ZOEPP were not using the same convention for the solid-solid, solid-fluid and solid-air cases, and in this respect were in error. Using the convention of figure 1 a single matrix formulation has been constructed that satisfies all media combinations.

7. DEPARTURES FROM THE INITIAL ASSUMPTIONS

7.1 The non-monochromatic incident wave

In principle we may superpose monochromatic waves to obtain any signal shape. The Zoeppritz equations have solutions which are independent of frequency in that the graphs of amplitude and resulting angle are independent of ω at pre-critical angles. However, in other respects there are important frequency-dependent effects to be considered.

First, any phase change that is independent of frequency corresponds to a shift in time or space which is a certain fraction of a wavelength or period respectively. Such phase changes therefore shift different frequencies by different amounts in time or space. In the case of a non-monochromatic waveform this results in a change in waveform shape associated with the phase change, except that a phase change of π will simply change the polarity of the waveform without changing its shape. A consequence of this is that the resulting propagating waves have a different shape from the incident waveform at super-critical angles—i.e. those angles for which the resulting waves suffer non-trivial phase changes (section 4.8). This change in shape depends upon the wave speed, so that the propagating waveforms in the two media will then in general have different shapes, as will the *P* and *S* waves in the same medium.

Secondly, the evanescent waves generated at the interface at super-critical angles decay away from the interface at a rate which depends upon frequency (section 4.8); longer wavelength waves decay away over a longer distance. It follows that the particle motion for a non-monochromatic evanescent wave is complicated and dependent upon the frequency content of the signal and the

distance from the interface. This is one reason why observed shear-wave particle motions become complex in the region of an interface at large angles of incidence.

A further complication arises at super-critical angles of incidence for an *S* wave which has an intermediate polarisation direction (i.e. it has components of both *SV* and *SH*). At incident angles super-critical for reflected or refracted *P*, the reflected and refracted *S* waves become elliptically polarised because the non-trivial phase change is suffered by *SV*, but not by *SH*. At incident angles super-critical for refracted *S*, both the *SV* and *SH* components suffer non-trivial phase changes but these are in general different (compare for example figures 3 and 4), so the reflected *S* wave is again elliptically polarised. The behaviour of the reflected and evanescent waves in this situation has been examined in detail by Hudson [54]. Because incident *S* waves are often super-critical for reflected or refracted *P* over a wide range of incident angles (outside a range that is often termed the "shear wave window"), it is easy to see how reflected or refracted *S* waveforms can have complex particle motions even for a simple wave-speed structure.

Most seismic waves are not stationary but are transient. In the simplest case a short monodirectional pulse may be incident at an interface. Such a transient pulse always contains a wide range of frequencies. The above frequency-dependent effects are then important; at super-critical angles of incidence the pulse changes its phase upon reflection or refraction, and so in general becomes bidirectional (i.e. an "N-shaped" wave).

7.2 The non-plane incident wave

If the incident wave is not planar this has a substantial effect on the behaviour at the interface. The wave motions substituted into the wave equation in section 4 are plane waves; plane waves are always an approximation to the non-plane waves of all real situations.

The behaviour of spherical or cylindrical waves incident at the surface (due to a buried point source and line source respectively) is referred to as "Lamb's problem". The situation is much more complicated than for the plane wave approximation, and includes critically refracted "head waves" and surface waves, which complicate the waveforms at any interface including the surface (see e.g. Aki and Richards [38] chapter 6, and Bullen and Bolt [18] page 146). Solutions for spherical and cylindrical waves are given by many authors. For example, exact solutions for the case of an incident *P* wave are given by Bortfeld [55], [56], and by Krail and Brysk [57], who give numerical results.

A spherical wave suffers geometrical spreading and this has associated with it a reduction of energy density on the wavefront as the wavefront expands. Upon abrupt change of wave speed there is an abrupt change in curvature of the wavefront, and this happens upon refraction, and upon change of mode between *P* and *S* for both reflection and refraction. This gives rise to an additional factor in the reflection coefficient for the phase *sP* (see e.g. Pearce [3]). This factor is always important for a mode-converted reflection because the ratio of the *P* and *S* wave speeds is always very different from 1.0. It was omitted by Fitch, McCowan and Shields [58], causing errors in *sP* amplitudes of the order of a factor of two, which were corrected by Fitch [59].

The detailed theory of head waves is given by Červený and Ravindra [60]. *P*- and *S*- wave energy is reflected from all points along the interface at their respective critical angles. These waves form the basis of seismic refraction surveying and equivalent arrivals do not exist for plane waves, for which the only arrival is an arrival reflected from the interface, having originated at the one point on the incident wave which has the correct lateral position. To explain head waves Huygens' principle can be used to conclude that a spherical wave can be described by a linear superposition of plane waves at a range of angles. This decomposition can be done formally using the Sommerfeld integral; in reflection seismology this is commonly referred to as the τ–p transform (see e.g. Treitel, Gutowski and Wagner [61]). We can then apply Zoeppritz' equations to each plane wave component.

As a result of the above effects the polarisation of an S wave incident at the free surface from a spherical wave may become elliptical, even at small (pre-critical) angles of incidence, and incident shear waves are contaminated by an S-to-P head wave. These effects have been studied in detail by Booth and Crampin [62], who show synthetic seismograms and particle-motion diagrams for surface motion due to a buried point source at various distances and frequencies. These diagrams show that the plane-wave surface motion presented in figures 50 and 51 are greatly modified in many situations appropriate to local observations of earthquakes, though shear-wave particle motions can remain less elliptical immediately beyond the critical angle than for plane waves. In general, the spherical-wave behaviour becomes more different from the plane-wave behaviour with increasing wavelength and increasing wavefront curvature (i.e. decreasing distance from the source). Results presented in [62] help to show when this effect is significant.

7.3 The curved interface

If the interface is significantly curved, then it will act as a lens to incoming plane waves and the resulting waves will not be planar. In these circumstances a transient wave will change its shape upon reflection or refraction (Aki and Richards [38] chapter 9). The Kirchhoff approximation may be used for such interfaces (see e.g. Wenzel, Stenzel and Zimmermann [63]). This situation is relevant in the Earth for longer period seismic waves, particularly at the core-mantle or inner-core boundaries which have greater curvatures than the Earth's surface.

7.4 The irregular interface

An irregular interface results in scattering of energy, which in general will be frequency-dependent. Behaviour will be different according to whether the variations are smaller than, similar to or greater than the seismic wavelength. A study of the reflection and refraction of plane waves at a periodic interface between two media has been made by Sato [64], and more recently by Fokkema [65], [66], and Fokkema and van den Berg [67]. Other methods used for rough interfaces are the method of Aki and Larner [68] and perturbation theory, e.g. by Gilbert and Knopoff [69].

7.5 The non-abrupt interface

If the change in wave-speed takes place over a distance which is long compared with the wavelength, then it will approximate to a wave-speed gradient, and the ray will curve through it, to the same final angle of refraction as if there were an abrupt interface. By Snell's law the ratio of the angles of incidence and refraction depends upon the ratio of the two wave speeds, and not upon any intermediate refractions. However, in this high-frequency extreme there is no energy partitioning, and so no reflected energy or conversion between P and S waves upon refraction.

Pilant [70] reviews work on determining reflection and transmission coefficients at non-abrupt interfaces. Gupta [71], [72] considers the case of a linear transition in wave-speed between two uniform layers. Lapwood, Hudson and Kembhavi [73], [74] and Lapwood and Hudson [75] consider a more general case.

In global seismology most interfaces appear abrupt at observable seismic wavelengths, but this is not so in exploration seismology. The wavelengths may then be comparable with the depth range over which the wave speed changes, while longer wavelengths may see an abrupt interface. The consequence is a tendency for more low-frequency energy to be reflected than high frequency energy. A similar effect is observed in the presence of anelastic attenuation, and therein lies an ambiguity which is difficult to disentangle (see Ziolkowski and Fokkema [76]).

7.6 The lubricated solid-solid interface

If the contact between two solid media is not welded, then the boundary conditions imposing tangential displacement continuity (equations (35a) and (35b)), and those imposing

continuity of tangential stresses (equations (35d) and (35e)) must be relaxed. In the extreme case, in which there is no stress transfer between the media, the tangential stresses fall to zero; this case has been considered by Chang [77]. A situation of more practical significance is where there is imperfect welding, so that slip is allowed but there is still friction. This might be realistic for waves passing through a medium with large-scale fluid-filled cracks with high pore pressure. This situation is considered by Murty [78], whose theory is developed further by Schoenberg [79]. The lubricated solid-solid interface is now important in non-destructive testing (see e.g. Nagy [80]).

7.7 Non-semi-infinite media: wave-speed gradients and proximity of other interfaces

As with irregular and non-abrupt interfaces, the effects of other interfaces depend upon the ratio of the linear dimensions to the wavelength. If a second interface is closer than about one wavelength, then the disturbances at the two interfaces interfere, and even if they are not close, there may be constructive or destructive interference as a function of angle. We can see how a succession of closely spaced interfaces approaches equivalence to a wave-speed gradient. A thin layer sandwiched between two halfspaces is not seen by waves whose wavelength is long compared with the separation. Such waves will see one interface, or if the two halfspaces are identical, no interface. It follows that a succession of closely-spaced interfaces may be traversed by a low-frequency wave as if passing through a single medium with a wave-speed gradient, while the same succession will result in energy partitioning according to the Zoeppritz equations for a high-frequency wave. Consequences of this for the frequency content of seismic reflection data are discussed by Ziolkowski and Fokkema [76].

At angles of incidence which are super-critical for both refracted P and refracted S, all energy is reflected. If such a layer is achieved by means of a non-abrupt interface, a high-frequency wave which does not "see" the interface will nevertheless be refracted back by the wave-speed gradient, so that it too will effectively be "reflected". One can therefore say that the reflection response of the sequence of interfaces is non-white at pre-critical angles of incidence and white at super-critical angles of incidence. This condition is formally expressed as the critical reflection theorem by Fokkema and Ziolkowski [81].

A common situation is the prevalence of low wave-speed surface layers, whose thickness may be of the order of a wavelength; this may be important both in global and exploration seismology, at their respective length scales. Interference between multiple reflections is possible, and such layers may not be seen by longer wavelengths. The composite effect of a near-surface structure may therefore be complicated and frequency-dependent.

Similar behaviour occurs at super-critical angles of incidence. If the separation of two interfaces is less than the penetration of the evanescent wave away from the interface, then the non-propagating wave may become a propagating wave again after refraction at the second interface. In these circumstance we have an incident evanescent wave, which is represented by a complex angle of incidence associated with the required horizontal slowness. Although the Zoeppritz equations include this case implicitly for a monochromatic incident wave, it must be remembered that the frequency-dependent decay of an evanescent wave away from the first interface will result in an incident amplitude at the second interface which decreases with increasing frequency.

7.8 Imperfectly elastic media

If the media either side of the interface are not perfectly elastic, the waves are attenuated as they pass through the media and their behaviour at the interface is affected. The wave amplitudes suffer an exponential decrease with distance and frequency if a constant Q model is assumed (i.e. if we assume that the fractional loss of energy per cycle is independent of frequency), and this attenuation can be described by making the elastic moduli, and hence the seismic wave speeds complex. This introduces the possibility of a real part in the complex exponential of the plane-wave trial solution. Borcherdt [82] and [83] investigate this, and Krebes [84], gives the corresponding modified equations and presents numerical results. Other examples are given by Bourbié and Gonzalez-Serrano [85] and

Kelamis [86]. We point out that those papers use different notation from ours, and from each other, so that their results require careful interpretation. Further work includes that of Cooper [87] and Buchen [88].

In general the effects are greatest for intermediate angles of incidence, and are unlikely to affect teleseismic observations significantly. They may be important in seismic exploration however, especially where target interfaces are close to zones of high attenuation.

7.9 Anisotropic media

If the *P*- and *S*- wave speeds depend upon the direction of particle displacement in the medium, the medium is said to exhibit seismic anisotropy and the behaviour of waves incident at an interface is more complicated, even in the case of plane waves. In general the particle motions are no longer parallel to or perpendicular to the ray direction, and the ray direction is not normal to the wavefront. Since *P*-wave particle motion is generally along the ray direction, the main effect on *P* waves is a variation in wave-speed with propagation direction. For *S*-waves the effects are much more complicated since particle motion may be in any direction in the plane normal to the ray; one result is the splitting of *S*-waves into near-orthogonally polarised components travelling at different wave speeds. The specific case of transverse isotropy (by which we mean that the wave speeds are the same in all directions in the plane of the interface) has been considered by Daley and Hron [89]; some comments on the more general problem are made by Evans [32].

8. AVO ANALYSIS AND APPROXIMATIONS TO THE ZOEPPRITZ EQUATIONS

As summarised in table 1, figures 2, 5, 8, 11, 14 and 19 all show results for a *P* wave incident at a solid-solid interface. Together these results suggest that the amplitude of a reflected *P* wave resulting from a near-normally incident *P* wave varies little with angle of incidence. Indeed this is normally assumed when multiple-offset traces are stacked in seismic reflection sections. However, there are special cases where the change with incident angle can be quite large, and this forms the basis of AVO analysis in seismic reflection processing. In 1955 Koefoed [90] found that large differences in U/V between the two media (corresponding to a large difference in Poisson's ratio) can give rise to larger variations in reflected *P* amplitude with angle of incidence. Although this variation is not especially large in our figure 14 (which shows a case of high contrast in Poisson's ratio—see table 1) the variation is more pronounced if U_{ii}/V_{ii} is larger than U_i/V_i (with $U_{ii}>U_i$); figure 14 shows the opposite case.

It happens that this large variation in U/V is prevalent in situations found in hydrocarbon exploration. A gas-bearing sandstone between shale layers provides a classic example, giving rise to high-amplitude reflections (sometimes referred to as "bright spots") together with a large variation in amplitude with incident angle. This can be contrasted with a similar situation in which the sandstone is instead water-saturated. First examples of observed AVO data interpreted in this way were given by Ostrander [91].

Shuey [92] has re-expressed the Zoeppritz equations in a way which isolates the combination of media properties which can be determined explicitly from the variation of amplitude with incident angle. He also derived analytic approximations to the equations which are valid for different ranges of incident angle. Further approximations relating incident and reflected *P* waves were derived by Mallick [93].

AVO analysis of seismic reflection data has become an important application of the Zoeppritz equations [94], and the program presented here can be used to predict the AVO behaviour for any media properties and any angle of incidence. It can also be used to predict the behaviour of incident and reflected shear waves, which is likely to become the subject of greater attention in the future.

9. ACKNOWLEDGEMENTS

We are indebted to Professor Alan Douglas for reviewing the manuscript, and for his many useful suggestions. We also thank Dr John Hudson for reading several versions and for providing much helpful criticism. Dr David Bowers helped with the graphic displays.

REFERENCES

1. R G Pearce: "Fault plane solutions using relative amplitudes of *P* and *pP*". Geophys J R Astr Soc **50**, 381–394 (1977)

2. R G Pearce: "Earthquake focal mechanisms from relative amplitudes of *P*, *pP* and *sP*: method and computer program". AWRE Report No. O 41/79, HMSO (1979)

3. R G Pearce: "Fault plane solutions using relative amplitudes of *P* and surface reflections: further studies". Geophys J R Astr Soc **60**, 459–488 (1980)

4. R G Pearce and R M Rogers: "Determination of earthquake moment tensors from teleseismic relative amplitude observations". J Geophys Res **94**, 775–786 (1989)

5. C G Knott: "Reflection and refraction of elastic waves with seismological applications". Phil Mag **48**, 64–97 (1899)

6. K Zoeppritz: "Erdbebenwellen VIIB: Über Reflexion und Durchgang seismischer Wellen durch Unstetigkeitsflächen". Nachr der Königlichen Gesell d Wiss Göttingen. math. phys. Kl: 66–84 (1919)

7. C Blamey: "Amplitude coefficients for *P* and *SV* waves on an interface and on a free surface". Unpublished Note AG/74 AWRE (1967)

8. K McCamy, R P Meyer and T J Smith: "Generally applicable solutions of Zoeppritz amplitude equations". Bull Seism Soc Am **52**, 923–955 (1962)

9. H Kolsky: "Stress waves in solids". Clarendon (1953)

10. K Ergin: "Energy ratio of the seismic waves reflected and refracted at a rock water boundary". Bull Seism Soc Am **42**, 349–372 (1952)

11. S Crampin: "An introduction to wave propagation in anisotropic media". Geophys J R Astr Soc **76**, 17–28 (1984)

12. J A Stratton: "Electromagnetic theory". McGraw Hill (1941)

13. H J J Braddick: "Vibrations, waves and diffraction". McGraw Hill (1965)

14. D S Jones and D W Jordan: "Introductory Analysis Vol. 1". Wiley and Sons (1969)

15. K E Bullen: "An introduction to the theory of seismology". Third edition. Cambridge University Press (1965)

16. W M Ewing, W S Jardetsky and F Press: "Elastic waves in layered media". McGraw-Hill (1957)

17. H Jeffreys: "The Earth". Sixth Edition. Cambridge University Press (1976)

18. K E Bullen and B A Bolt: "An Introduction to the Theory of Seismology". Fourth Edition. Cambridge University Press (1985)

19. J A Hudson: "The excitation and propagation of elastic waves". Cambridge University Press (1980)

20. C B Officer: "Introduction to theoretical geophysics". Springer-Verlag (1974)

21. J K Costain, K L Cook and S T Algermissen: "Amplitude, energy and phase angles of plane *SV* waves and their application to Earth crustal studies". Bull Seism Soc Am **53**, 1039–1074 (1963)

22. S Mueller and M Landisman: "Seismic studies of the Earth's crust in continents I. Evidence for a low velocity zone in the upper part of the lithosphere". Geophys J R astr Soc **10**, 525–538 (1966)

23. G P Woollard: "Regional isostatic relations in the United States". In: "The Earth beneath the Continents". pp 557–594. J S Steinhart and T J Smith Eds. Geophysics Monograph No. 10, American Geophysical Union, Washington, D C (1966)

24. M Ewing: "The sediments of the Argentine basin". Q J R Astr Soc **6**, 10–27 (1965)

25. F K Levin: "When reflection coefficients are zero". Geophysics **51**, 736–741 (1986)

26. A Dziewonski and D L Anderson: "Preliminary Reference Earth Model". Phys Earth Planet Inter **25**, 297–356 (1981)

27. B A Bolt: "The velocity of seismic waves near the Earth's centre". Bull Seism Soc Am **54**, 191–208 (1964)

28. A B Wood: "A textbook of sound". Bell (1931)

29. E L Hamilton and R T Bachman: "Sound velocity and related properties of marine sediments". J Acoust Soc Am **72**, 1891–1903 (1982)

30. J A Mendiguren: "Focal mechanism of a shock in the middle of the Nazca plate". J Geophys Res **76**, 3861–3879 (1971)

31. R G Pearce: "Complex *P* waveforms from a Gulf of Aden earthquake". Geophys J R Astr Soc **64**, 187–200 (1981)

32. R Evans: "Effects of the free surface on shear wavetrains". Geophys J R Astr Soc **76**, 165–172 (1984)

33. C Y Fu: "Studies on seismic waves: I. Reflection and refraction of plane waves". Geophysics **11**, 1–9 (1946)

34. C E Richter: "Elementary Seismology". Freeman and Co (1958)

35. J K Costain, K L Cook and S T Algermissen: "Corrigendum: Amplitude, energy and phase angles of plane *SV* waves and their application to Earth crustal studies". Bull Seism Soc Am **55**, 567–575 (1965)

36. J S Singh, A Ben-Menahem and M Shimshoni: "Comments on papers by Costain et al on the solution of Zoeppritz' amplitude equations". Bull Seism Soc Am **60**, 277–280 (1970)

37. A L Hales and J L Roberts: "The Zoeppritz amplitude equations: more errors". Bull Seism Soc Am **64**, 285 (1974)

38. K Aki and P G Richards: "Quantitative Seismology, theory and methods". Vol. I. Freeman and Co (1980)

39. G B Young and L W Braile: "A computer program for the application of Zoeppritz's amplitude equations and Knott's energy equations". Bull Seism Soc Am **66**, 1881–1885 (1976)

40. J B Macelwane: "Introduction to theoretical seismology, Part 1 Geodynamics". Wiley (1936)

41. D Gubbins: "Seismology and plate tectonics". Cambridge University Press (1990)

42. M Muskat and M W Meres: "Reflection and transmission coefficients for plane waves in elastic media". Geophysics **5**, 115–148 (1940)

43. M Muskat: "The seismic wave energy reflected from various types of stratified horizon". Geophysics **5**, 149–155 (1940)

44. R Bortfeld: "Approximations to the reflection and transmission coefficients of plane longitudinal and transverse waves". Geophys Prosp **9**, 485–502 (1961)

45. O Koefoed: "Reflection and transmission coefficients for plane longitudinal incident waves". Geophys Prosp **10**, 304–351 (1962)

46. P F Daley and F Hron: "Wave methods for shear waves in elastic media". In: G Dohr Ed. "Seismic shear waves". Handbook of Geophysical Exploration Vol 15A, Geophysical Press (1985)

47. R D Tooley, T W Spencer and H F Sagoci: "Reflection and transmission of plane compressional waves". Geophysics **30**, 552–570 (1965)

48. D R Miles: "Three component seismic data: researchers' toy or interpreter's tool?". Leading Edge **7**, 28–31 (1988)

49. K H Waters: "Reflection seismology". John Wiley (1978)

50. R E Sheriff: "Encyclopedic Dictionary of Exploration Geophysics". Society of Exploration Geophysicists (1973)

51. R E Sheriff amended. Geophysics **40**, Supplement 2 No 213

52. H Jeffreys: "The Earth". Fourth Edition. Cambridge University Press (1962)

53. J D Achenbach: "Wave propagation in elastic solids". North Holland (1975)

54. J A Hudson: "The total internal reflection of *SH* waves". Geophys J R Astr Soc **6**, 509–531 (1962)

55. R Bortfeld: "Exact solution of the reflection and refraction of arbitrary spherical compressional waves at liquid-liquid interfaces and at solid-solid interfaces with equal shear velocities and equal densities". Geophys Prosp **10**, 35–67 (1962)

56. R Bortfeld: "Reflection and refraction of spherical compressional waves at arbitrary plane interfaces". Geophys Prosp **10**, 517–538 (1962)

57. P M Krail and H Brysk: "Reflection of spherical seismic waves in layered elastic media". Geophysics **48**, 655–664 (1983)

58. T J Fitch, D W McCowan and M W Shields: "Estimation of the seismic moment tensor from teleseismic body wave data with applications to intraplate and mantle earthquakes". J Geophys Res **85**, 3817–3828 (1980)

59. T W Fitch: "Correction and addition to 'Estimation of the seismic moment tensor from teleseismic body wave data with applications to intraplate and mantle earthquakes', by T J Fitch, D W McCowan and M W Shields". J Geophys Res **86**, 9375–9376 (1981)

60. V Červený and R Ravindra: "Theory of seismic headwaves". University of Toronto Press, Toronto (1971)

61. S Treitel, P R Gutowski and D E Wagner: "Plane-wave decomposition of seismograms". Geophysics **47**, 1375–1401 (1982)

62. D C Booth and S Crampin: "Shear wave polarisations on a curved wavefront at an isotropic free surface". Geophys J R Astr Soc **83**, 31–45 (1985)

63. F Wenzel, K-J Stenzel and U Zimmermann: "Wave propagation in laterally heterogeneous layered media". Geophys J Int **103**, 675–684 (1991)

64. R Sato: "The reflection of elastic waves on corrugated surface" Zisin(ii) **8**, 8–22 (1955)

65. J T Fokkema: "Reflection and refraction of time-harmonic elastic waves by the periodic interface between two elastic media". PhD Thesis, Delft University of Technology, The Netherlands (1979)

66. J T Fokkema: "Diffraction of elastic waves by the periodic rigid boundary of a semi-infinite solid". Proc Roy Soc Lond **A363**, 487–502 (1978)

67. J T Fokkema and P M van den Berg: "Elastodynamic diffraction by a periodic rough surface (stress-free boundary)". J Acoust Soc Am **62**, 1095–1101 (1977)

68. K Aki and K L Larner: "Surface motion of a layered medium having an irregular interface due to incident plane *SH* waves". J Geophys Res **75**, 933–954 (1970)

69. F Gilbert and L Knopoff: "Seismic scattering from topographic irregularities". J Geophys Res **65**, 3437–3444 (1960)

70. W L Pilant: "Elastic waves in the Earth". Developments in Solid Earth Geophysics 11. Elsevier (1979)

71. R N Gupta: "Reflection of elastic waves from a linear transition layer". Bull Seism Soc Am 56, 511–526 (1966)

72. R N Gupta: "Reflection of plane elastic waves from transition layers with arbitrary variation of velocity and density". Bull Seism Soc Am **56**, 633–642 (1966)

73. E R Lapwood, J A Hudson and V K Kembhavi: "The passage of elastic waves through an anomalous region—I. Transmission of body waves through a soft layer". Geophys J R Astr Soc **31**, 457–467 (1973)

74. E R Lapwood, J A Hudson and V K Kembhavi: "The passage of elastic waves through an anomalous region—II. Transmission through a layer between two different media". Geophys J R Astr Soc **40**, 241–254 (1975)

75. E R Lapwood and J A Hudson: "The passage of elastic waves through an anomalous region—III. Transmission of obliquely incident body waves". Geophys J R Astr Soc **40**, 255–268 (1975)

76. A M Ziolkowski and J T Fokkema: "The progressive attenuation of high-frequency energy in seismic reflection data". Geophys Prosp **34**, 981–1001 (1986)

77. S-J Chang: "Diffraction of plane dilatational waves by a finite crack". Q J Mech Appl Math **24**, 423–443 (1971)

78. G S Murty: "Reflection, transmission and attenuation of elastic waves at a loosely-bonded interface of two half spaces". Geophys J R Astr Soc **44**, 389–404 (1976)

79. M Schoenberg: "Elastic wave behaviour across linear slip interfaces". J Acoust Soc Am **68**, 1516–1521 (1980)

80. P B Nagy: "Ultrasonic classification of imperfect interfaces". J Non-destructive Evaluation **11**, 127–140 (1992)

81. J T Fokkema and A M Ziolkowski: "The critical reflection theorem". Geophysics **52**, 965–972 (1987)

82. R D Borcherdt: "Energy and plane waves in linear viscoelastic media". J Geophys Res **78**, 2442–2453 (1973)

83. R D Borcherdt: "Reflection and refraction of type-II *S* waves in elastic and anelastic media". Bull Seism Soc Am **67**, 43–67 (1977)

84. E S Krebes: "On the reflection and transmission of viscoelastic waves—some numerical results". Geophysics **49**, 1374–1380 (1984)

85. T Bourbié and A Gonzalez-Serrano: "Synthetic seismograms in attenuating media". Geophysics **48**, 1575–1587 (1983)

86. P G Kelamis, P G Kanasewich and F Abramovici: "Attenuation of seismograms obtained by the Cagniard-Pekeris method". Geophysics **48**, 1204–1211 (1983)

87. H F Cooper: "Reflection and transmission of oblique plane waves at a plane interface between two viscoelastic media." J Acoust Soc Am **42**, 1064–1069 (1967)

88. P W Buchen: "Reflection, transmission and diffraction of *SH* waves in linear viscoelastic solids". Geophys J R Astr Soc **23**, 531–542 (1971)

89. P F Daley and F Hron: "Reflection and transmission coefficients for transversely isotropic media". Bull Seism Soc Am **67**, 661–675 (1977)

90. O Koefoed: "On the effect of Poisson's ratios of rock strata on the reflection coefficients of plane waves". Geophys Prosp **3**, 381–387 (1955)

91. W J Ostrander: "Plane-wave reflection coefficients for gas sands at nonnormal angles of incidence". Geophysics **49**, 1637–1648 (1984)

92. R T Shuey: "A simplification of the Zoeppritz equations". Geophysics **50**, 609–614 (1985)

93. S Mallick: "A simple approximation to the *P*-wave reflection coefficient and its implication in the inversion of amplitude variation with offset data". Geophysics **58**, 544–552 (1993)

94. J P Castagna and M M Backus eds: "Theory and practice of AVO analysis". Investigations in Geophysics vol. 8, Society of Exploration Geophysicists, Tulsa, USA.

APPENDIX A

COMPUTER PROGRAM—BRIEF DESCRIPTION

The computer program for calculating the Zoeppritz equations was originally written as a series of subroutines in Fortran IV based upon the conventions given in Blamey [7]. This new version follows the sign convention established in this Report as summarised in figure 1. Justification for this convention is given in section 3.1, and differences from other work are explained in section 6. The new version is written in Fortran 77 with some extensions, and is compatible with Fortran 90.

The amplitude, phase and resulting angles of reflected and refracted *P* and *S* waves for a given incident *P* or *S* wave are computed by subroutine ZOMAT, which is given with its dependent subroutines in Appendix B1. The arguments in ZOMAT are used to input the wave type (*P* or *S*) and its incident amplitude and phase, with *S* separated for convenience into *S* in the ray plane normal to the interface (*SV*) and *S* in the plane of the interface (*SH*). Wave speed, density and layer type (solid, fluid or void) for each layer are input via COMMON blocks, which are used also for output. Full details are given in Appendix B1.

Appendix B2 gives an example of a driver for subroutine ZOMAT—subroutine ZOEPP. Subroutine ZOEPP is called once to generate output for any chosen combination of media types and incident wave type(s). ZOEPP calls subroutine ZOMAT once for each of a sweep of incident angles. This package, with added graphics, was used to generate the results shown in figures 2–49 of this report. Combinations of media are solid/solid, solid/fluid, fluid/solid, fluid/fluid, solid/void and fluid/void. Input data comprise the *P*-and *S*-wave speeds and density of the two media, with a switch to indicate whether the medium is solid, fluid, or void, and whether the incident wave is *P* or *S*. The output is available in an array and consists of tables of resulting angle, displacement amplitude, and phase of the incident and all resulting waves, as a function of incident angle. Full details are given in Appendix B2. The results may easily be graphed as in figures 2–49.

APPENDIX B

COMPUTER PROGRAM—LISTING AND DOCUMENTATION

B1. SUBROUTINE ZOMAT AND DEPENDENT SUBPROGRAMS

```
!
!
!
C     SUBROUTINE ZOMAT(TYPE,ANG,AMP1,PHASE1,AMP2,PHASE2)
C
C     Solution of the Zoeppritz equations for a single incident wave
C
C
Caveat : These subroutines are part of a suite of programs which is
C        software quality registered.  Software is supplied on the
C        understanding the  user  is responsible for validation and
C        accepts that the authors have no  liability for its use or
C        misuse.
C
C
C     This subroutine calculates the displacement amplitude, phase, and
C     resulting angle of each wave (in general reflected P, reflected S,
C     refracted P and refracted S) resulting from a P or S wave incident
C     at a given angle at the interface between two media with given
C     parameters.  The subroutine uses complex algebra so that both the
C     displacement amplitude and phase of each wave are calculated, and
C     evanescent waves (corresponding to super-critical and hence
C     complex angles of reflection and/or refraction) are fully treated.
C     Even the incident wave may be evanescent; this is useful if a
C     succession of interfaces is concatenated, and waves become super-
C     critical only in intermediate layers.  (However, because an
C     evanescent wave suffers frequency-dependent decay away from the
C     originating interface, an appropriate correction must be applied
C     to its amplitude before using it as an incident wave at a
C     subsequent interface.  If this is not done, amplitudes will only
C     be valid for transmission of an evanscent wave through a zero-
C     thickness layer.)
C
C     For definition of sign convention and other information see:
C     'Amplitude versus offset (AVO) and the Zoeppritz equations for
C     partitioning of seismic waves at an interface: theory, new
C     computer program, examples and review of past errors' by
C     R G Pearce and J B Young, AWE Report 03/96, HMSO 1997.
C
C     INPUT
C
C     Incident wave information is passed in as arguments thus:
C
C          TYPE     CHARACTER*2   'P ' for incident P; 'S ' for incident
C                                 S.  Often SV (the component of S in the
C                                 ray plane) or SH (the component of S
C                                 parallel to the interface) is considered
C                                 alone, in which case either AMP1 or AMP2
C                                 can be set to 0.0; see below)
C
C          ANG      COMPLEX*16    Angle of incidence in degrees.  For real
C                                 angles (normal travelling-wave case) set
C                                 the real part to the angle (between 0.0
C                                 and 90.0) and the imaginary part to 0.0.
C                                 For an evanescent incident wave the
C                                 imaginary part will be non-zero, and ANG
C                                 will normally be derived from the output
```

```
C                                 of a previous call to ZOMAT.
C
C          AMP1     REAL*8  )     If TYPE='P ', then AMP1 and PHASE1 are
C          PHASE1   REAL*8  )     the amplitude and phase of the incident
C          AMP2     REAL*8  )     P wave and AMP2 and PHASE2 are unused.
C          PHASE2   REAL*8  )     If TYPE='S ', then AMP1 and PHASE1 are
C                                 the amplitude and phase of the SV
C                                 component (ie in the ray plane) and AMP2
C                                 and PHASE2 are the amplitude and phase
C                                 of the SH component (ie parallel to the
C                                 interface).  PHASE1 and PHASE2 may be
C                                 set to 0.0 unless the incident wave is
C                                 an S wave which is not plane-polarised,
C                                 in which case PHASE1 and PHASE2 will be
C                                 different.  Normally AMP1 and AMP2
C                                 should be positive, with 'negative
C                                 polarity' being indicated by PHASE1
C                                 and/or PHASE2 being set to 180.0.  If
C                                 AMP1 or AMP2 are negative, its sign is
C                                 changed and 180.0 added to PHASE1 or
C                                 PHASE2 as appropriate.
C
C     The layer parameters are input via COMMON thus:
C
C       COMMON /LAYER1/
C
C          TYPE1    CHARACTER*8  Medium of incident layer.  'SOLID    '
C                                 or 'FLUID    '
C
C          URLI     REAL*8       P-wave speed in incident layer
C
C          VRLI     REAL*8       S-wave speed in incident layer.
C                                 Defaults to URLI/SQRT(3.0) (Poisson
C                                 solid).  Not used if TYPE1='FLUID    '
C
C          RRLI     REAL*8       Density of incident layer
C
C       COMMON /LAYER2/
C
C          TYPE2    CHARACTER*8  Medium of second layer.  'SOLID    ',
C                                 'FLUID    ' or 'VOID    '
C
C          URFII    REAL*8       P-wave speed in second layer.  Not used
C                                 if TYPE2='VOID    '
C
C          VRFII    REAL*8       S-wave speed in second layer.  Defaults
C                                 to URFII/SQRT(3.0) (Poisson solid).
C                                 Not used if TYPE2='FLUID    ' or
C                                 'VOID    '
C
C          RRFII    REAL*8       Density of second layer.  Not used if
C                                 TYPE2='VOID    '
C
C          Note: Wave speeds only appear as ratios in the formulae, as
C          do densities.  Any units may therefore be used for wave
C          speeds and densities
C
C     OUTPUT
C
C     The input and computed values of angle, amplitude, and phase of
C     each wave are stored in COMMON /ZOCOM/ thus:
C
C          AP,AAMP,APHASE       Angle, amplitude and phase of Incident P
C          ASV,BAMP,BPHASE      Angle, amplitude and phase of Incident SV
C          ARLP,CAMP,CPHASE     Angle, amplitude and phase of Reflected P
```

```
C           ARLSV,DAMP,DPHASE   Angle, amplitude and phase of Reflected SV
C           ARFP,EAMP,EPHASE    Angle, amplitude and phase of Refracted P
C           ARFSV,FAMP,FPHASE   Angle, amplitude and phase of Refracted SV
C           ASH,GAMP,GPHASE     Angle, amplitude and phase of Incident SH
C           ARLSH,HAMP,HPHASE   Angle, amplitude and phase of Reflected SH
C           ARFSH,IAMP,IPHASE   Angle, amplitude and phase of Refracted SH
C
C     In each case the angle is COMPLEX*16 and the amplitude and phase are
C     REAL*8.  For travelling waves the real part of angle will contain
C     the angle of incidence/reflection/refraction in degrees, and the
C     imaginary part will be zero.  For evansecent waves the imaginary
C     part will be non-zero.
C
C     The COMMON /ZOLOG/ contains logical variables defining the
C           existence (or otherwise) of the above waves.
C     The COMMON /ZOCMT/ defines constants required by the program
C           and can be changed to satisfy the precision of the host
C           computer.
C     The COMMON /ZOWSP/ is working space for the program including
C           space for the matrices defined by the formulae.
C
C     Subroutine ZOMAT calls associated subroutines SETUP and CINVERT,
C     and associated functions AMPLIT, PHASE, RESULT and CDASIN
C     (complex double-precision arc-sine) in addition to standard
C     library functions
C
      SUBROUTINE ZOMAT(TYPE,ANG,AMP1,PHASE1,AMP2,PHASE2)
      COMMON /LAYER1/TYPE1,URLI,VRLI,RRLI
      COMMON /LAYER2/TYPE2,URFII,VRFII,RRFII
      COMMON /ZOLOG/ LP,LSV,LRLP,LRLSV,LRFP,LRFSV,LSH,LRLSH,LRFSH
      COMMON /ZOCOM/ AP,AAMP,APHASE,ASV,BAMP,BPHASE,
     1               ARLP,CAMP,CPHASE,ARLSV,DAMP,DPHASE,
     2               ARFP,EAMP,EPHASE,ARFSV,FAMP,FPHASE,
     3               ASH,GAMP,GPHASE,ARLSH,HAMP,HPHASE,
     4               ARFSH,IAMP,IPHASE
      COMMON /ZOCMT/ RADEG,ZERO,SMALL,HALF,ONE,TWO,THREE,PI,NINETY,ONE80
      COMMON /ZOWSP/ TYPE8,U,UR,US,W,V,VR,X
      DIMENSION      O(4),T2(4),TYPE8(2),U(4,4),UR(4),US(4),W(4),
     1               V(2,2),VR(2),X(2)
      INTEGER I,J
      LOGICAL        LP,LSV,LRLP,LRLSV,LRFP,LRFSV,LSH,LRLSH,LRFSH
      COMPLEX*16     CRLA,CRLA2,CRLB,CRLB2,CRFE,CRFE2,CRFF,CRFF2,
     1               U,UR,US,W,V,VR,X,ANG,DANG,SDANG,CDASIN,A,B,G,
     2               AP,ASV,ARLP,ARLSV,ARFP,ARFSV,ASH,ARLSH,ARFSH,
     3               RESULT
      REAL*8         URLI,VRLI,RRLI,URFII,VRFII,RRFII,
     1               AMP1,PHASE1,AMP2,PHASE2,O,R,RADEG,
     2               ZERO,SMALL,HALF,ONE,TWO,THREE,PI,NINETY,ONE80,
     3               AAMP,APHASE,BAMP,BPHASE,CAMP,CPHASE,DAMP,DPHASE,
     4               EAMP,EPHASE,FAMP,FPHASE,GAMP,GPHASE,HAMP,HPHASE,
     5               IAMP,IPHASE,AMPLIT,PHASE
      CHARACTER*2    TYPE,T2,P,S,SH,SV
      CHARACTER*8    TYPE1,TYPE2,TYPE8,SOLID,FLUID,VOID,INCDNT,BLANK
      EQUIVALENCE (T2(1),TYPE8(2))
      DATA P/'P '/,S/'S '/,SV/'SV'/,SH/'SH'/,
     1     SOLID/'SOLID   '/,FLUID/'FLUID   '/,VOID/'VOID    '/,
     2     INCDNT/'Incident'/,BLANK/'        '/
C
C     INITIALISE ZOCMT VALUES, RESET ZOCOM TO ZERO AND ZOLOG TO FALSE
      CALL SETUP
      TYPE8(1)=INCDNT
      TYPE8(2)=BLANK
C
C     SET DENSITY RATIO
      R=RRFII/RRLI
```

```
C
C     SET DEFAULT WAVE SPEEDS
      IF(TYPE1.EQ.SOLID.AND.VRLI.LE.ZERO)VRLI=URLI/DSQRT(THREE)
      IF(TYPE2.EQ.SOLID.AND.VRFII.LE.ZERO)VRFII=URFII/DSQRT(THREE)
C
C     PROCESS INPUT FOR INCIDENT S
      IF(TYPE.NE.P)THEN
        T2(2)=S
C       INCIDENT SV PARAMETERS
        IF(AMP1.NE.ZERO)THEN
          LSV=.TRUE.
          ASV=ANG
          BAMP=AMP1
          BPHASE=PHASE1
          IF(AMP1.LT.ZERO)THEN
            BAMP=-BAMP
            BPHASE=BPHASE+ONE80
          ENDIF
        ENDIF
C       INCIDENT SH PARAMETERS
        IF(AMP2.NE.ZERO)THEN
          LSH=.TRUE.
          ASH=ANG
          GAMP=AMP2
          GPHASE=PHASE2
          IF(AMP2.LT.ZERO)THEN
            GAMP=-GAMP
            GPHASE=GPHASE+ONE80
          ENDIF
        ENDIF
C       WAVE-SPEED RATIOS FOR SNELL'S LAW
        O(1)=URLI/VRLI
        O(2)=ONE
        O(3)=URFII/VRLI
        O(4)=VRFII/VRLI
C
C      PROCESS INPUT FOR INCIDENT P
       ELSE
        T2(2)=P
C       INCIDENT P PARAMETERS
        IF(AMP1.NE.ZERO)THEN
          LP=.TRUE.
          AP=ANG
          AAMP=AMP1
          APHASE=PHASE1
          IF(AMP1.LT.ZERO)THEN
            AAMP=-AAMP
            APHASE=APHASE+ONE80
          ENDIF
        ENDIF
C       WAVE-SPEED RATIOS FOR SNELL'S LAW
        O(1)=ONE
        O(2)=VRLI/URLI
        O(3)=URFII/URLI
        O(4)=VRFII/URLI
      ENDIF
C
C     SET COMPLEX INCIDENT AMPLITUDES
      A=DCMPLX(AAMP*DCOS(APHASE/RADEG),AAMP*DSIN(APHASE/RADEG))
      B=DCMPLX(BAMP*DCOS(BPHASE/RADEG),BAMP*DSIN(BPHASE/RADEG))
      G=DCMPLX(GAMP*DCOS(GPHASE/RADEG),GAMP*DSIN(GPHASE/RADEG))
C
C     SET RESULTING ANGLES BY COMPLEX SNELL'S LAW
      DANG=ANG/RADEG
      SDANG=CDSIN(DANG)
```

```
      CRLA=CDASIN(SDANG*O(1))
      CRLA2=CRLA+CRLA
      CRLB=CDASIN(SDANG*O(2))
      CRLB2=CRLB+CRLB
      CRFE=CDASIN(SDANG*O(3))
      CRFE2=CRFE+CRFE
      CRFF=CDASIN(SDANG*O(4))
      CRFF2=CRFF+CRFF
C
C     SET UP P-SV MATRIX STANDARD EQUATION
      U(1,1) =  CDSIN(CRLA)
      U(1,2) =  CDCOS(CRLB)
      U(1,3) = -CDSIN(CRFE)
      U(1,4) =  CDCOS(CRFF)
      UR(1)  = -CDSIN(CRLA)*A
      US(1)  =  CDCOS(CRLB)*B
      U(2,1) =  CDCOS(CRLA)
      U(2,2) = -CDSIN(CRLB)
      U(2,3) =  CDCOS(CRFE)
      U(2,4) =  CDSIN(CRFF)
      UR(2)  =  CDCOS(CRLA)*A
      US(2)  =  CDSIN(CRLB)*B
      U(3,1) =  CDSIN(CRLA2)*VRLI*VRLI*URFII
      U(3,2) =  CDCOS(CRLB2)*VRLI*URLI*URFII
      U(3,3) =  CDSIN(CRFE2)*VRFII*VRFII*URLI*R
      U(3,4) = -CDCOS(CRFF2)*VRFII*URFII*URLI*R
      UR(3)  =  CDSIN(CRLA2)*VRLI*VRLI*URFII*A
      US(3)  = -CDCOS(CRLB2)*VRLI*URLI*URFII*B
      U(4,1) = -CDCOS(CRLB2)
      U(4,2) =  CDSIN(CRLB2)*(VRLI/URLI)
      U(4,3) =  CDCOS(CRFF2)*(URFII/URLI)*R
      U(4,4) =  CDSIN(CRFF2)*(VRFII/URLI)*R
      UR(4)  =  CDCOS(CRLB2)*A
      US(4)  =  CDSIN(CRLB2)*(VRLI/URLI)*B
C     SET UP P-SV MATRIX EQUATION ROW 3 FOR VOID LAYER
      IF(R.EQ.ZERO)THEN
        U(3,1) =  CDSIN(CRLA2)*VRLI
        U(3,2) =  CDCOS(CRLB2)*URLI
        U(3,3) =  ZERO
        U(3,4) =  ZERO
        UR(3)  =  CDSIN(CRLA2)*VRLI*A
        US(3)  = -CDCOS(CRLB2)*URLI*B
      ENDIF
C     SET UP P-SV MATRIX EQUATION ROW 3 FOR FLUID/FLUID
      IF(R.GT.ZERO.AND.VRLI.LE.ZERO.AND.VRFII.LE.ZERO)THEN
        U(3,1) =  ZERO
        U(3,2) =  CDCOS(CRLB2)*URLI*URFII
        U(3,3) =  ZERO
        U(3,4) = -CDCOS(CRFF2)*URFII*URLI*R
        UR(3)  =  ZERO
        US(3)  = -CDCOS(CRLB2)*URLI*URFII*B
      ENDIF
C
C     IF INCIDENT S, SET UP SH MATRIX EQUATION AND REORDER RH
C     COLUMNS OF P-SV MATRIX EQUATION
      IF(TYPE.NE.P)THEN
        V(1,1) =  DCMPLX(ONE,ZERO)
        V(1,2) = -DCMPLX(ONE,ZERO)
        VR(1)  = -DCMPLX(ONE,ZERO)*G
        V(2,1) =  CDCOS(CRLB)*VRLI
        V(2,2) =  CDCOS(CRFF)*VRFII*R
        VR(2)  =  CDCOS(CRLB)*VRLI*G
        UR(1)  =  US(1)
        UR(2)  =  US(2)
        UR(3)  =  US(3)
```

```
        UR(4)  =  US(4)
C
C     IF INCIDENT S, SOLVE SH MATRIX EQUATION AND SET OUTPUT PARAMETERS
        CALL CINVERT(V,2,2)
        DO J=1,2
          X(J)=DCMPLX(ZERO,ZERO)
          DO I=1,2
            X(J)=X(J) + V(J,I)*VR(I)
          ENDDO
        ENDDO
        HAMP = AMPLIT(X(1),VRLI)
        IAMP = AMPLIT(X(2),VRFII)
        HPHASE = PHASE(X(1),VRLI) * RADEG
        IPHASE = PHASE(X(2),VRFII) * RADEG
        IF(AMP2.NE.ZERO)THEN
          LSH = .TRUE.
          ARLSH = RESULT(CRLB,VRLI) * RADEG
          ARFSH = RESULT(CRFF,VRFII) * RADEG
          IF(TYPE1.EQ.SOLID)LRLSH = .TRUE.
          IF(TYPE2.EQ.SOLID)LRFSH = .TRUE.
        ENDIF
      ENDIF
C
C     SOLVE P-SV MATRIX EQUATION AND SET OUTPUT PARAMETERS
      CALL CINVERT(U,4,4)
      DO J=1,4
        W(J)=DCMPLX(ZERO,ZERO)
        DO I=1,4
          W(J)=W(J) + U(J,I)*UR(I)
        ENDDO
      ENDDO
      CAMP = AMPLIT(W(1),RRLI)
      DAMP = AMPLIT(W(2),VRLI)
      EAMP = AMPLIT(W(3),RRFII)
      FAMP = AMPLIT(W(4),VRFII)
      CPHASE = PHASE(W(1),RRLI) * RADEG
      DPHASE = PHASE(W(2),VRLI) * RADEG
      EPHASE = PHASE(W(3),RRFII) * RADEG
      FPHASE = PHASE(W(4),VRFII) * RADEG
      IF(AMP1.NE.ZERO)THEN
        ARLP  = RESULT(CRLA,RRLI) * RADEG
        ARLSV = RESULT(CRLB,VRLI) * RADEG
        ARFP  = RESULT(CRFE,RRFII) * RADEG
        ARFSV = RESULT(CRFF,VRFII) * RADEG
      ENDIF
      IF(.NOT.LP.AND..NOT.LSV.AND.LSH)RETURN
      IF(TYPE1.EQ.SOLID.OR.TYPE1.EQ.FLUID)LRLP = .TRUE.
      IF(TYPE2.EQ.SOLID.OR.TYPE2.EQ.FLUID)LRFP = .TRUE.
      IF(TYPE1.EQ.SOLID)LRLSV = .TRUE.
      IF(TYPE2.EQ.SOLID)LRFSV = .TRUE.
C
      RETURN
      END
!
!
!
      FUNCTION AMPLIT(UDE,VEL)
      COMMON /ZOCMT/ RADEG,ZERO,SMALL
      REAL*8         RADEG,ZERO,SMALL,AMPLIT,VEL
      COMPLEX*16 UDE
C
      AMPLIT=ZERO
      IF(DABS(VEL).LE.SMALL)RETURN
      AMPLIT=CDABS(UDE)
      RETURN
```

```
      END
!
!
!
      FUNCTION PHASE(ANGLE,VELOC)
      COMMON /ZOCMT/ RADEG,ZERO,SMALL,HALF,ONE,TWO,THREE,PI
      REAL*8         RADEG,ZERO,SMALL,HALF,ONE,TWO,THREE,PI
      REAL*8 VELOC,PHASE,AMPLIT,IMAGIN
      COMPLEX*16 ANGLE
C
      PHASE=ZERO
      IF(DABS(VELOC).LE.SMALL)RETURN
      AMPLIT=DREAL(ANGLE)
      IMAGIN=DIMAG(ANGLE)
      IF(DABS(AMPLIT).LE.SMALL)RETURN
      PHASE=DATAN2(IMAGIN,AMPLIT)
      RETURN
      END
!
!
!
      FUNCTION RESULT(ANGLE,VELOC)
      COMMON /ZOCMT/ RADEG,ZERO,SMALL
      REAL*8         RADEG,ZERO,SMALL,VELOC
      COMPLEX*16 ANGLE,RESULT
C
      RESULT=DCMPLX(ZERO,ZERO)
      IF(DABS(VELOC).LE.SMALL)RETURN
      RESULT=ANGLE
      IF(DABS(DIMAG(ANGLE)).LE.SMALL)THEN
        RESULT=DCMPLX(DREAL(ANGLE),ZERO)
      ENDIF
      RETURN
      END
!
!
!
      FUNCTION CDASIN(Z)
C
C     COMPLEX DOUBLE PRECISION ARC-SINE FUNCTION
C     (USES STANDARD FORMULA - E.G. J W DETTMAN 'APPLIED COMPLEX
C     VARIABLES' MACMILLAN (1965) P61)
C
      COMMON /ZOCMT/ RADEG,ZERO,SMALL,HALF,ONE,TWO,THREE,PI,NINETY,ONE80
      REAL*8         RADEG,ZERO,SMALL,HALF,ONE,TWO,THREE,PI,NINETY,ONE80
      COMPLEX*16 CDASIN,Z,W
C
      W=CDSQRT(Z*Z-ONE)
      W=CDLOG(Z+W)
      CDASIN=DCMPLX(PI/TWO-DIMAG(W),DREAL(W))
      RETURN
      END
!
!
!
C     Complex matrix inversion routine
C     ********************************
C
C     Method : Direct Gaussian Elimination With Full Pivoting
C     Restriction on matrix type (symmetric etc) : None
C
C     This is a modifed version of the 'gaussj' routine from
C     Numerical Recipes in FORTRAN
C
C     Calling cinvert(A,n,np)
```

```
C     ***********************
C
C     A(1:n,1:n) is the complex input matrix
C     A is stored in a matrix of dimension np*np (A(np,np))
C     n is the number of rows (or columns) of A that are used
C     On exit from the routine, A contains the inverse
C
      SUBROUTINE CINVERT(A,N,NP)
      INTEGER N,NP,NMAX,I,ICOL,IROW,J,K,L,LL,INDXC,INDXR,IPIV
      COMPLEX*16 A,DUM,PIVINV
      DOUBLE PRECISION BIG
      DIMENSION A(NP,NP),INDXC(50),INDXR(50),IPIV(50)
      DATA NMAX/50/
C
      DO J=1,NMAX
         IPIV(J)=0
      ENDDO
C
      DO I=1,N
         BIG=0.0D0
         DO J=1,N
          IF(IPIV(J).NE.1)THEN
            DO K=1,N
              IF (IPIV(K).EQ.0) THEN
                IF (CDABS(A(J,K)).GE.BIG)THEN
                  BIG=CDABS(A(J,K))
                  IROW=J
                  ICOL=K
                ENDIF
              ELSE IF (IPIV(K).GT.1) THEN
                WRITE (6,6)
    6           FORMAT(' Singular Matrix In CINVERT ')
              ENDIF
            ENDDO
          ENDIF
        ENDDO
C
        IPIV(ICOL)=IPIV(ICOL)+1
        IF (IROW.NE.ICOL) THEN
          DO L=1,N
            DUM=A(IROW,L)
            A(IROW,L)=A(ICOL,L)
            A(ICOL,L)=DUM
          ENDDO
        ENDIF
        INDXR(I)=IROW
        INDXC(I)=ICOL
        IF (A(ICOL,ICOL).EQ.0.0) WRITE (6,6)
        PIVINV=1.0/A(ICOL,ICOL)
        A(ICOL,ICOL)=(1.0D0,0.0D0)
        DO L=1,N
          A(ICOL,L)=A(ICOL,L)*PIVINV
        ENDDO
        DO LL=1,N
          IF(LL.NE.ICOL)THEN
            DUM=A(LL,ICOL)
            A(LL,ICOL)=(0.0D0,0.0D0)
            DO L=1,N
              A(LL,L)=A(LL,L)-A(ICOL,L)*DUM
            ENDDO
          ENDIF
        ENDDO
      ENDDO
      DO L=N,1,-1
        IF(INDXR(L).NE.INDXC(L))THEN
```

```
            DO K=1,N
              DUM=A(K,INDXR(L))
              A(K,INDXR(L))=A(K,INDXC(L))
              A(K,INDXC(L))=DUM
            ENDDO
          ENDIF
        ENDDO
C
        RETURN
        END
```

B2. SUBROUTINES ZOEPP AND SET—EXAMPLE OF A DRIVER FOR ZOMAT

```
!
!
!
C     SOLUTION OF ZOEPPRITZ' AMPLITUDE EQUATIONS FOR VARIOUS MEDIA
C
C
Caveat : These subroutines are part of a suite of programs which is
C        software quality registered.  Software is supplied on the
C        understanding the user is responsible for validation and
C        accepts that the authors have no liability for its use or
C        misuse.
C
C
C        SUBROUTINE ZOEPP(ALF1,BET1,RHO1,IND1,LAY1,
C                         ALF2,BET2,RHO2,IND2,LAY2,
C                         AMP1,PHASE1,AMP2,PHASE2,
C                         T,N,M,SANG,DANG,WAVE)
C
C     SUBROUTINE ZOEPP        This is an example driver for the
C     Zoeppritz coefficient subroutine ZOMAT.  It generates results for
C     a range of incident angles for either an incident P wave, pure SV
C     wave, pure SH wave, or S wave (resolved into SV and SH).  The
C     angles of incidence may comprise a single value or a sweep of
C     values with constant increment up to the complete range of angles
C     from normal to glancing incidence.  The same displacement
C     amplitude and phase for all angles of incidence in the sweep is
C     used.  This subroutine does not exploit the full generality
C     of subroutine ZOMAT in that only real angles of incidence are
C     permitted (ie evanescent incident waves are excluded - see
C     subroutine ZOMAT).  Treatment of evanescent reflected and
C     refracted waves is included.  An associated subroutine SET sets
C     up the output results matrix (see below).
C
C     For definition of sign convention and other information see:
C     'Amplitude versus offset (AVO) and the Zoeppritz equations for
C     partitioning of seismic waves at an interface: theory, new
C     computer program, examples and review of past errors' by
C     R G Pearce and J B Young, AWE Report 03/96, HMSO 1997.
C
C     DESCRIPTION OF PARAMETERS (all double precision)
C
C     ALF1   P-wave speed in the incident layer  (inout)
C     BET1   S-wave speed in the incident layer  (inout)
C     RHO1   Density of incident layer  (inout)
C            (Note: Wave speeds only appear as ratios in the formulae,
C            as do densities.  Any units may therefore be used for wave
C            speeds and densities)
C     IND1   Indicator for the incident layer  (in)
C            IND1 = 0   Fluid layer, Incident P
```

```
C             IND1 = 1   Solid layer, Incident P
C             IND1 = 2   Solid layer, Incident SV
C             IND1 = 3   Solid layer, Incident SH
C             IND1 = 4   Solid layer, Incident S (resolved into SV and SH)
C      LAY1   Medium of incident layer  (out) ('SOLID   ' or
C             'FLUID   ')
C      ALF2   P-wave speed in second layer  (inout)
C      BET2   S-wave speed in second layer  (inout)
C      RHO2   Density of second layer (use zero for void)  (inout)
C      IND2   Indicator for second layer  (in)
C             IND2 = 0   Fluid layer
C             IND2.GT.0  Solid layer
C      LAY2   Medium of second layer  (out) ('SOLID   ', 'FLUID   '
C             or 'VOID    ')
C      AMP1,PHASE1 Displacement amplitude and phase in degrees of
C             incident P, SV or SH wave according to the value of IND1.
C             If IND1=4, these refer to incident SV  (in)
C      AMP2,PHASE2 Unused unless IND1=4, in which case these refer to
C             the amplitude and phase in degrees of incident SH  (in)
C      SANG   Value of first incident angle in degrees  (in)
C      DANG   Increment of incident angle for a sweep of angles  (in)
C             (If zero the single value of SANG only is computed)
C      M      is the number of real angles computed  (out)
C      N      is the total number of angles computed  (in)
C
C      Note.  In this subroutine, layer types (solid, fluid or void)
C      are determined by the values of IND1, IND2 and RHO2 alone, as
C      indicated above.  If BETA1 and/or BETA2 are zero, these will
C      default to Poisson solid values (see subroutine ZOMAT for
C      details)
C
C      RESULTS MATRIX
C
C      The results matrix is of the form (c.f. subroutine SET)
C             T(N,3,9)  (out)
C             WAVE(9)   (out)
C
C      The nine blocks in T(N,3,9) contain
C      1)   Incident P
C      2)   Incident SV
C      3)   Incident SH
C      4)   Reflected P
C      5)   Reflected SV
C      6)   Reflected SH
C      7)   Refracted P
C      8)   Refracted SV
C      9)   Refracted SH
C
C           WAVE contains the information on which blocks exist
C
C      The three blocks in T(N,3,9) contain, for each of the nine
C      blocks
C      1)   Incident or resulting angle in degrees
C      2)   Displacement amplitude (modulus)
C      3)   Phase in degrees
C
C      SPECIFIC CALLS FOR DIFFERENT INCIDENT WAVE TYPE AND MEDIA TYPE
C      COMBINATIONS
C
C      Although any combination of incident wave type an media types can
C      be specified in a call to ZOEPP as above, using appropriate values
C      of IND1 and IND2, subroutine ZOEPP is also provided with nine entry
C      points for the specific incident wave type and media type
C      combinations.  The arguments in these entry points have the same
C      meaning as in the call to ZOEPP.  In all incident S cases, AMP1 and
```

```
C     PHASE1 refer to the SV component, and AMP2 and PHASE2 refer to the
C     SH component.  Use of these calls is as follows
C
C     INCIDENT P   SOLID / SOLID  (statements 100)
C     CALL ZIPS2S(ALF1,BET1,RHO1,ALF2,BET2,RHO2,AMP1,PHASE1,
C     T,N,M,SANG,DANG)
C
C     INCIDENT S   SOLID / SOLID  (statements 200)
C     CALL ZISS2S(ALF1,BET1,RHO1,ALF2,BET2,RHO2,AMP1,PHASE1,AMP2,PHASE2,
C     T,N,M,SANG,DANG)
C
C     INCIDENT P   SOLID / VOID   (statements 300)
C     CALL ZIPS2V(ALF1,BET1,RHO1,AMP1,PHASE1,T,N,M,SANG,DANG)
C
C     INCIDENT S   SOLID / VOID   (statements 400)
C     CALL ZISS2V(ALF1,BET1,RHO1,AMP1,PHASE1,AMP2,PHASE2,
C     T,N,M,SANG,DANG)
C
C     INCIDENT P   SOLID / FLUID  (statements 500)
C     CALL ZIPS2F(ALF1,BET1,RHO1,ALF2,RHO2,AMP1,PHASE1,T,N,M,SANG,DANG)
C
C     INCIDENT S   SOLID / FLUID  (statements 600)
C     CALL ZISS2F(ALF1,BET1,RHO1,ALF2,RHO2,AMP1,PHASE1,AMP2,PHASE2,
C     T,N,M,SANG,DANG)
C
C     INCIDENT P   FLUID / SOLID  (statements 700)
C     CALL ZIPF2S(ALF1,RHO1,ALF2,BET2,RHO2,AMP1,PHASE1,T,N,M,SANG,DANG)
C
C     INCIDENT P   FLUID / FLUID  (statements 800)
C     CALL ZIPF2F(ALF1,RHO1,ALF2,RHO2,AMP1,PHASE1,T,N,M,SANG,DANG)
C
C     INCIDENT P   FLUID / VOID   (statements 900)
C     CALL ZIPF2V(ALF1,RHO1,AMP1,PHASE1,T,N,M,SANG,DANG)
C
      SUBROUTINE ZOEPP(ALF1,BET1,RHO1,IND1,LAY1,ALF2,BET2,RHO2,IND2,
     1LAY2,AMP1,PHASE1,AMP2,PHASE2,T,N,M,SANG,DANG,WAVE)
C
      DIMENSION T(181,3,9),WAVE(9),LAYER(3)
C
      COMMON /LAYER1/TYPE1,URLI,VRLI,RRLI
      COMMON /LAYER2/TYPE2,URFII,VRFII,RRFII
      COMMON /ZOLOG/ LP,LSV,LRLP,LRLSV,LRFP,LRFSV,LSH,LRLSH,LRFSH
      COMMON /ZOCOM/ AP,AAMP,APHASE,ASV,BAMP,BPHASE,
     1               ARLP,CAMP,CPHASE,ARLSV,DAMP,DPHASE,
     2               ARFP,EAMP,EPHASE,ARFSV,FAMP,FPHASE,
     3               ASH,GAMP,GPHASE,ARLSH,HAMP,HPHASE,
     4               ARFSH,IAMP,IPHASE
      COMMON /ZOCMT/ RADEG,ZERO,SMALL,HALF,ONE,TWO,THREE,PI,NINETY,ONE80
C
      COMPLEX*16 AP,ASV,ARLP,ARLSV,ARFP,ARFSV,ASH,ARLSH,ARFSH,ANG
      REAL*8 ALF1,BET1,RHO1,ALF2,BET2,RHO2,AMP1,PHASE1,AMP2,PHASE2,
     1AMPF1,PHASF1,AMPF2,PHASF2,T,SANG,DANG
      REAL*8 AAMP,BAMP,CAMP,DAMP,EAMP,FAMP,GAMP,HAMP,IAMP,
     1APHASE,BPHASE,CPHASE,DPHASE,EPHASE,FPHASE,GPHASE,HPHASE,IPHASE,
     2ANGMAX,URLI,VRLI,RRLI,URFII,VRFII,RRFII,
     3RADEG,ZERO,SMALL,HALF,ONE,TWO,THREE,PI,NINETY,ONE80
      INTEGER L,M,N,IND,IND1,IND2
      CHARACTER*8 TYPE1,LAY1,TYPE2,LAY2,LAYER
      LOGICAL WAVE,LP,LSV,LRLP,LRLSV,LRFP,LRFSV,LSH,LRLSH,LRFSH,FINISH
      DATA LAYER/'SOLID   ','FLUID   ','VOID    '/
C
      L=0
      M=N
      ANG=DCMPLX(SANG,ZERO)
C
```

```
      IND=IND1+1
      AMPF1=AMP1
      PHASF1=PHASE1
      AMPF2=AMP2
      PHASF2=PHASE2
      GO TO (1,1,1,4,5) IND
 1    AMPF2=ZERO
      PHASF2=ZERO
      GO TO 5
 4    AMPF1=ZERO
      PHASF1=ZERO
      AMPF2=AMP1
      PHASF2=PHASE1
C
 5    GO TO (10,40,70,70,70),IND
 10   IF(RHO2.NE.ZERO)GO TO 20
C     ZIPF2V
      TYPE1=LAYER(2)
      TYPE2=LAYER(3)
      GO TO 900
 20   IF(IND2.LE.0)GO TO 30
C     ZIPF2S
      TYPE1=LAYER(2)
      TYPE2=LAYER(1)
      GO TO 700
C     ZIPF2F
 30   TYPE1=LAYER(2)
      TYPE2=LAYER(2)
      GO TO 800
 40   IF(RHO2.NE.ZERO)GO TO 50
C     ZIPS2V
      TYPE1=LAYER(1)
      TYPE2=LAYER(3)
      GO TO 300
 50   IF(IND2.LE.0)GO TO 60
C     ZIPS2S
      TYPE1=LAYER(1)
      TYPE2=LAYER(1)
      GO TO 100
C     ZIPS2F
 60   TYPE1=LAYER(1)
      TYPE2=LAYER(2)
      GO TO 500
 70   IF(RHO2.NE.ZERO)GO TO 80
C     ZISS2V
      TYPE1=LAYER(1)
      TYPE2=LAYER(3)
      GO TO 400
 80   IF(IND2.LE.0)GO TO 90
C     ZISS2S
      TYPE1=LAYER(1)
      TYPE2=LAYER(1)
      GO TO 200
C     ZISS2F
 90   TYPE1=LAYER(1)
      TYPE2=LAYER(2)
      GO TO 600
C
C     INCIDENT P     SOLID / SOLID
C
      ENTRY ZIPS2S(ALF1,BET1,RHO1,ALF2,BET2,RHO2,AMP1,PHASE1,
     1T,N,M,SANG,DANG)
C
      L=0
      M=N
```

```
      AMPF1=AMP1
      PHASF1=PHASE1
      AMPF2=ZERO
      PHASF2=ZERO
      ANG=DCMPLX(SANG,ZERO)
      TYPE1=LAYER(1)
      TYPE2=LAYER(1)
      IND=2
C
 100  URLI=ALF1
      VRLI=BET1
      RRLI=RHO1
      URFII=ALF2
      VRFII=BET2
      RRFII=RHO2
      IF(URLI.LT.URFII)THEN
        ANGMAX=DASIN(URLI/URFII)*RADEG
       ELSE
        ANGMAX=NINETY
      ENDIF
 150  CALL ZOMAT('P ',ANG,AMPF1,PHASF1,ZERO,ZERO)
      CALL SET(T,L,M,ANG,DANG,ANGMAX,FINISH)
      IF(.NOT.FINISH)GO TO 150
      GO TO 1000
C
C     INCIDENT S     SOLID / SOLID
C
      ENTRY ZISS2S(ALF1,BET1,RHO1,ALF2,BET2,RHO2,AMP1,PHASE1,AMP2,
     1PHASE2,T,N,M,SANG,DANG)
C
      L=0
      M=N
      AMPF1=AMP1
      PHASF1=PHASE1
      AMPF2=AMP2
      PHASF2=PHASE2
      ANG=DCMPLX(SANG,ZERO)
      TYPE1=LAYER(1)
      TYPE2=LAYER(1)
      IND=5
C
 200  URLI=ALF1
      VRLI=BET1
      RRLI=RHO1
      URFII=ALF2
      VRFII=BET2
      RRFII=RHO2
      IF(URLI.LT.URFII)THEN
        ANGMAX=DMIN1(DASIN(VRLI/URLI),DASIN(VRLI/URFII))*RADEG
       ELSE
        ANGMAX=DASIN(VRLI/URLI)*RADEG
      ENDIF
 250  GO TO (290,290,260,270,280),IND
 260  CALL ZOMAT('S ',ANG,AMPF1,PHASF1,ZERO,ZERO)
      CALL SET(T,L,M,ANG,DANG,ANGMAX,FINISH)
      IF(.NOT.FINISH)GO TO 260
      GO TO 1000
 270  CALL ZOMAT('S ',ANG,ZERO,ZERO,AMPF2,PHASF2)
      CALL SET(T,L,M,ANG,DANG,ANGMAX,FINISH)
      IF(.NOT.FINISH)GO TO 270
      GO TO 1000
 280  CALL ZOMAT('S ',ANG,AMPF1,PHASF1,AMPF2,PHASF2)
      CALL SET(T,L,M,ANG,DANG,ANGMAX,FINISH)
      IF(.NOT.FINISH)GO TO 280
 290  GO TO 1000
```

```
C
C     INCIDENT P     SOLID / VOID
C
      ENTRY ZIPS2V(ALF1,BET1,RHO1,AMP1,PHASE1,T,N,M,SANG,DANG)
C
      L=0
      M=N
      AMPF1=AMP1
      PHASF1=PHASE1
      AMPF2=ZERO
      PHASF2=ZERO
      ANG=DCMPLX(SANG,ZERO)
      TYPE1=LAYER(1)
      TYPE2=LAYER(3)
      IND=2
C
 300  URLI=ALF1
      VRLI=BET1
      RRLI=RHO1
      URFII=ZERO
      VRFII=ZERO
      RRFII=ZERO
      ANGMAX=NINETY
 350  CALL ZOMAT('P ',ANG,AMPF1,PHASF1,ZERO,ZERO)
      CALL SET(T,L,M,ANG,DANG,ANGMAX,FINISH)
      IF(.NOT.FINISH)GO TO 350
      GO TO 1000
C
C     INCIDENT S     SOLID / VOID
C
      ENTRY ZISS2V(ALF1,BET1,RHO1,AMP1,PHASE1,AMP2,PHASE2,
     1T,N,M,SANG,DANG)
C
      L=0
      M=N
      AMPF1=AMP1
      PHASF1=PHASE1
      AMPF2=AMP2
      PHASF2=PHASE2
      ANG=DCMPLX(SANG,ZERO)
      TYPE1=LAYER(1)
      TYPE2=LAYER(3)
      IND=5
C
 400  URLI=ALF1
      VRLI=BET1
      RRLI=RHO1
      URFII=ZERO
      VRFII=ZERO
      RRFII=ZERO
      ANGMAX=DASIN(VRLI/URLI)*RADEG
 450  GO TO (490,490,460,470,480),IND
 460  CALL ZOMAT('S ',ANG,AMPF1,PHASF1,ZERO,ZERO)
      CALL SET(T,L,M,ANG,DANG,ANGMAX,FINISH)
      IF(.NOT.FINISH)GO TO 460
      GO TO 1000
 470  CALL ZOMAT('S ',ANG,ZERO,ZERO,AMPF2,PHASF2)
      CALL SET(T,L,M,ANG,DANG,ANGMAX,FINISH)
      IF(.NOT.FINISH)GO TO 470
      GO TO 1000
 480  CALL ZOMAT('S ',ANG,AMPF1,PHASF1,AMPF2,PHASF2)
      CALL SET(T,L,M,ANG,DANG,ANGMAX,FINISH)
      IF(.NOT.FINISH)GO TO 480
 490  GO TO 1000
C
```

```
C     INCIDENT P     SOLID / FLUID
C
      ENTRY ZIPS2F(ALF1,BET1,RHO1,ALF2,RHO2,AMP1,PHASE1,T,N,M,SANG,DANG)
C
      L=0
      M=N
      AMPF1=AMP1
      PHASF1=PHASE1
      AMPF2=ZERO
      PHASF2=ZERO
      ANG=DCMPLX(SANG,ZERO)
      TYPE1=LAYER(1)
      TYPE2=LAYER(2)
      IND=2
C
 500  URLI=ALF1
      VRLI=BET1
      RRLI=RHO1
      URFII=ALF2
      VRFII=ZERO
      RRFII=RHO2
      IF(URLI.LT.URFII)THEN
        ANGMAX=DASIN(URLI/URFII)*RADEG
       ELSE
        ANGMAX=NINETY
      ENDIF
 550  CALL ZOMAT('P ',ANG,AMPF1,PHASF1,ZERO,ZERO)
      CALL SET(T,L,M,ANG,DANG,ANGMAX,FINISH)
      IF(.NOT.FINISH)GO TO 550
      GO TO 1000
C
C     INCIDENT S     SOLID / FLUID
C
      ENTRY ZISS2F(ALF1,BET1,RHO1,ALF2,RHO2,AMP1,PHASE1,AMP2,PHASE2,
     1T,N,M,SANG,DANG)
C
      L=0
      M=N
      AMPF1=AMP1
      PHASF1=PHASE1
      AMPF2=AMP2
      PHASF2=PHASE2
      ANG=DCMPLX(SANG,ZERO)
      TYPE1=LAYER(1)
      TYPE2=LAYER(2)
      IND=5
C
 600  URLI=ALF1
      VRLI=BET1
      RRLI=RHO1
      URFII=ALF2
      VRFII=ZERO
      RRFII=RHO2
      IF(URLI.LT.URFII)THEN
        ANGMAX=DMIN1(DASIN(VRLI/URLI),DASIN(VRLI/URFII))*RADEG
       ELSE
        ANGMAX=DASIN(VRLI/URLI)*RADEG
      ENDIF
 650  GO TO (690,690,660,670,680),IND
 660  CALL ZOMAT('S ',ANG,AMPF1,PHASF1,ZERO,ZERO)
      CALL SET(T,L,M,ANG,DANG,ANGMAX,FINISH)
      IF(.NOT.FINISH)GO TO 660
      GO TO 1000
 670  CALL ZOMAT('S ',ANG,ZERO,ZERO,AMPF2,PHASF2)
      CALL SET(T,L,M,ANG,DANG,ANGMAX,FINISH)
```

```
      IF(.NOT.FINISH)GO TO 670
      GO TO 1000
 680  CALL ZOMAT('S ',ANG,AMPF1,PHASF1,AMPF2,PHASF2)
      CALL SET(T,L,M,ANG,DANG,ANGMAX,FINISH)
      IF(.NOT.FINISH)GO TO 680
 690  GO TO 1000
C
C     INCIDENT P     FLUID / SOLID
C
      ENTRY ZIPF2S(ALF1,RHO1,ALF2,BET2,RHO2,AMP1,PHASE1,T,N,M,SANG,DANG)
C
      L=0
      M=N
      AMPF1=AMP1
      PHASF1=PHASE1
      AMPF2=ZERO
      PHASF2=ZERO
      ANG=DCMPLX(SANG,ZERO)
      TYPE1=LAYER(2)
      TYPE2=LAYER(1)
      IND=1
C
 700  URLI=ALF1
      VRLI=ZERO
      RRLI=RHO1
      URFII=ALF2
      VRFII=BET2
      RRFII=RHO2
      ANGMAX=NINETY
 750  CALL ZOMAT('P ',ANG,AMPF1,PHASF1,ZERO,ZERO)
      CALL SET(T,L,M,ANG,DANG,ANGMAX,FINISH)
      IF(.NOT.FINISH)GO TO 750
      GO TO 1000
C
C     INCIDENT P     FLUID / FLUID
C
      ENTRY ZIPF2F(ALF1,RHO1,ALF2,RHO2,AMP1,PHASE1,T,N,M,SANG,DANG)
C
      L=0
      M=N
      AMPF1=AMP1
      PHASF1=PHASE1
      AMPF2=ZERO
      PHASF2=ZERO
      ANG=DCMPLX(SANG,ZERO)
      TYPE1=LAYER(2)
      TYPE2=LAYER(3)
      IND=1
C
 900  URLI=ALF1
      VRLI=ZERO
      RRLI=RHO1
      URFII=ZERO
      VRFII=ZERO
      RRFII=ZERO
      ANGMAX=NINETY
 950  CALL ZOMAT('P ',ANG,AMPF1,PHASF1,ZERO,ZERO)
      CALL SET(T,L,M,ANG,DANG,ANGMAX,FINISH)
      IF(.NOT.FINISH)GO TO 950
C
 1000 LAY1=TYPE1
      ALF1=URLI
      BET1=VRLI
      RHO1=RRLI
      LAY2=TYPE2
```

```
      ALF2=URFII
      BET2=VRFII
      RHO2=RRFII
      WAVE(1)=LP
      WAVE(2)=LSV
      WAVE(3)=LSH
      WAVE(4)=LRLP
      WAVE(5)=LRLSV
      WAVE(6)=LRLSH
      WAVE(7)=LRFP
      WAVE(8)=LRFSV
      WAVE(9)=LRFSH
C
      RETURN
      END
!
!
!
      SUBROUTINE SET(T,L,M,ANG,DANG,ANGMAX,FINIS)
      DIMENSION T(181,27)
C
C     This subroutine sets up the results matrix T in the form
C      1-3     Incident P
C      4-6     Incident SV
C      7-9     Incident SH
C     10-12    Reflected P
C     13-15    Reflected SV
C     16-18    Reflected SH
C     19-21    Refracted P
C     22-24    Refracted SV
C     25-27    Refracted SH
C
C     The three items for each of nine blocks are
C       1      Angle in degrees.  (The modulus of the complex angle
C              is given - this is equal to the real angle for angles
C              less than 90 degrees.  For evanescent waves the real
C              part equals 90 degrees but the imaginary part is non-
C              zero, so the modulus is greater than 90 degrees.  This
C              test can thus be used on Angle to determine whether a wave
C              is evanescent)
C       2      Amplitude (modulus)
C       3      Phase in degrees
C
C     This subroutine can be changed to suit any output requirements
C     (In particular, in its present form it does not preserve the
C     imaginary part of evanescent resulting angles)
C
      COMMON /ZOCOM/ AP,AAMP,APHASE,ASV,BAMP,BPHASE,
     1               ARLP,CAMP,CPHASE,ARLSV,DAMP,DPHASE,
     2               ARFP,EAMP,EPHASE,ARFSV,FAMP,FPHASE,
     3               ASH,GAMP,GPHASE,ARLSH,HAMP,HPHASE,
     4               ARFSH,IAMP,IPHASE
      COMMON /ZOCMT/ RADEG,ZERO,SMALL,HALF,ONE,TWO,THREE,PI,NINETY,ONE80
C
      COMPLEX*16 AP,ASV,ARLP,ARLSV,ARFP,ARFSV,ASH,ARLSH,ARFSH,ANG
      REAL*8 T,AAMP,BAMP,CAMP,DAMP,EAMP,FAMP,GAMP,HAMP,IAMP,
     1APHASE,BPHASE,CPHASE,DPHASE,EPHASE,FPHASE,GPHASE,HPHASE,IPHASE,
     2DANG,ANGMAX,RADEG,ZERO,SMALL,HALF,ONE,TWO,THREE,PI,NINETY,ONE80
      INTEGER L,M
      LOGICAL FINIS
C
      FINIS=.FALSE.
      L=L+1
C
      T(L,1)  = CDABS(AP)
```

```
      T(L,2)  = AAMP
      T(L,3)  = APHASE
      T(L,4)  = CDABS(ASV)
      T(L,5)  = BAMP
      T(L,6)  = BPHASE
      T(L,7)  = CDABS(ASH)
      T(L,8)  = GAMP
      T(L,9)  = GPHASE
      T(L,10) = CDABS(ARLP)
      T(L,11) = CAMP
      T(L,12) = CPHASE
      T(L,13) = CDABS(ARLSV)
      T(L,14) = DAMP
      T(L,15) = DPHASE
      T(L,16) = CDABS(ARLSH)
      T(L,17) = HAMP
      T(L,18) = HPHASE
      T(L,19) = CDABS(ARFP)
      T(L,20) = EAMP
      T(L,21) = EPHASE
      T(L,22) = CDABS(ARFSV)
      T(L,23) = FAMP
      T(L,24) = FPHASE
      T(L,25) = CDABS(ARFSH)
      T(L,26) = IAMP
      T(L,27) = IPHASE
C
      IF(DANG.EQ.ZERO)THEN
        M=L
        FINIS=.TRUE.
       RETURN
       ELSE
        ANG=ANG+DCMPLX(DANG,ZERO)
      ENDIF
C
      IF(DREAL(ANG).GT.NINETY)THEN
        FINIS=.TRUE.
       ELSEIF(DREAL(ANG).GT.ANGMAX)THEN
         M=L
         ANGMAX=NINETY
      ENDIF
C
      RETURN
      END
```

TABLE 1. Summary of cases classified according to wave-speed contrast and media type, showing Report section numbers (and figure numbers in parentheses). The wave-speed contrast is given as "high" if the *P*-wave speed in one medium is less than the *S*-wave speed in the other. For a solid/fluid interface, it is given as "anomalous" if the fluid has the higher *P*-wave speed; for a solid/solid interface it is given as "anomalous" if the *S* wave-speed contrast is opposite to that of the *P*-wave speed (this implies an anomalous Poisson's ratio). If none of these conditions applies it is given as "normal", or left blank if there is no option. * denotes that the density contrast is opposite to the *P* wave-speed contrast. See text for explanation of abbreviations.

	Medium i fluid				Medium i solid				
	Incident *P*	Real example used, if any	Wave-speed contrast		Incident *P*	Incident *SV*	Incident *SH*	Real example used, if any	Wave-speed contrast
Medium ii void	5.6 (49)	fluid free surface			5.5 (46)	5.5 (47)	5.5 (48)	solid free surface	
Medium ii fluid									
$U_{ii}>U_i$	5.4 (44)	deep-sea sediment/water			5.3.4 (40)	5.3.4 (41)	5.3.4 (42)		anomalous
$U_{ii}<U_i$	5.4 (45)	deep-sea sediment/water		$V_i<U_{ii}$	5.3.2 (24)	5.3.2 (25)	5.3.2 (26)	CMB–JB	normal*
					5.3.2 (28)	5.3.2 (29)	5.3.2 (30)	CMB–PREM	normal*
					5.3.3 (32)	5.3.3 (33)	5.3.3 (34)	ICB–JB	normal
					5.3.3 (36)	5.3.3 (37)	5.3.3 (38)	ICB–PREM	normal
				$V_i>U_{ii}$	5.3.1 (20)	5.3.1 (21)	5.3.1 (22)	sea bed	high
Medium ii solid									
$U_{ii}>U_i$ $V_{ii}<U_i$	5.3.2 (27)	CMB–JB	normal*	$V_i<V_{ii}$	5.2.1.2 (2)	5.2.1.3 (3)	5.2.1.4 (4)	Moho	normal
	5.3.2 (31)	CMB–PREM	normal*						
	5.3.3 (35)	ICB–JB	normal	$V_i>V_{ii}$	5.2.3 (14)	5.2.3 (15)	5.2.3 (16)		anomalous
	5.3.3 (39)	ICB–PREM	normal						
$V_{ii}>U_i$	5.3.1 (23)	sea bed	high		5.2.2 (8)	5.2.2 (9)	5.2.2 (10)		high
$U_{ii}<U_i$	5.3.4 (43)		anomalous	$V_i<U_{ii}$ $V_{ii}<V_i$	5.2.1.5 (5)	5.2.1.6 (6)	5.2.1.7 (7)	Moho	normal
				$V_{ii}>V_i$	5.2.3 (17)	5.2.3 (18)	5.2.3 (19)		anomalous
				$V_i>U_{ii}$	5.2.2 (11)	5.2.2 (12)	5.2.2 (13)		high

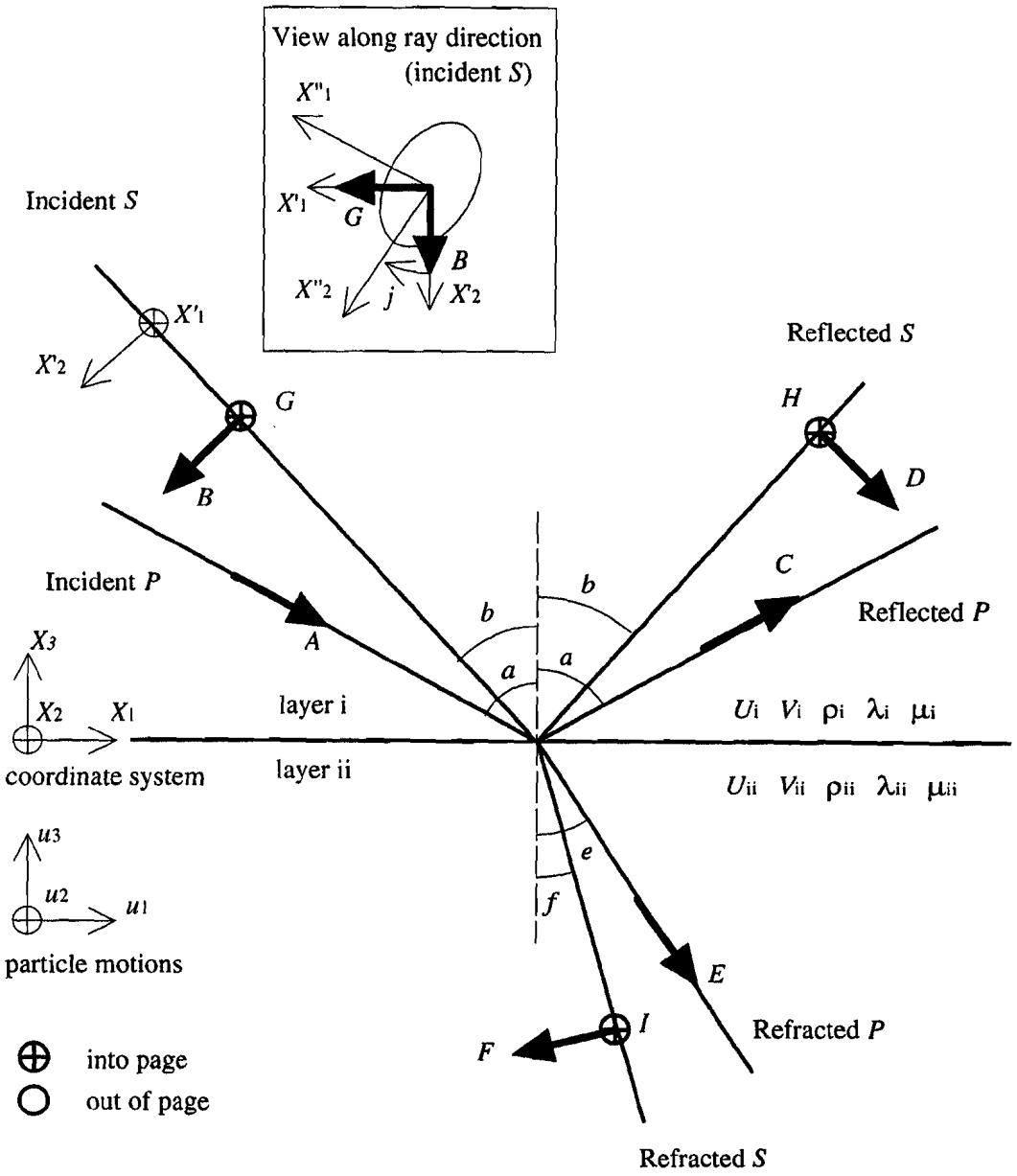

Figure 1 Notation used in this report for displacement amplitudes *A–I*, angles *a*, *b*, *e* and *f*, wave speeds and densities (see text for full description). Inset is a diagram to show the notation of *S*-wave polarisation characteristics.

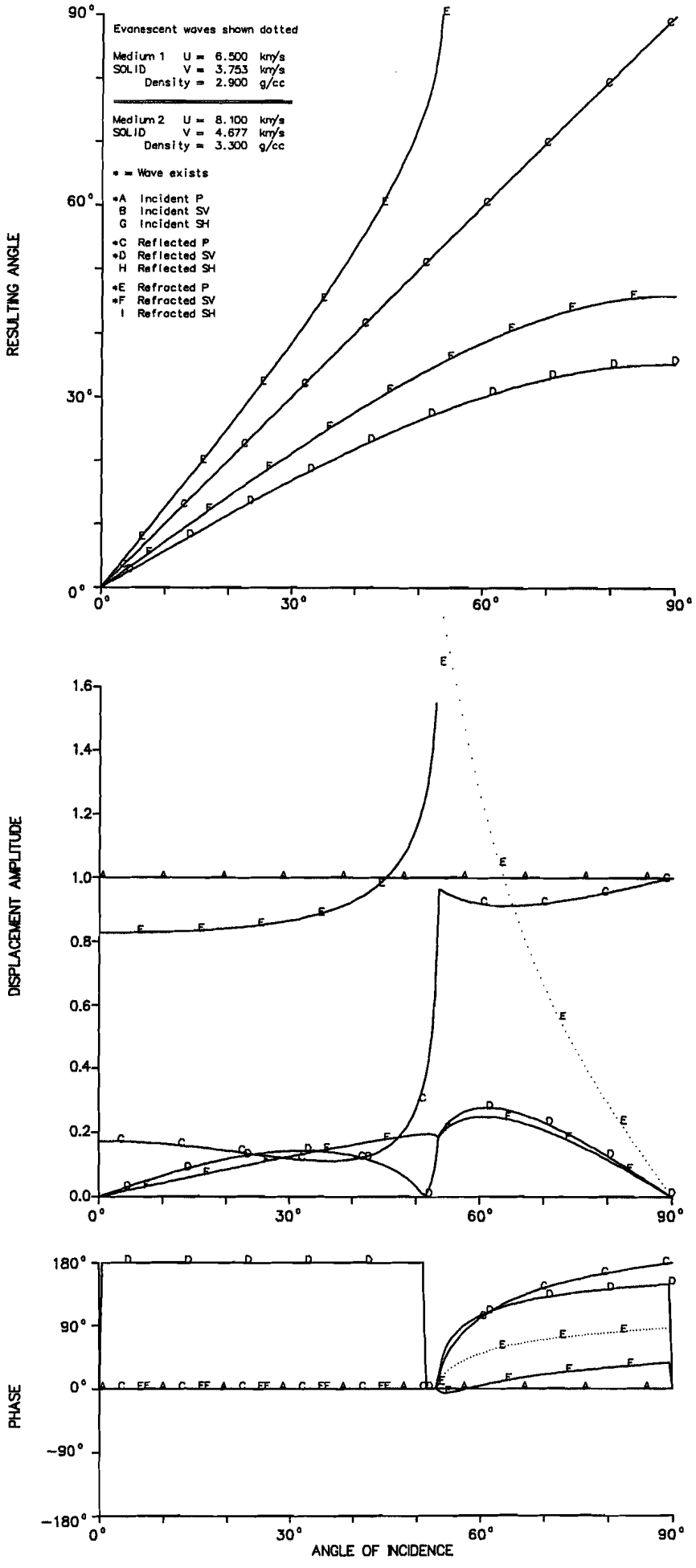

Figure 2. Solid–solid interface (Moho). Incident P from above.

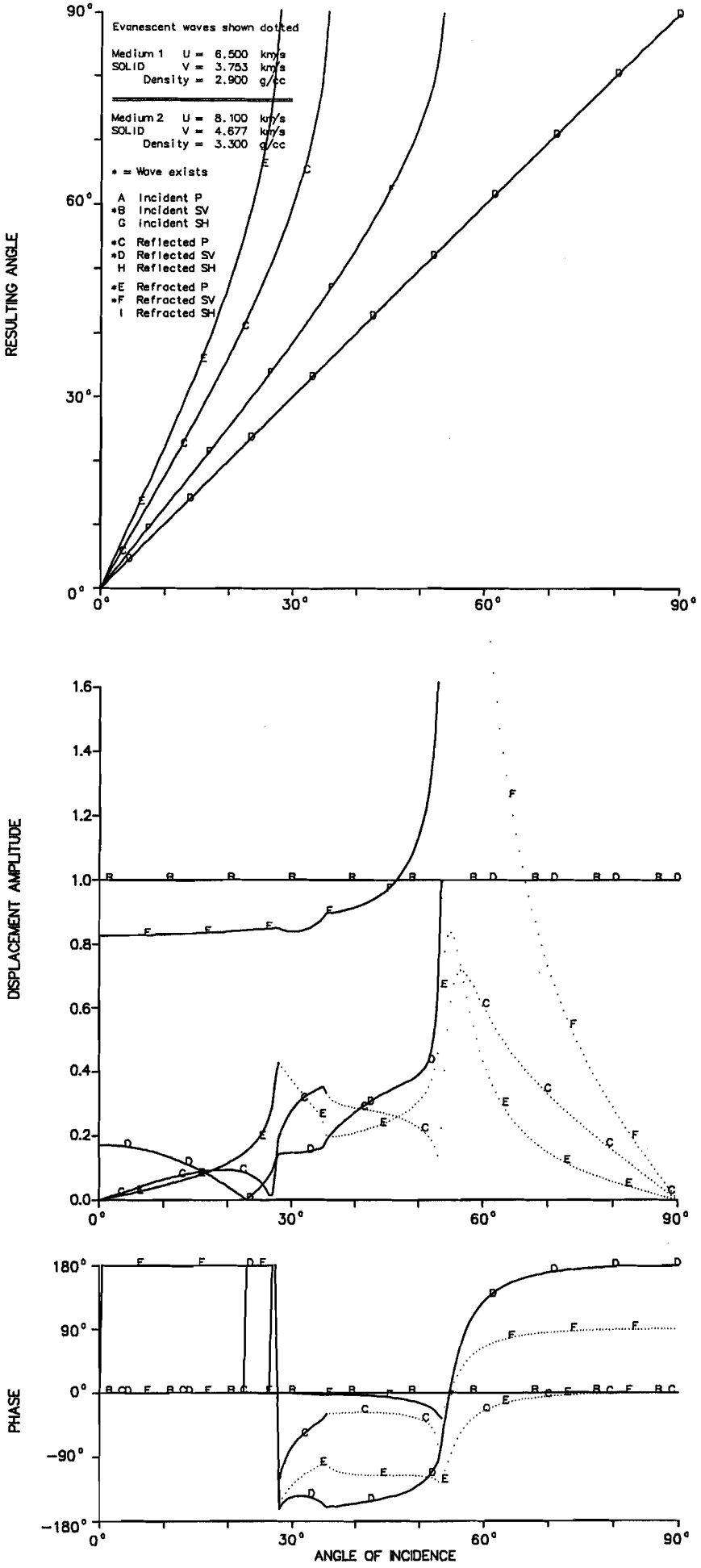

Figure 3. Solid–solid interface (Moho). Incident SV from above.

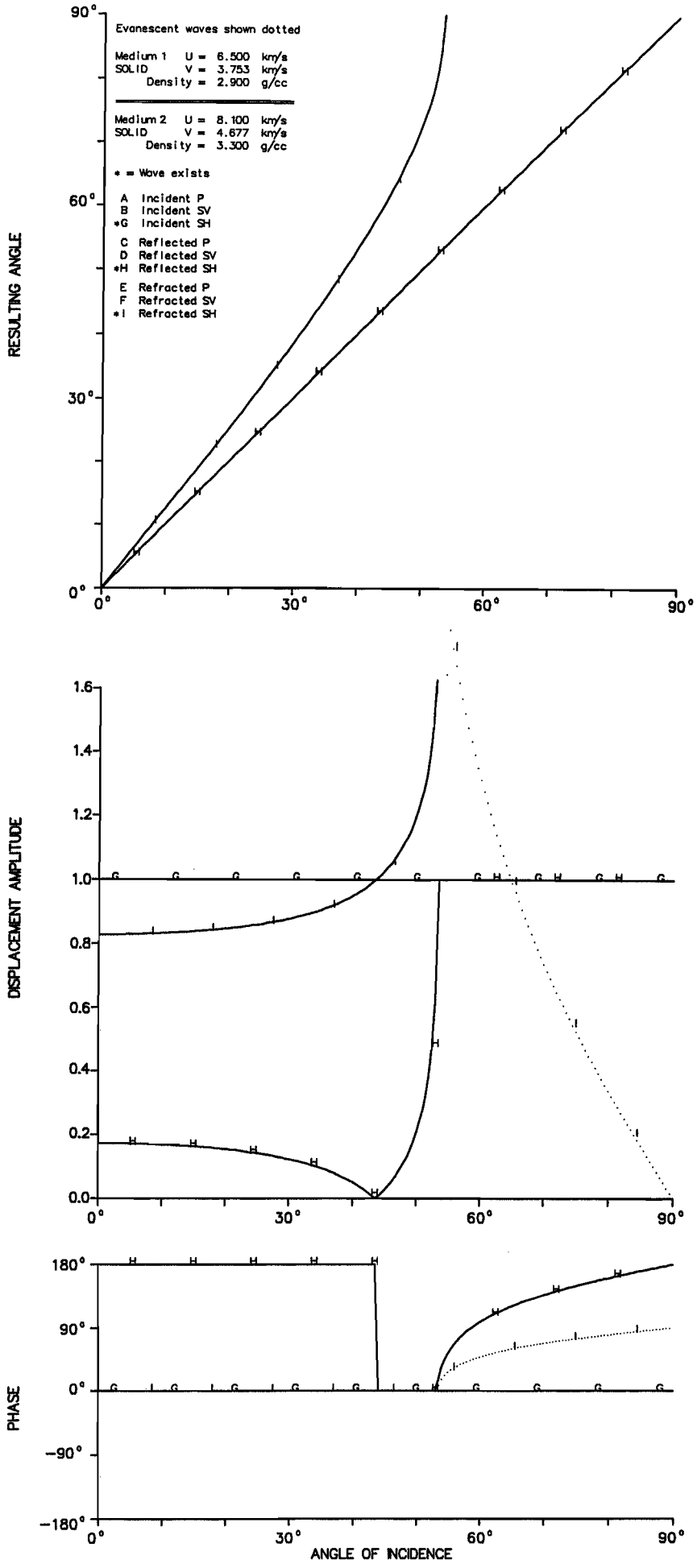

Figure 4. Solid–solid interface (Moho). Incident SH from above.

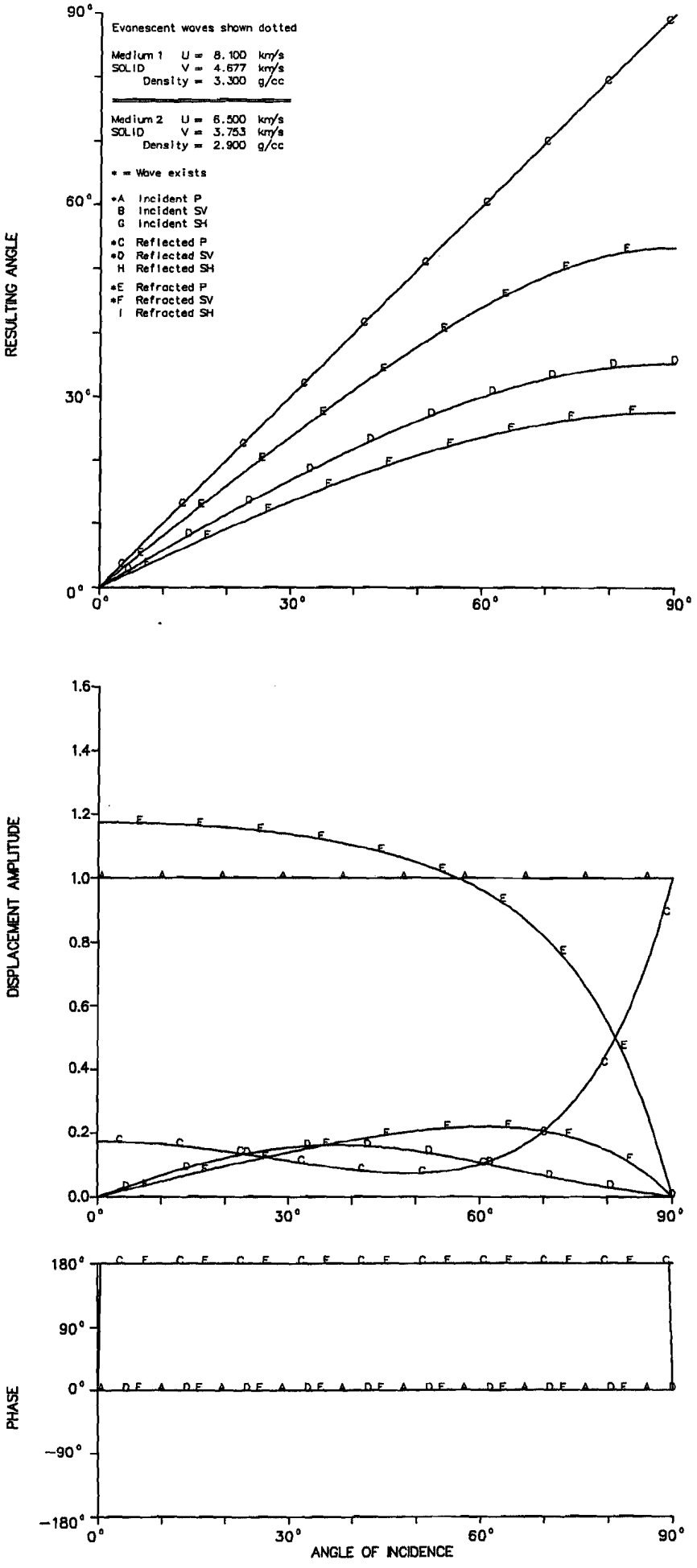

Figure 5. Solid–solid interface (Moho). Incident P from below.

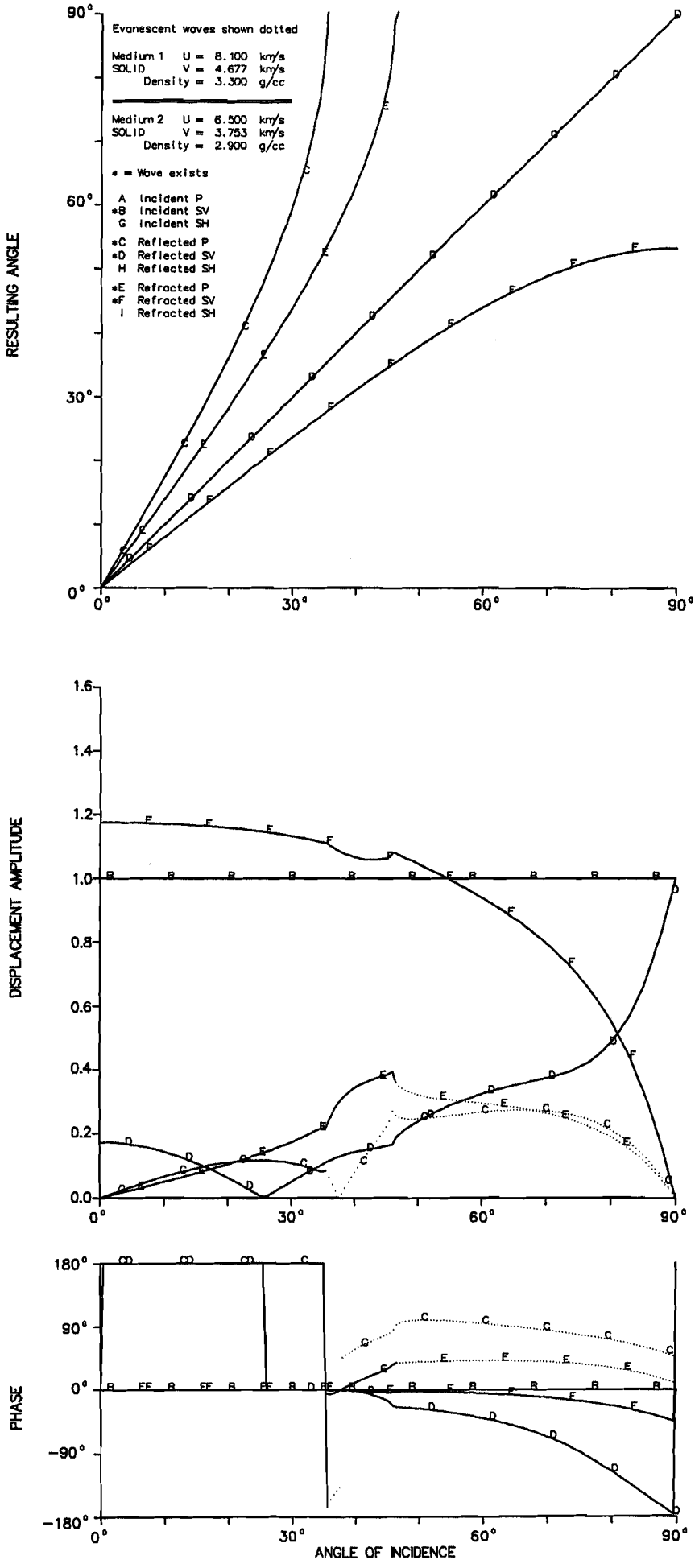

Figure 6. Solid–solid interface (Moho). Incident SV from below.

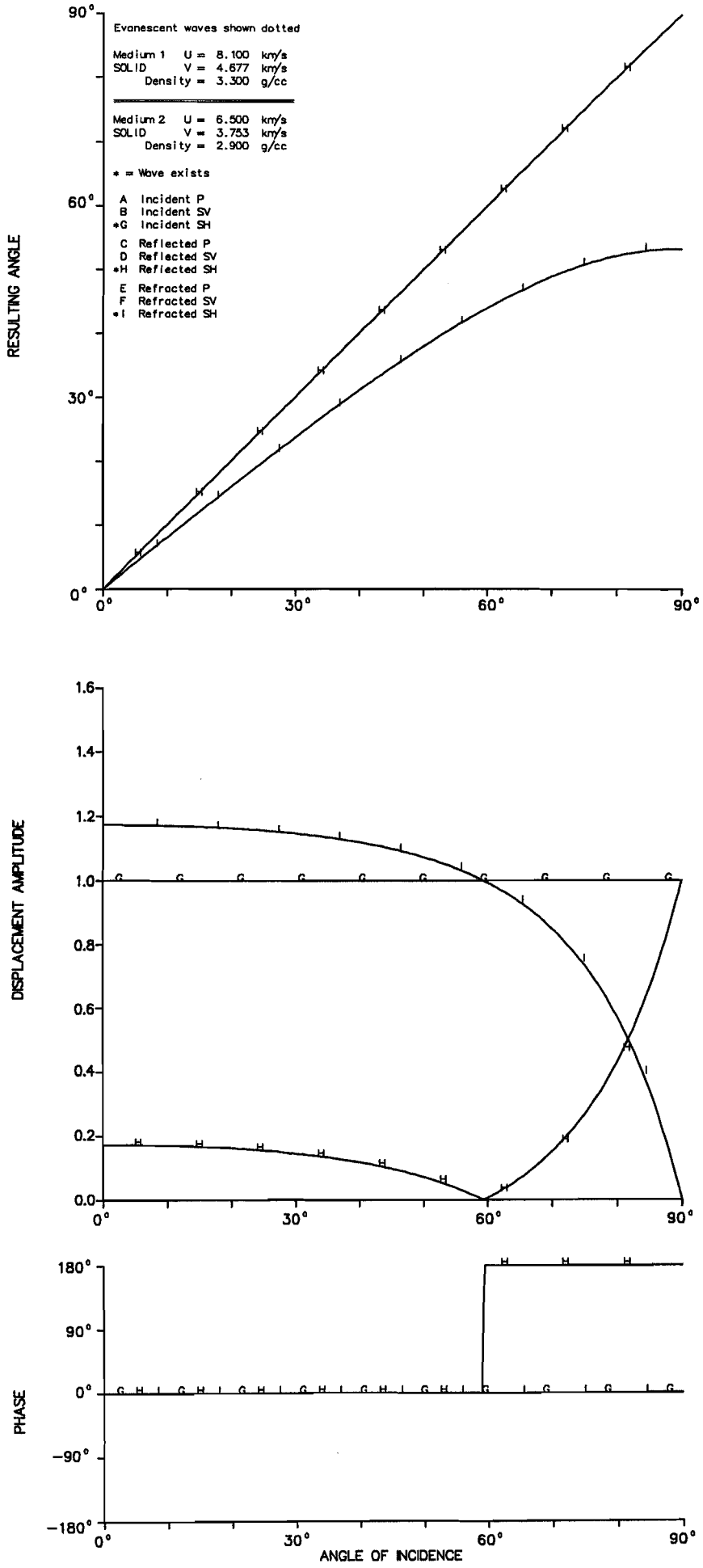

Figure 7. Solid–solid interface (Moho). Incident SH from below.

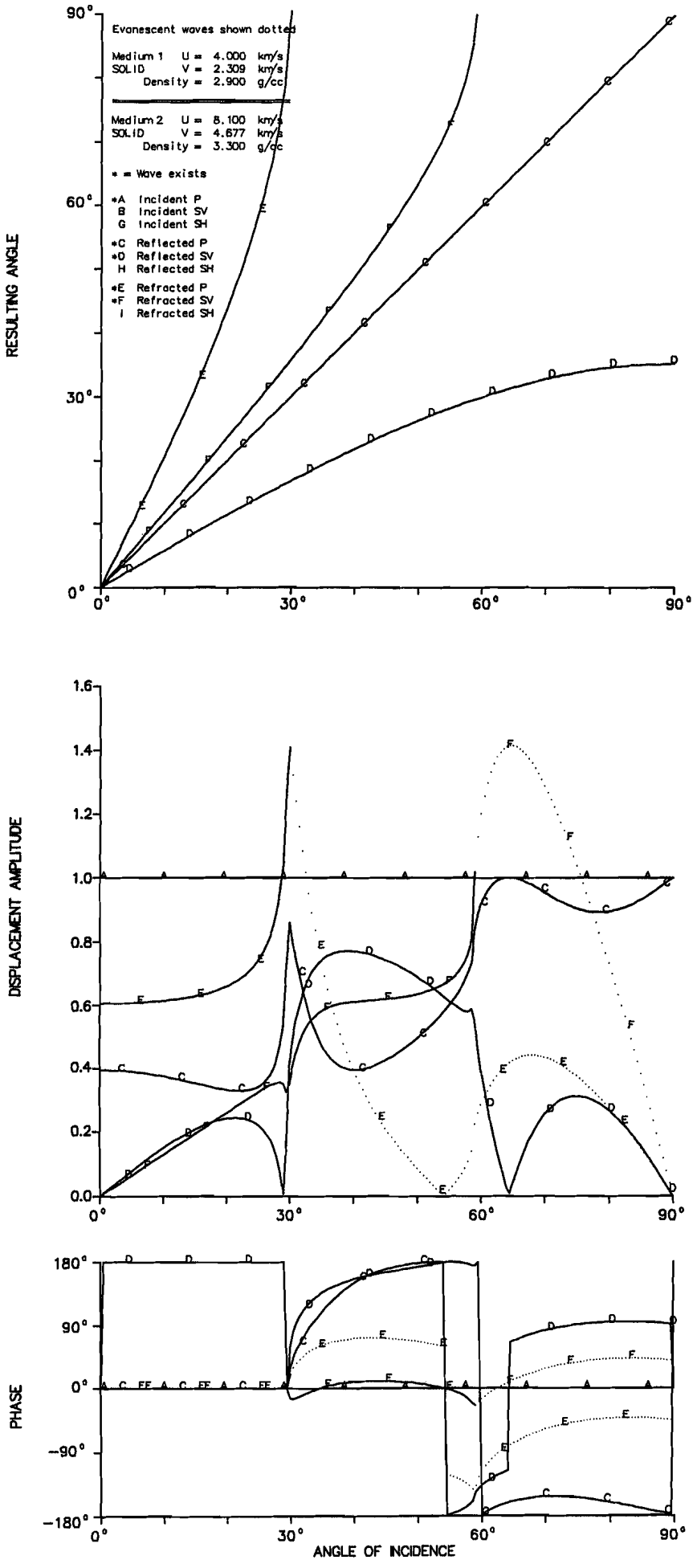

Figure 8. Solid–solid interface (high contrast). Incident P from above.

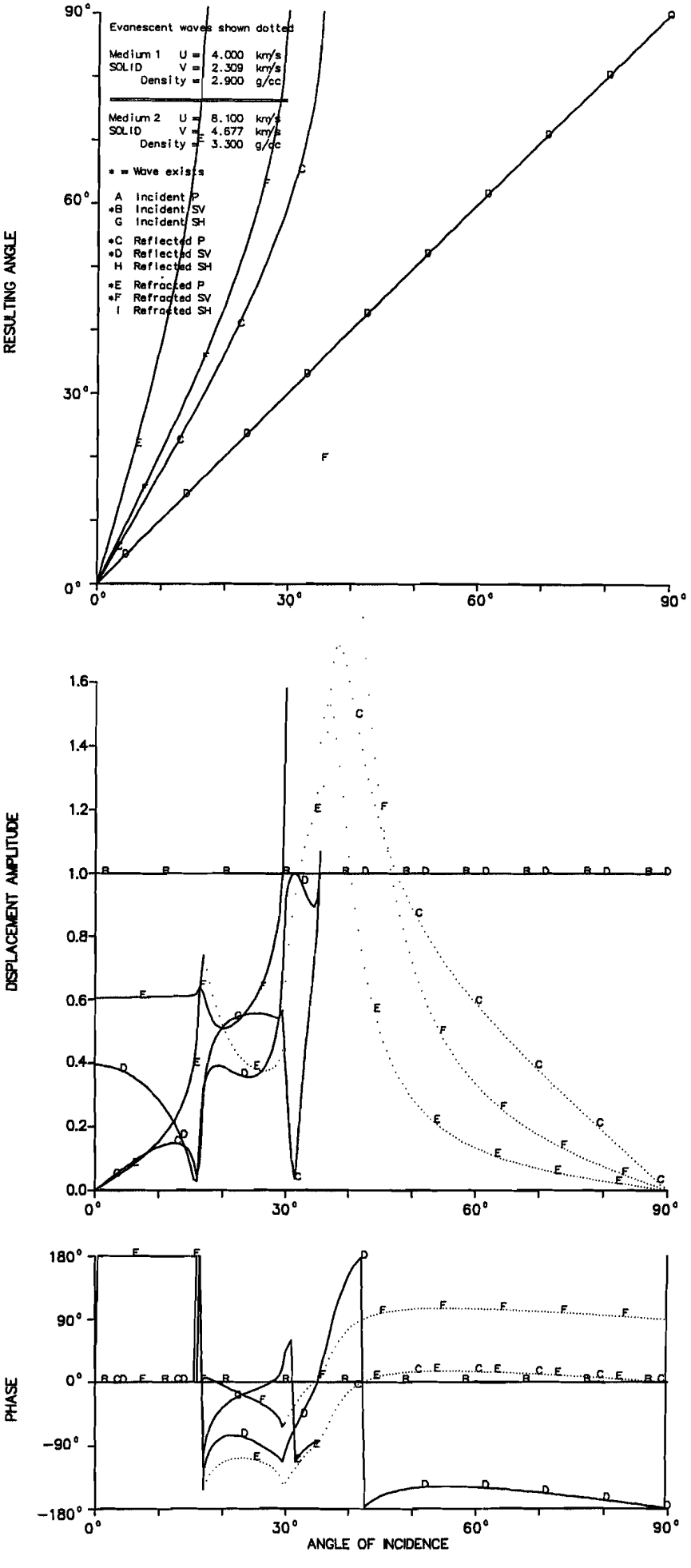

Figure 9. Solid–solid interface (high contrast). Incident SV from above.

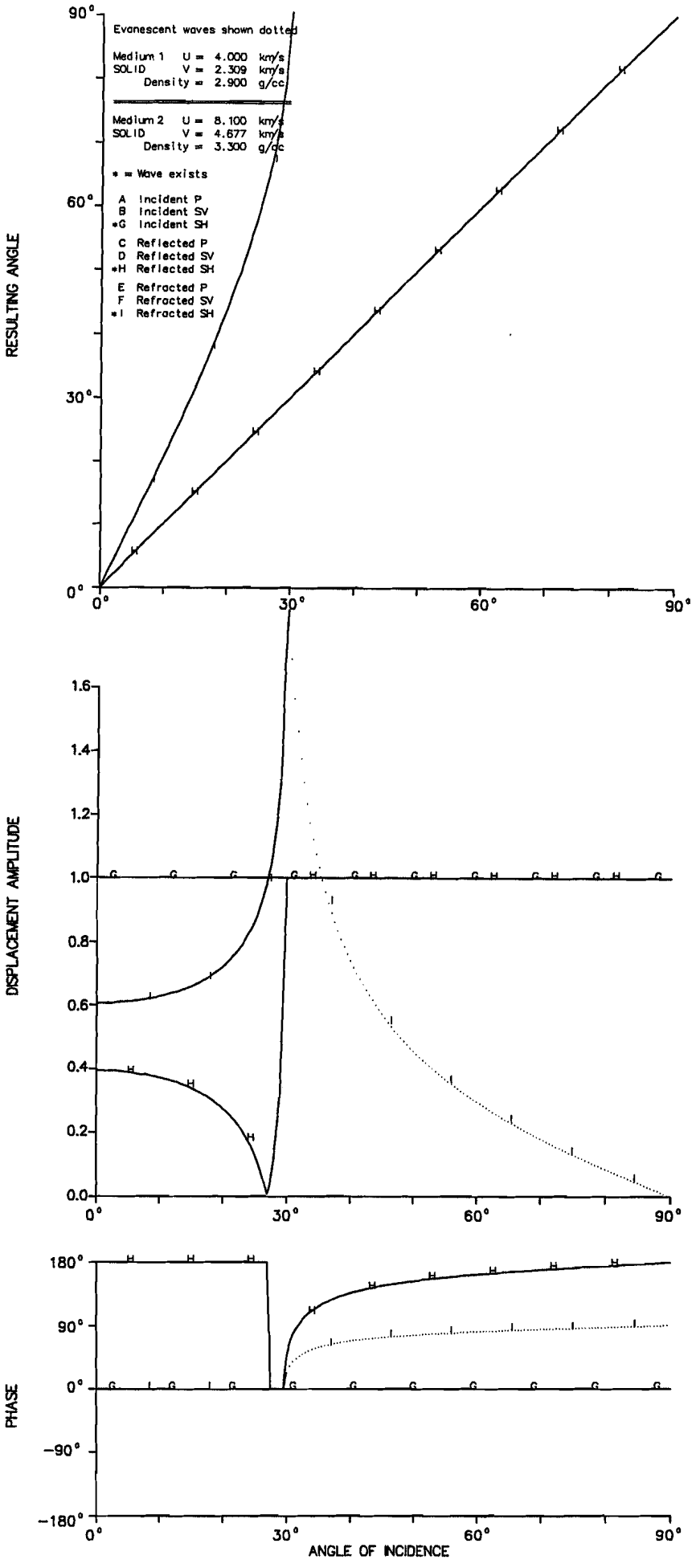

Figure 10. Solid–solid interface (high contrast). Incident SH from above.

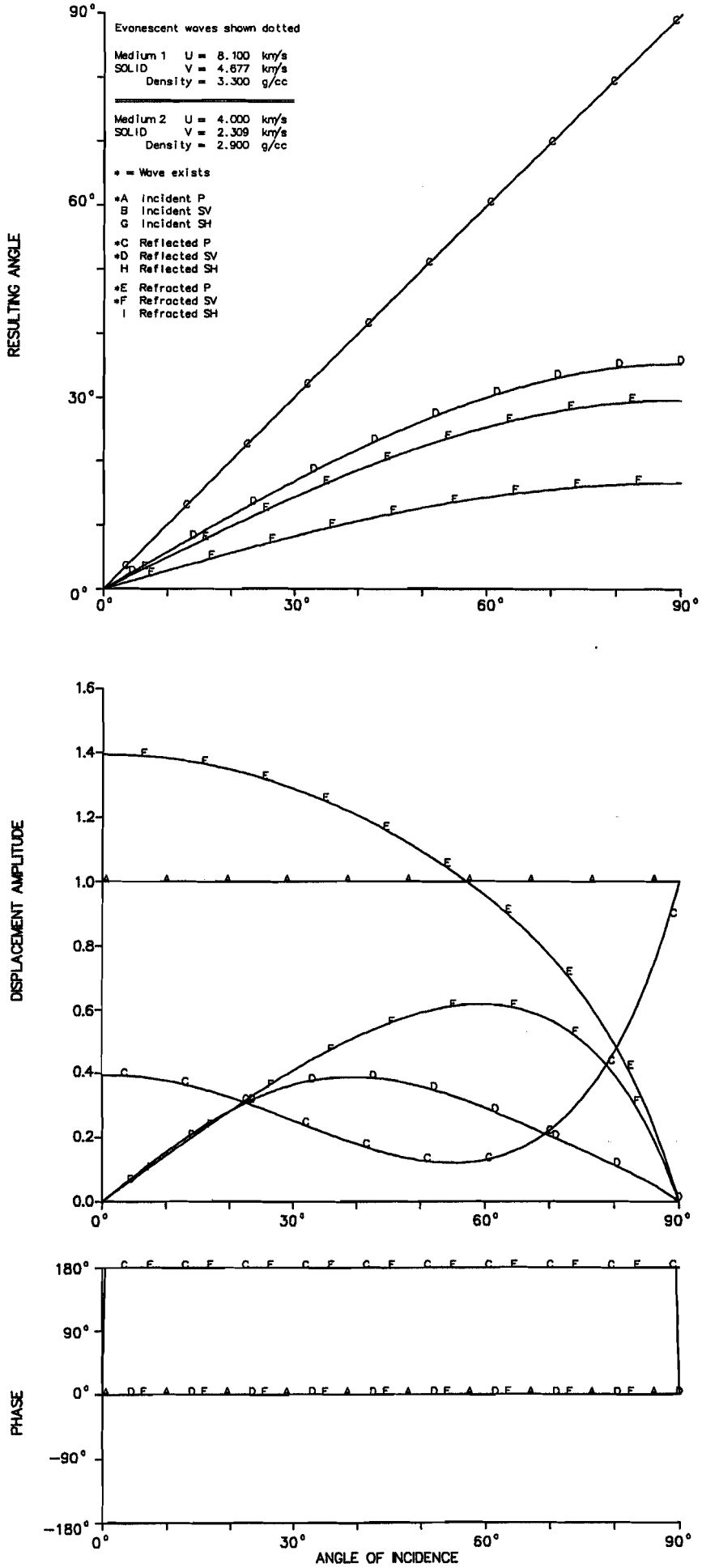

Figure 11. Solid–solid interface (high contrast). Incident P from below.

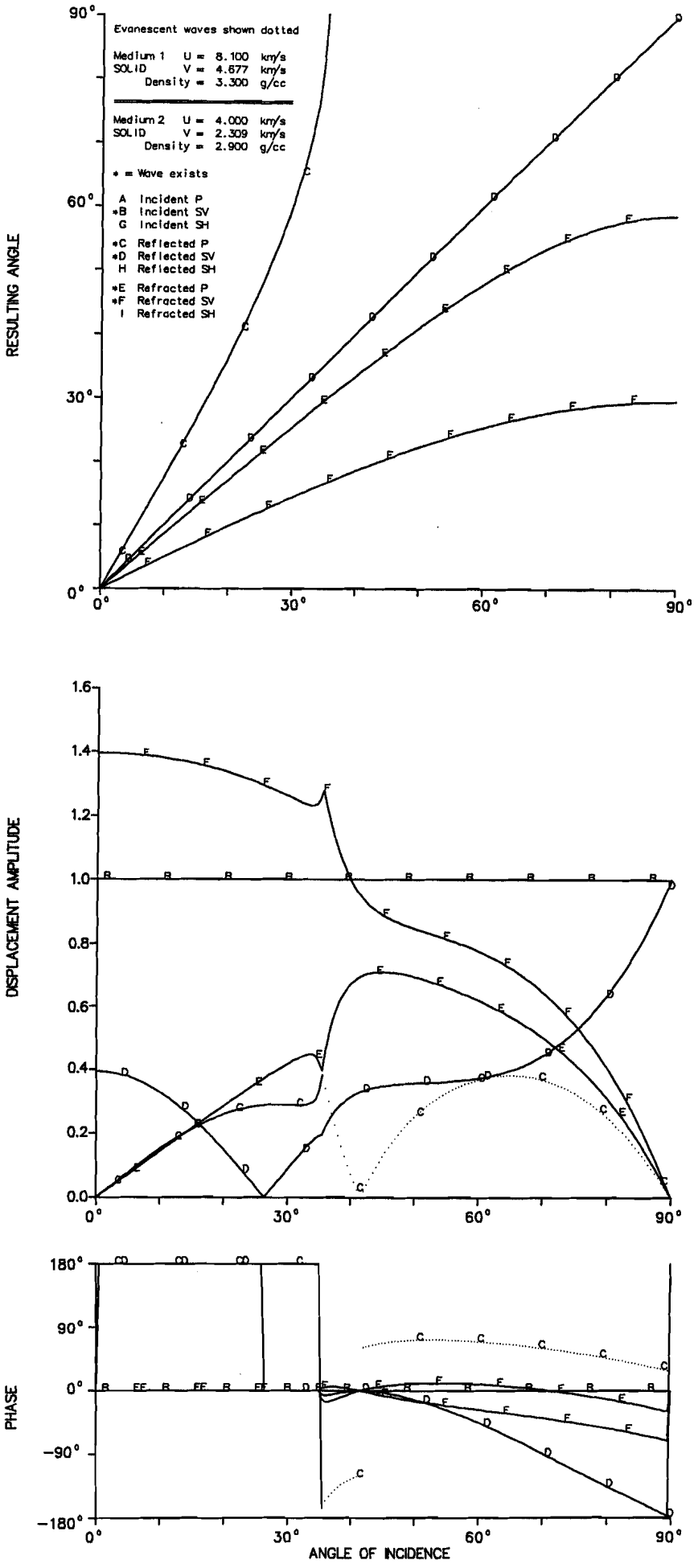

Figure 12. Solid–solid interface (high contrast). Incident SV from below.

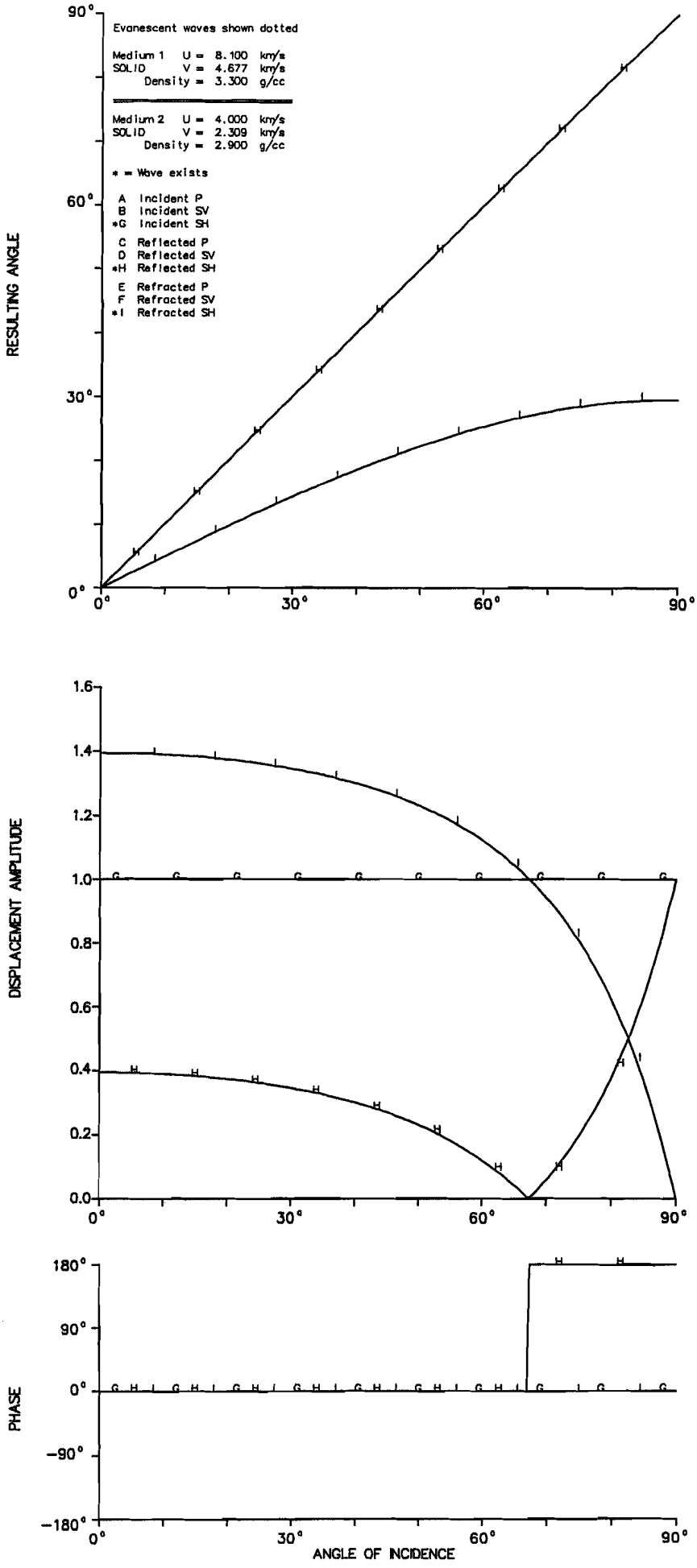

Figure 13. Solid–solid interface (high contrast). Incident SH from below.

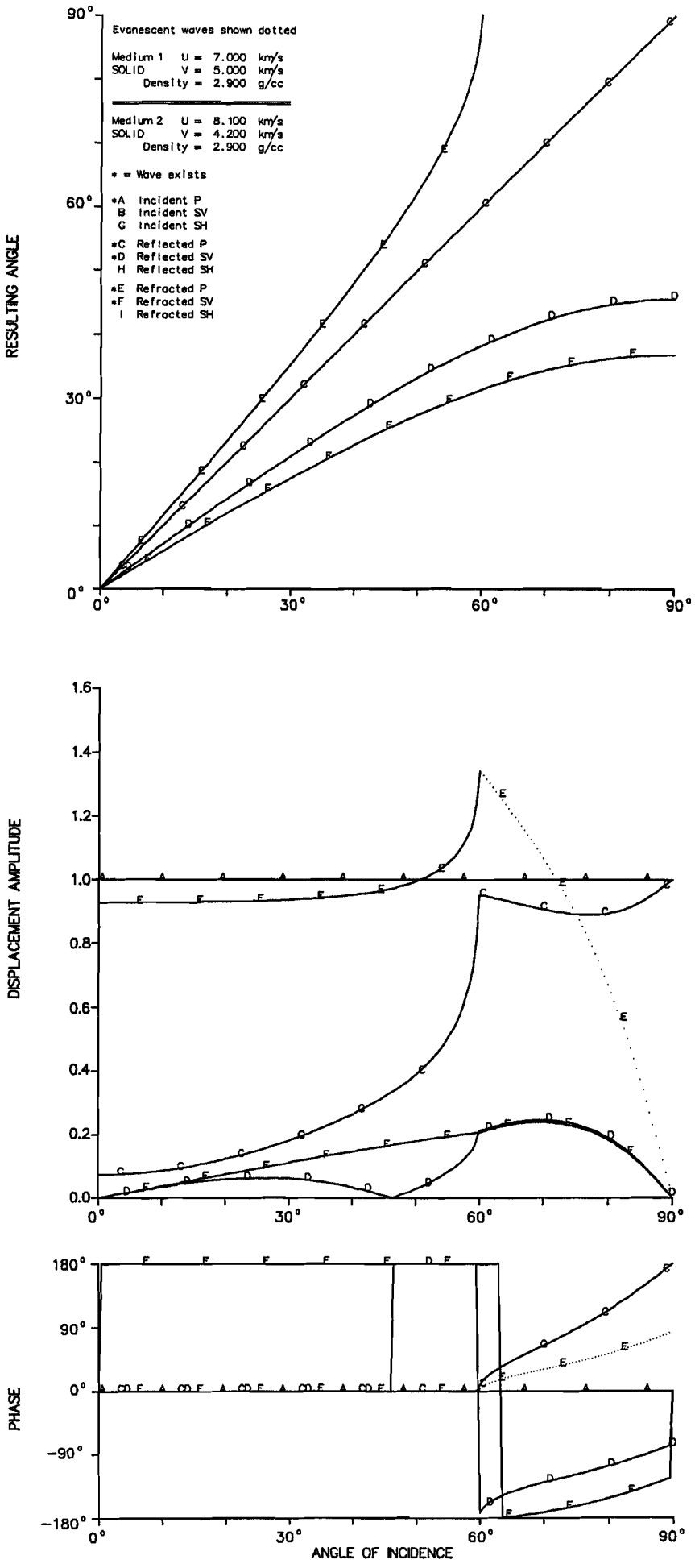

Figure 14. Solid–solid interface (anomalous U/V). Incident P from above.

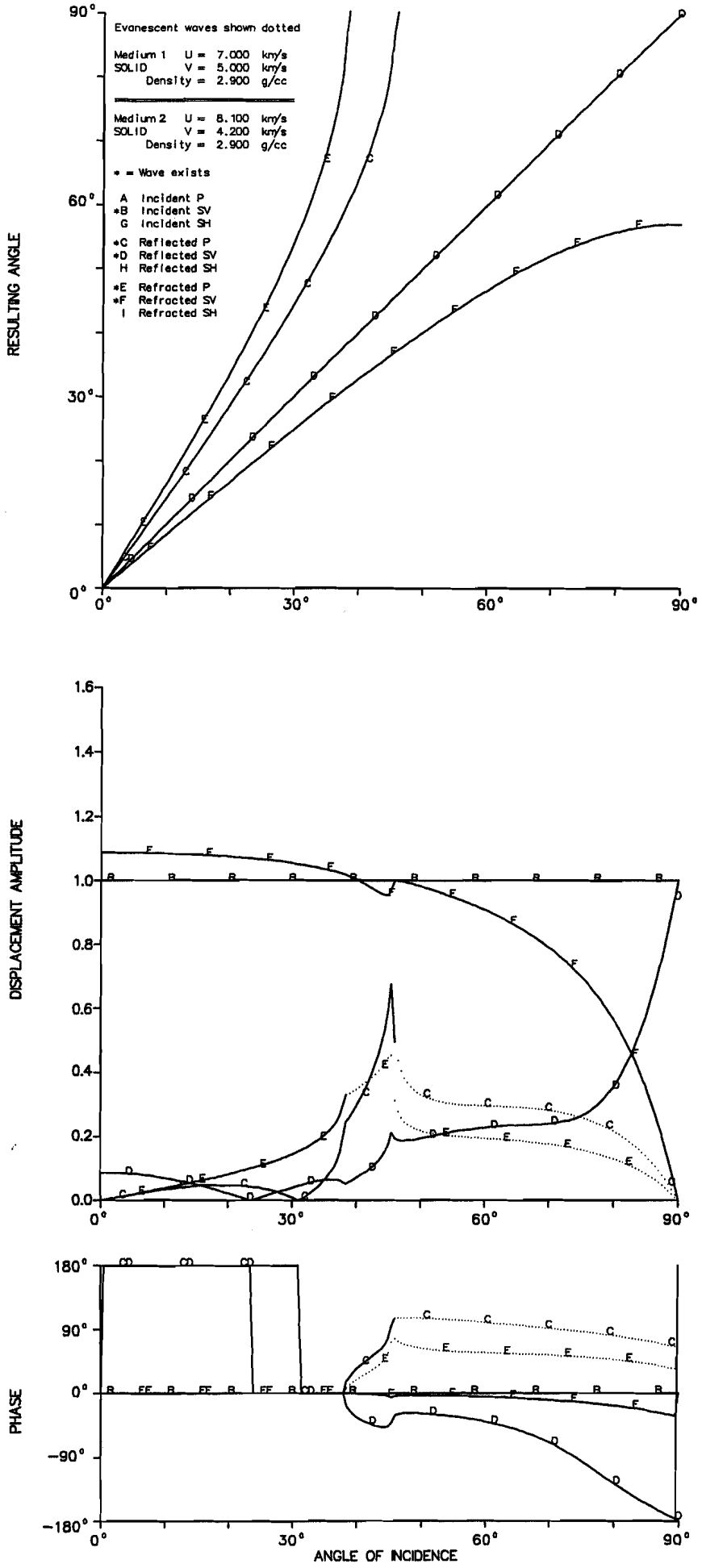

Figure 15. Solid–solid interface (anomalous U/V). Incident SV from above.

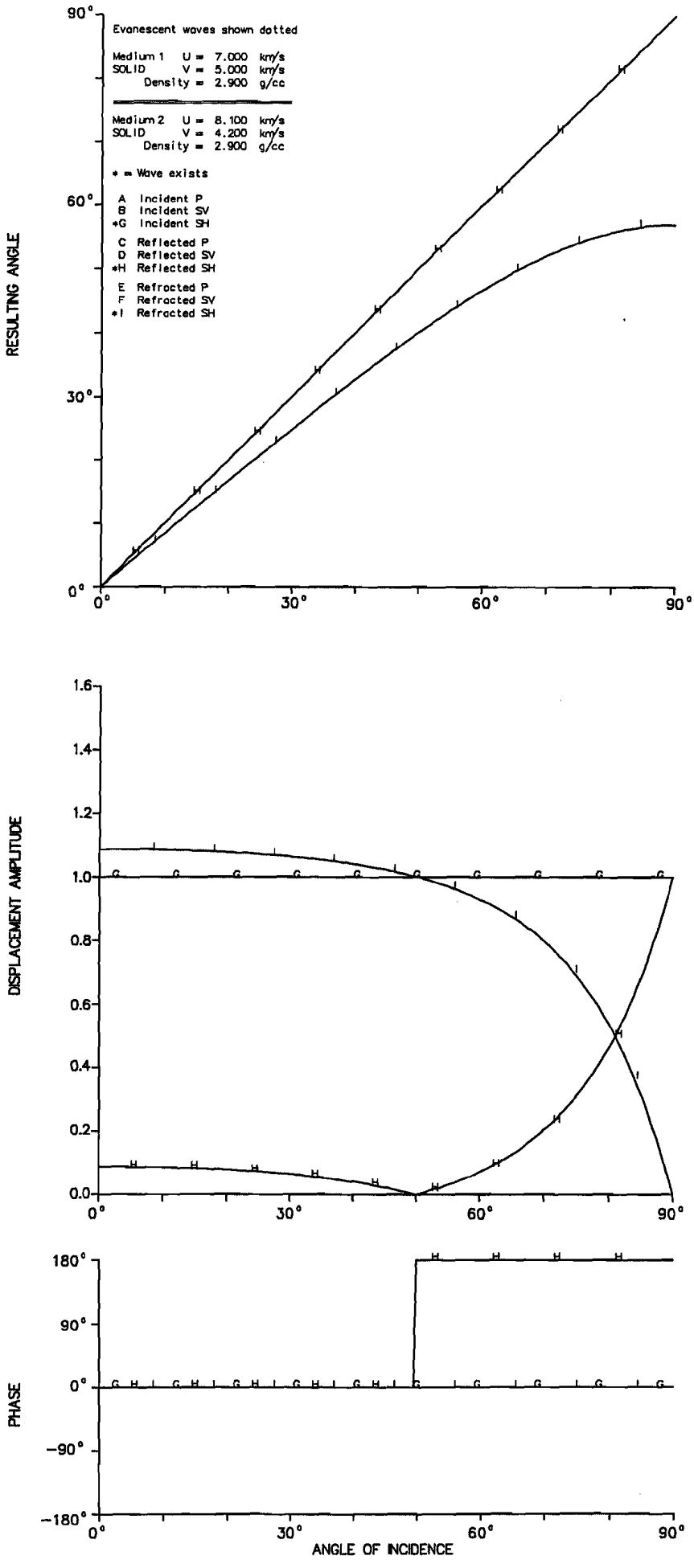

Figure 16. Solid–solid interface (anomalous U/V). Incident SH from above.

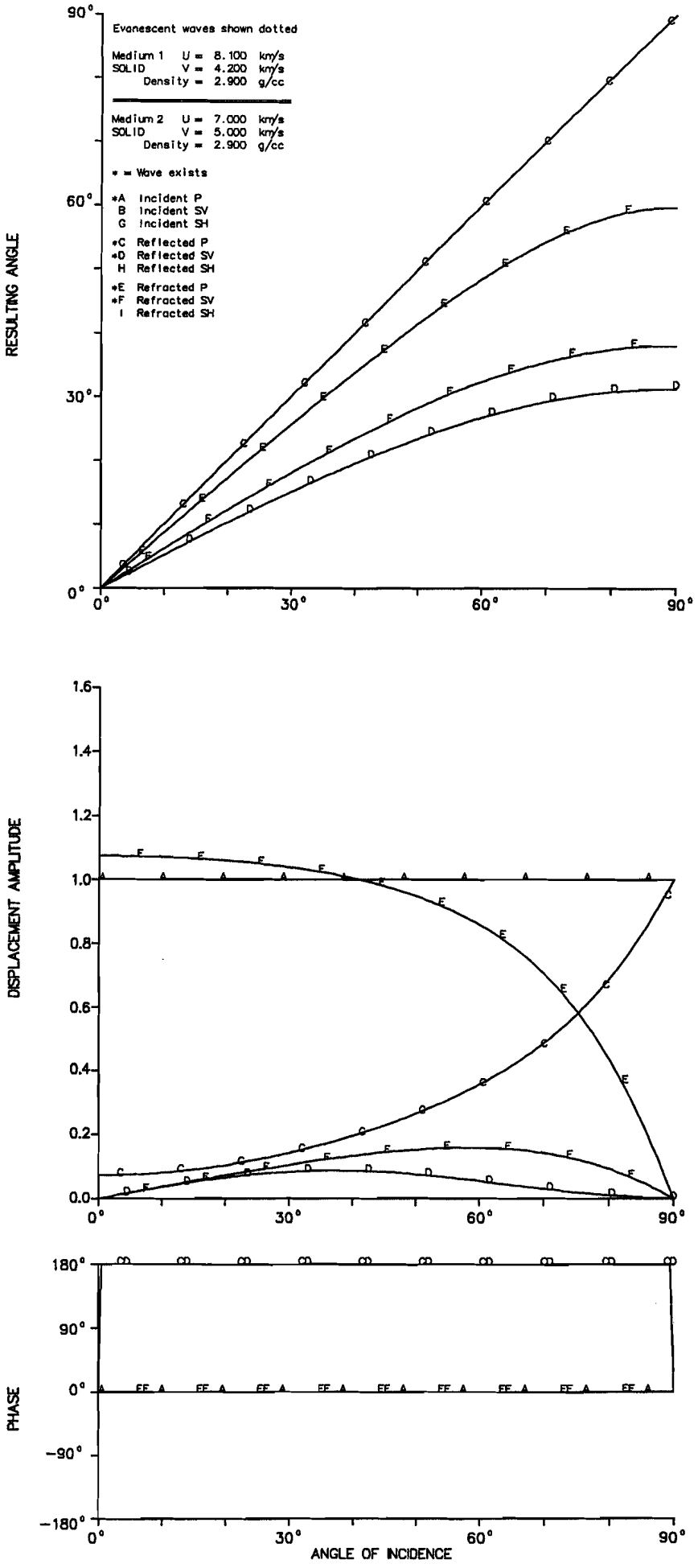

Figure 17. Solid–solid interface (anomalous U/V). Incident P from below.

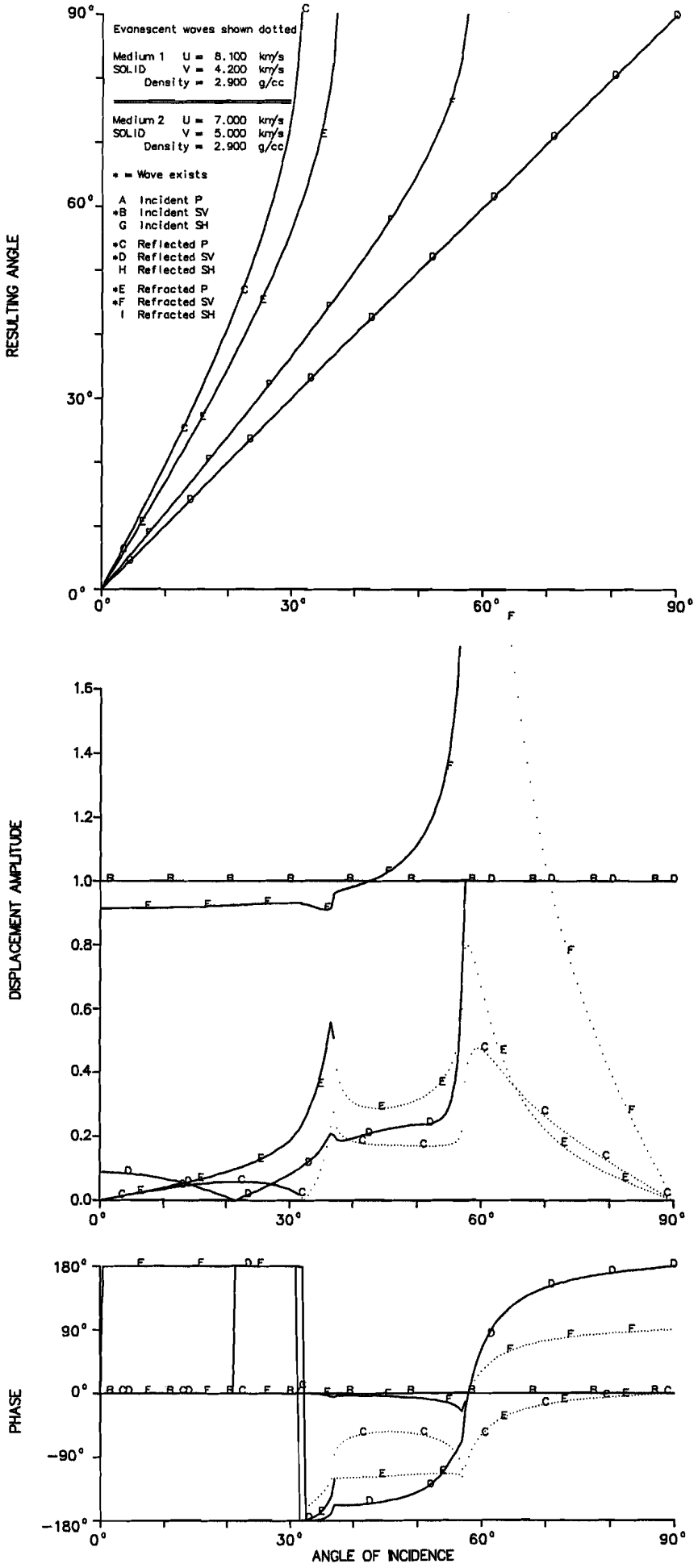

Figure 18. Solid–solid interface (anomalous U/V). Incident SV from below.

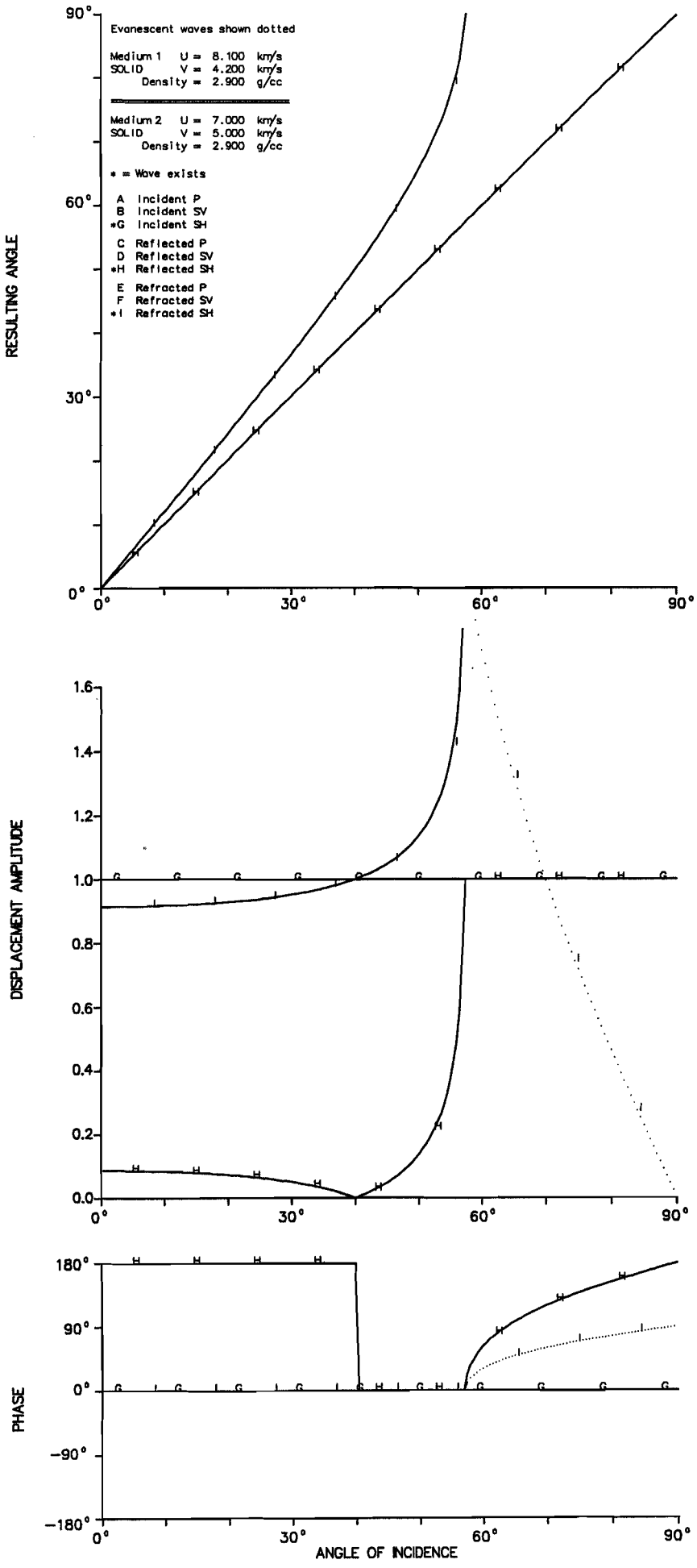

Figure 19. Solid–solid interface (anomalous U/V). Incident SH from below.

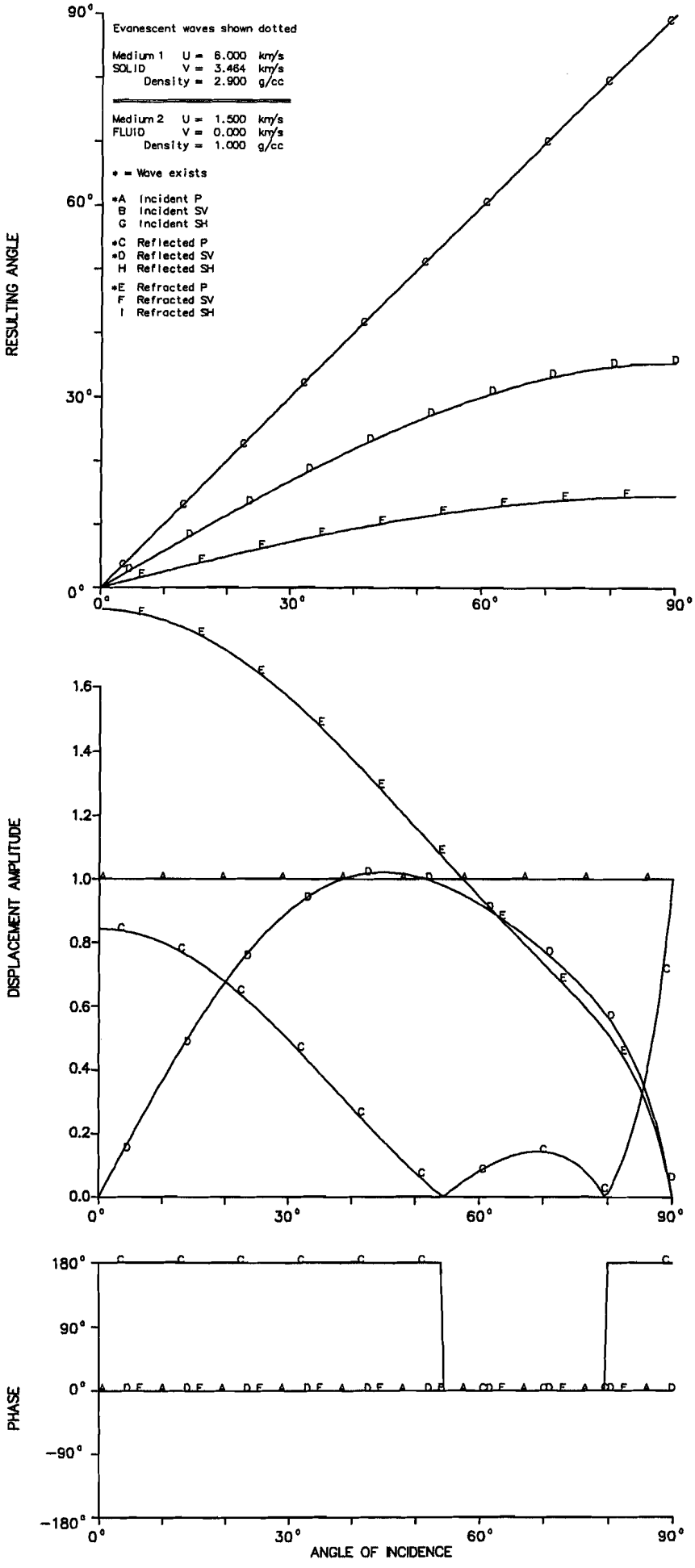

Figure 20. Solid–fluid interface (sea bed). Incident P from below.

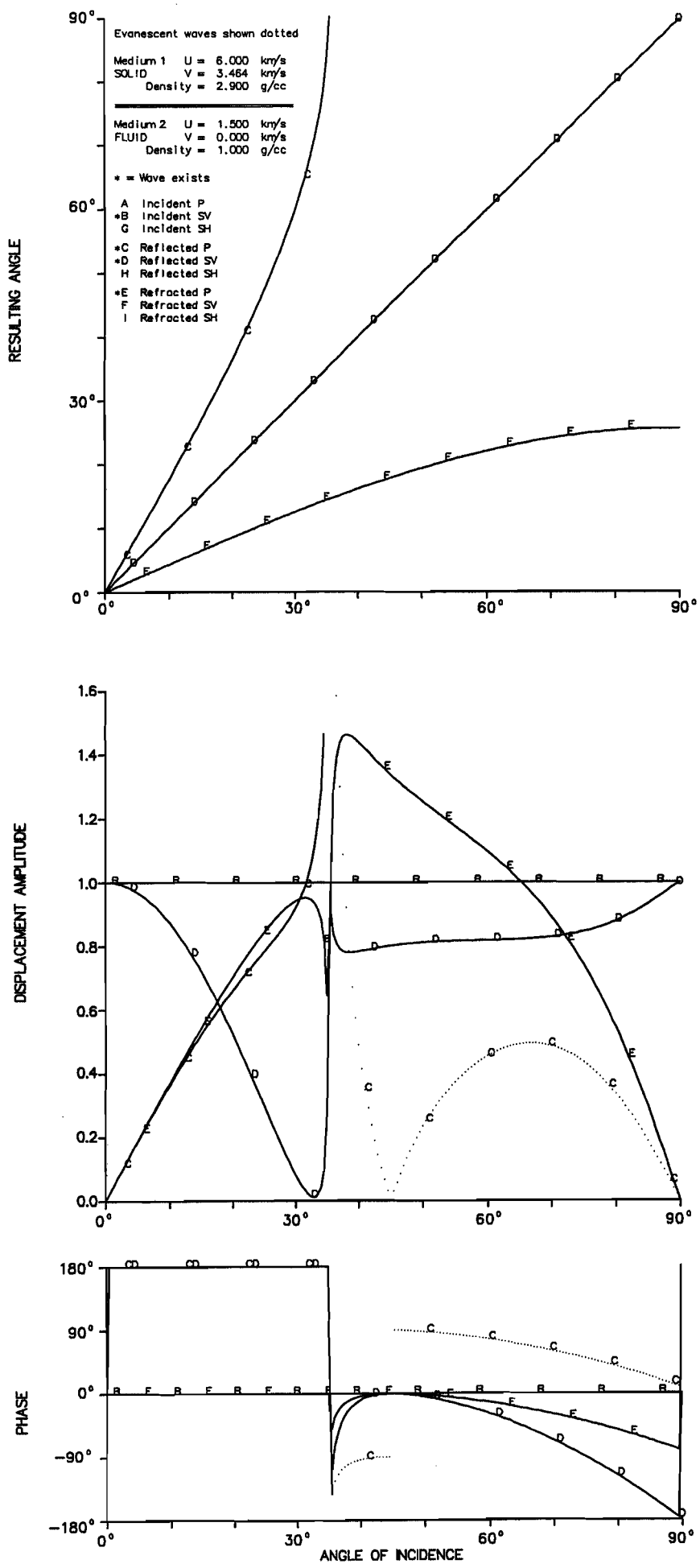

Figure 21. Solid–fluid interface (sea bed). Incident SV from below.

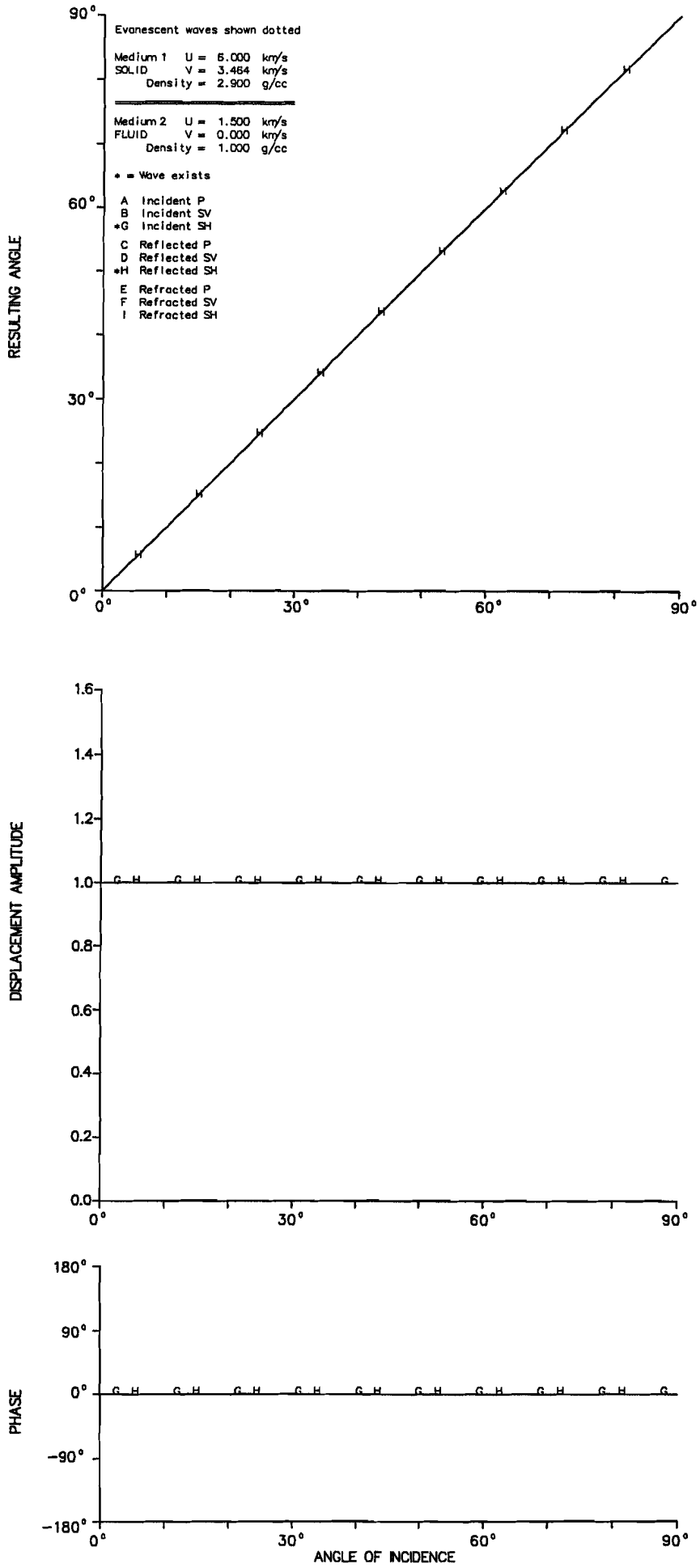

Figure 22. Solid–fluid interface (sea bed). Incident SH from below.

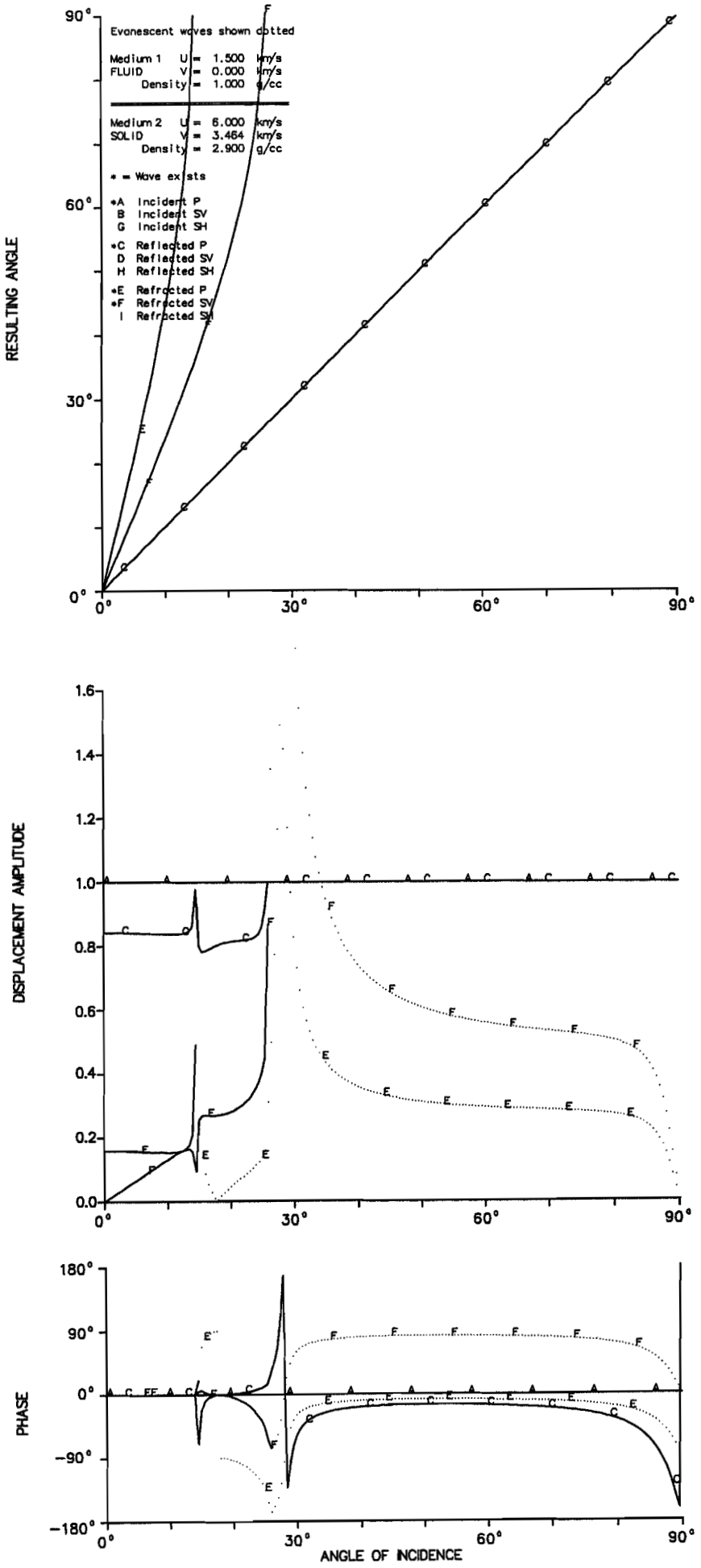

Figure 23. Solid–fluid interface (sea bed). Incident P from above.

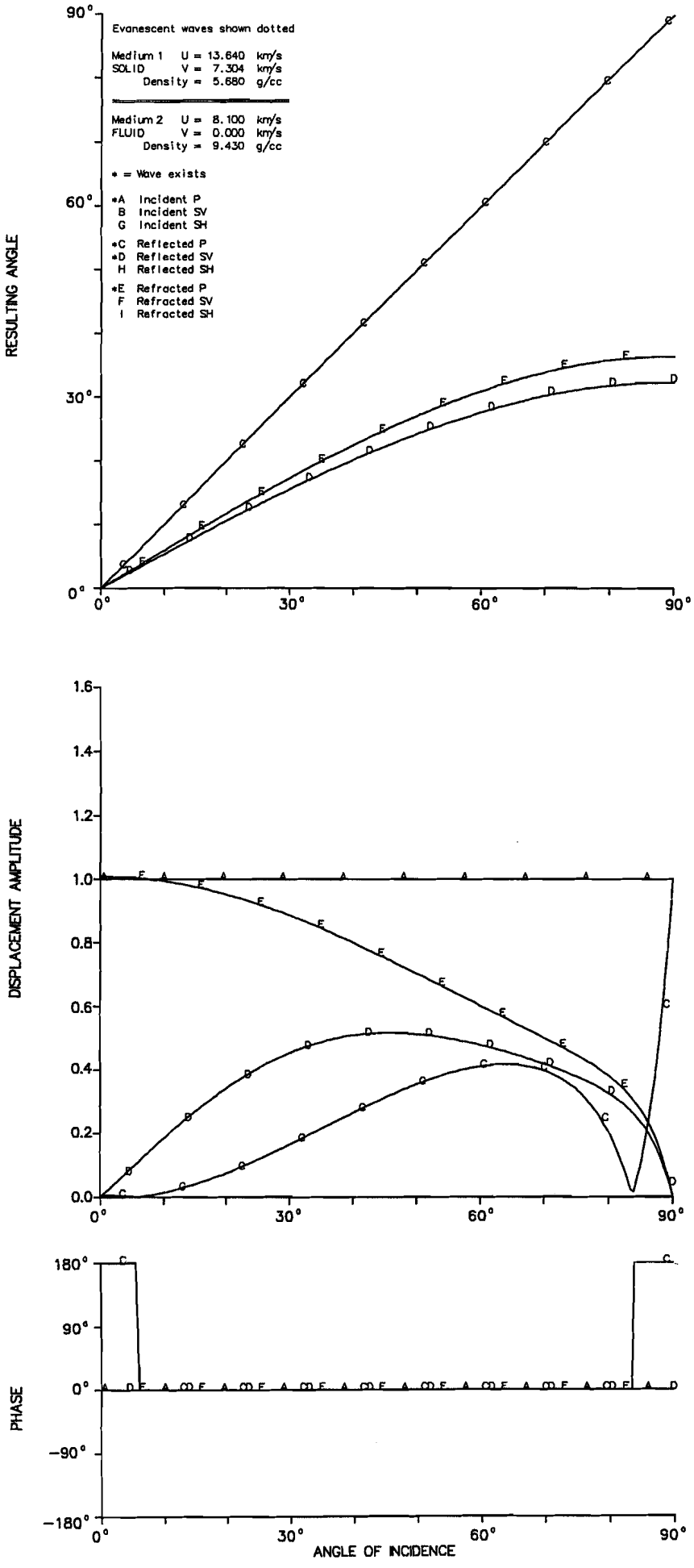

Figure 24. Solid–fluid interface (CMB–JB). Incident P from above.

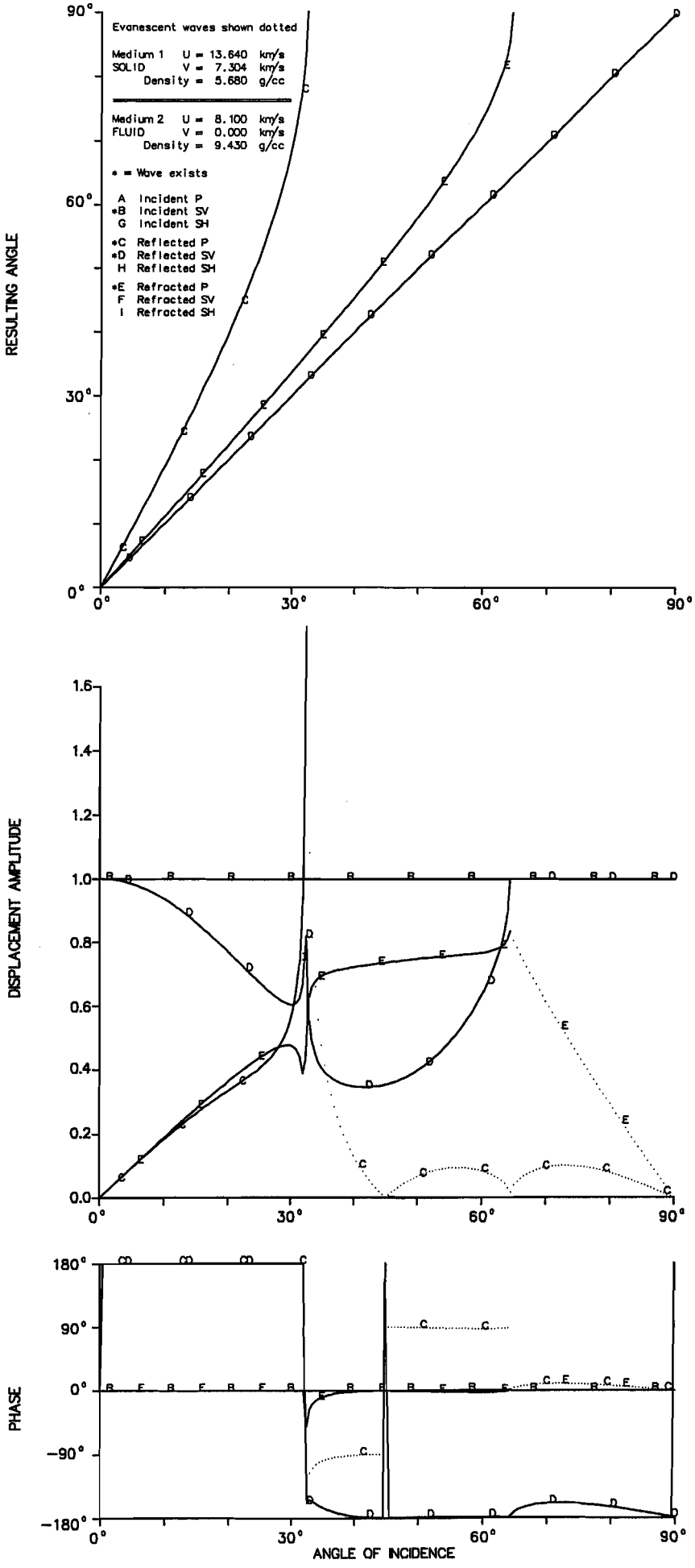

Figure 25. Solid–fluid interface (CMB–JB). Incident SV from above.

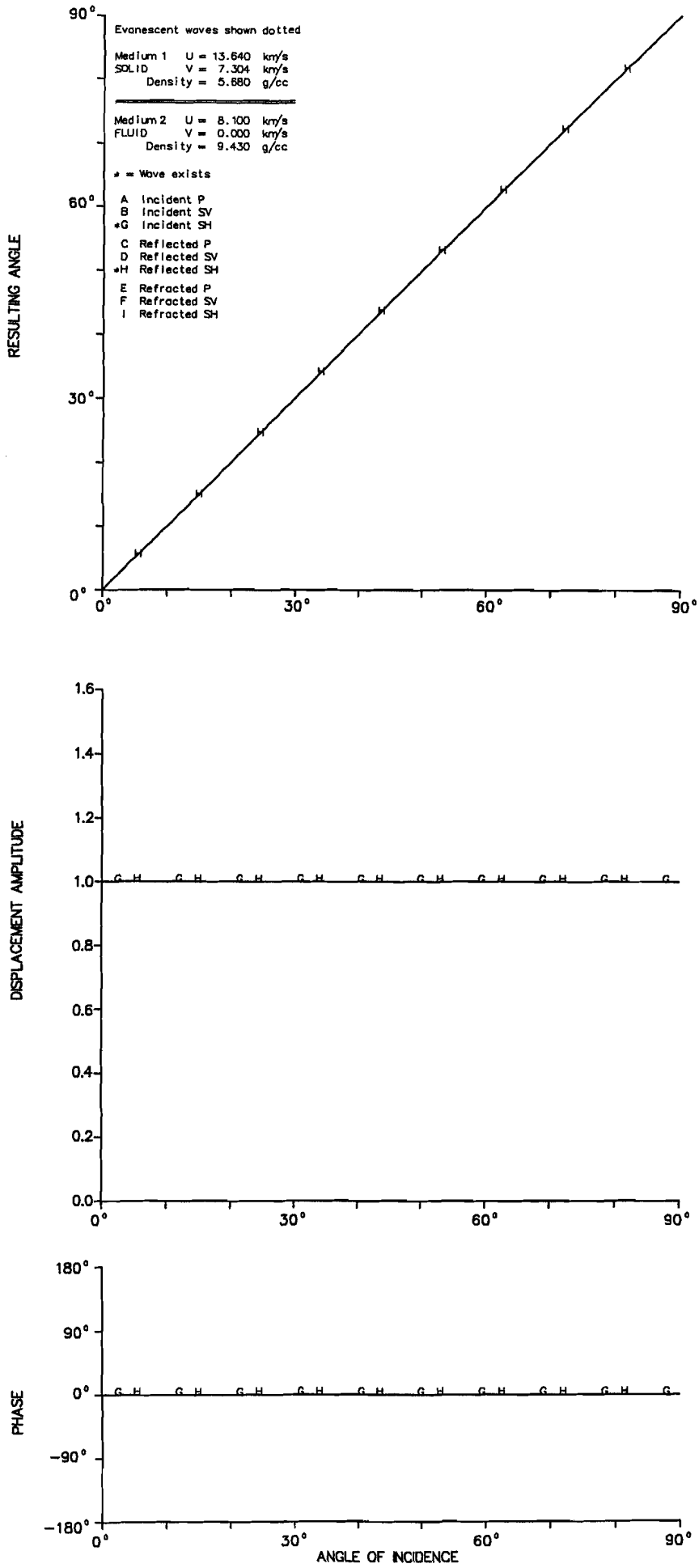

Figure 26. Solid–fluid interface (CMB–JB). Incident SH from above.

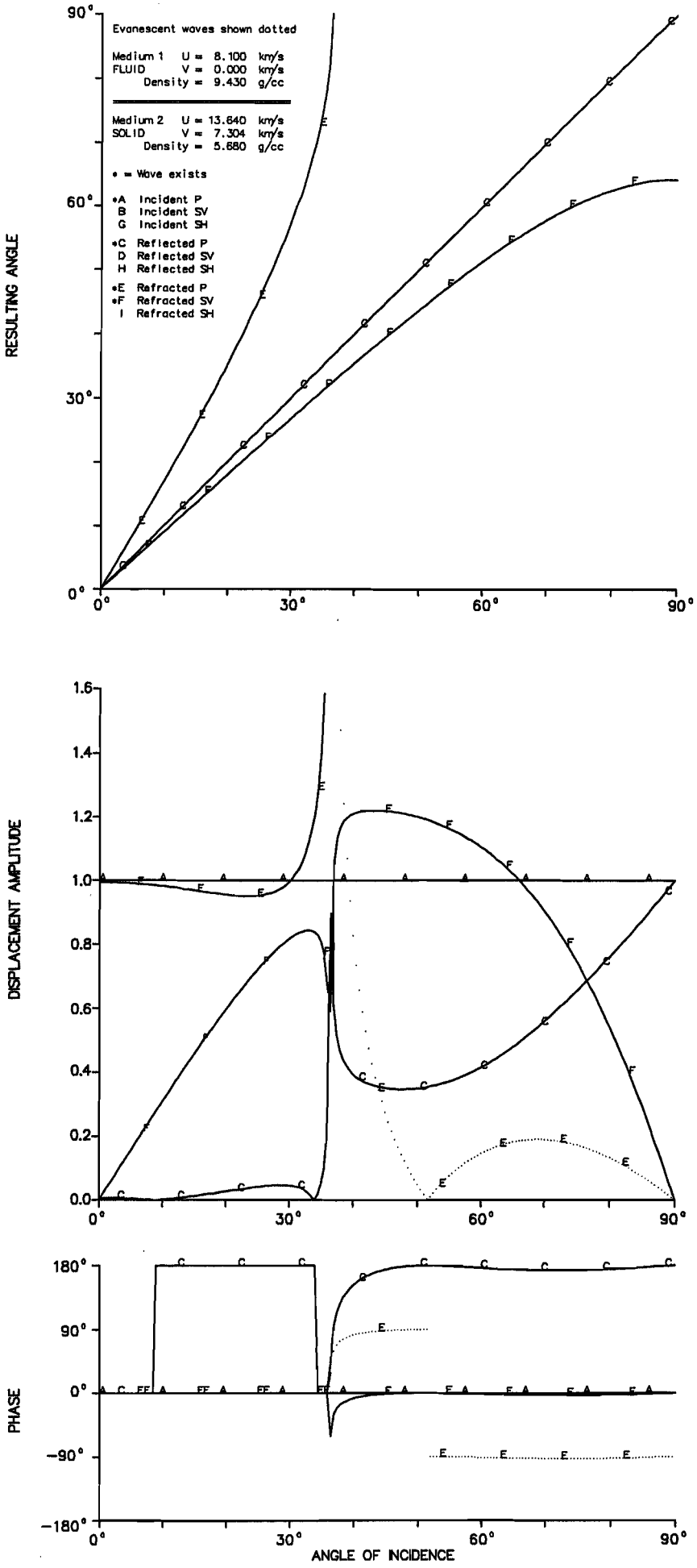

Figure 27. Solid–fluid interface (CMB–JB). Incident P from below.

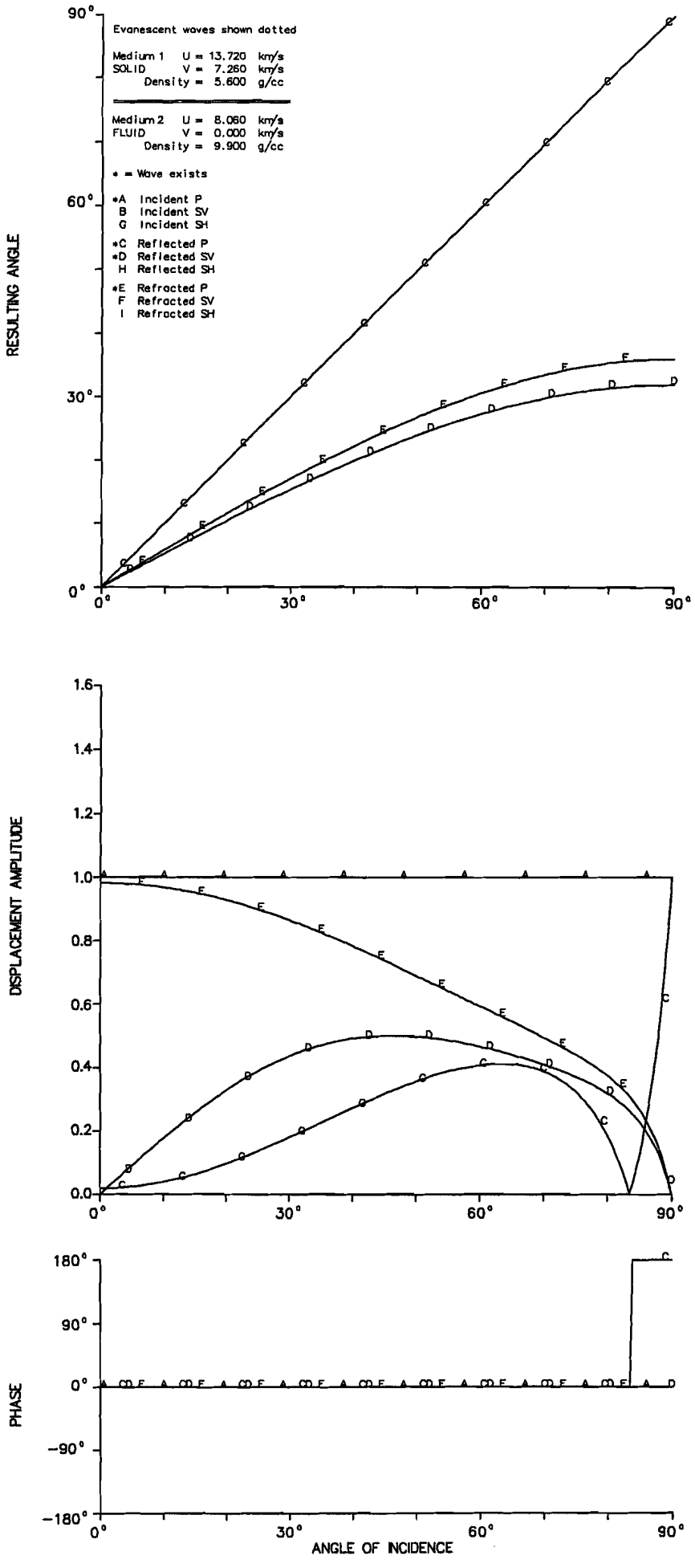

Figure 28. Solid–fluid interface (CMB–PREM). Incident P from above.

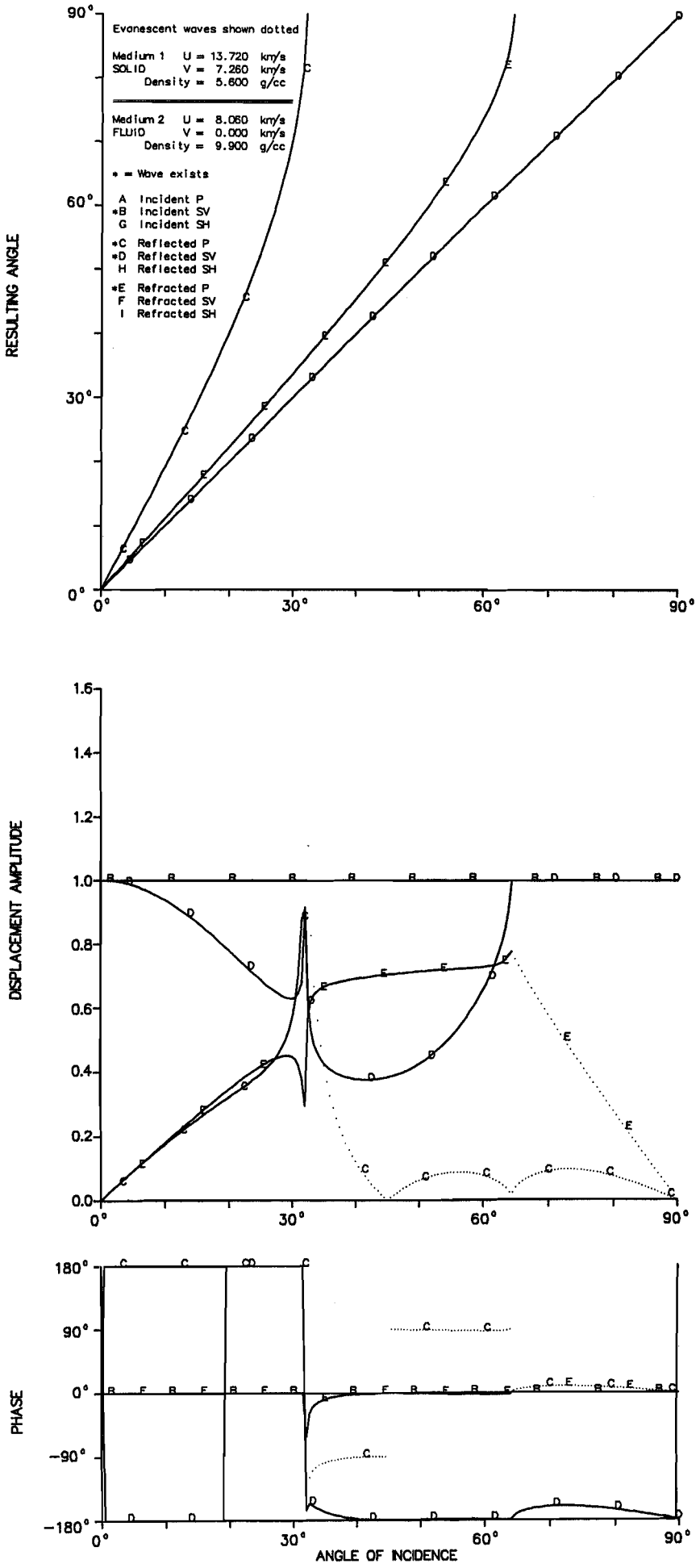

Figure 29. Solid–fluid interface (CMB–PREM). Incident SV from above.

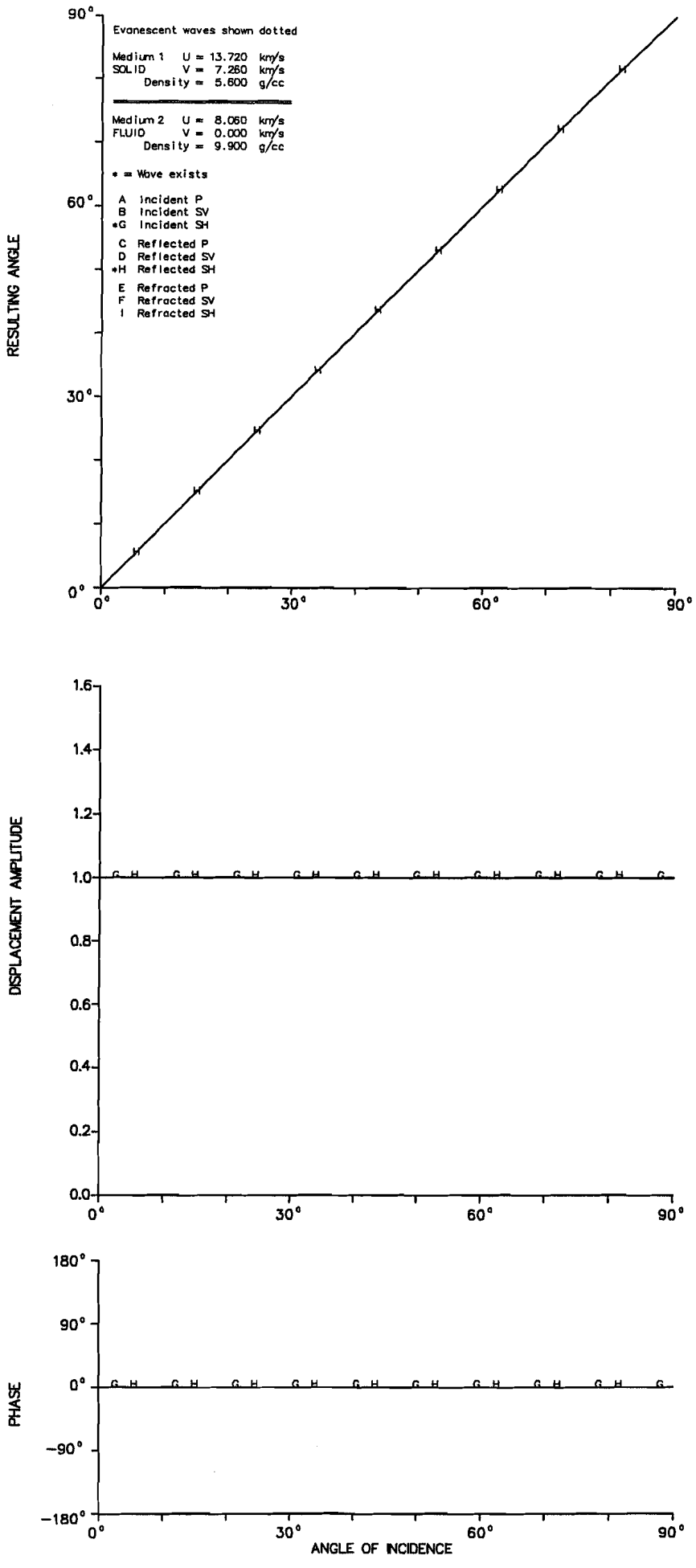

Figure 30. Solid–fluid interface (CMB–PREM). Incident SH from above.

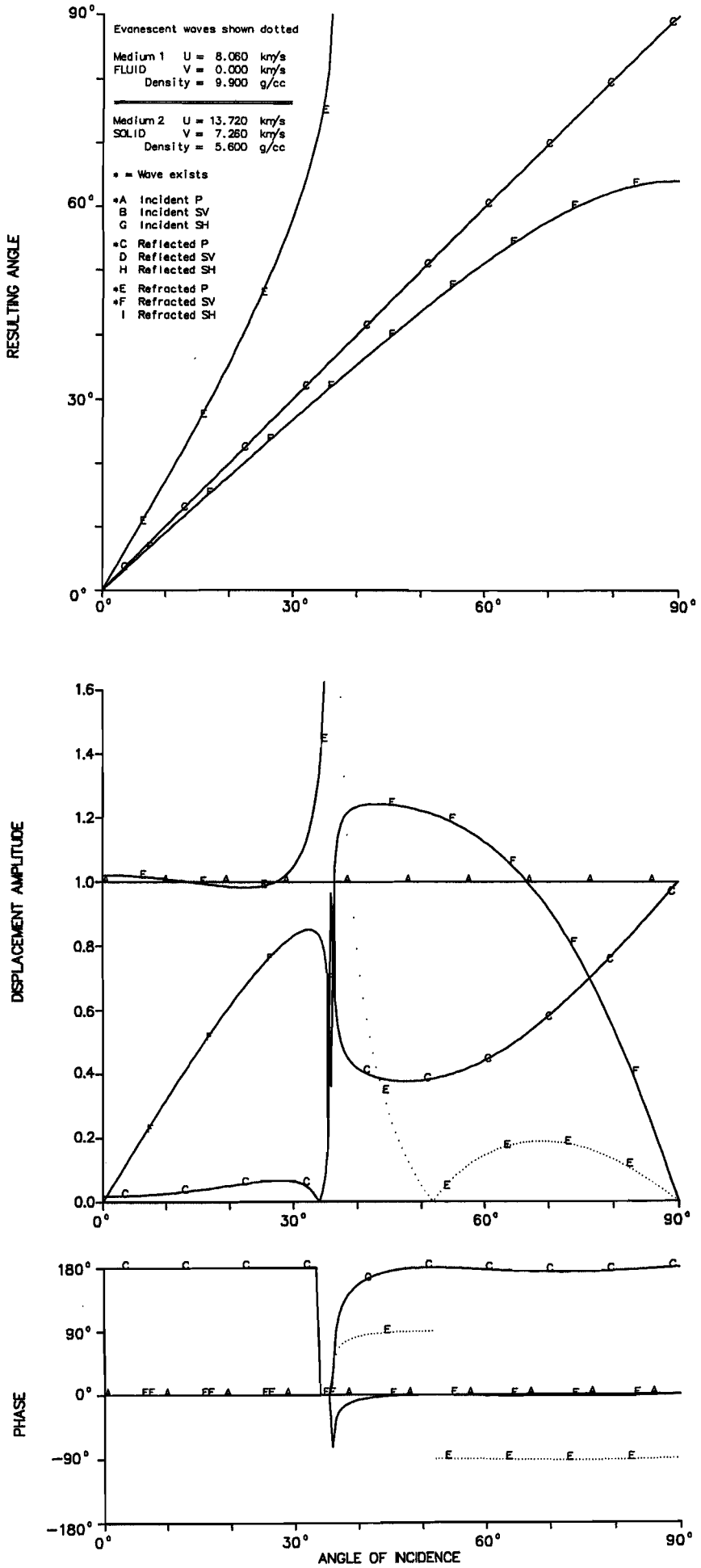

Figure 31. Solid–fluid interface (CMB–PREM). Incident P from below.

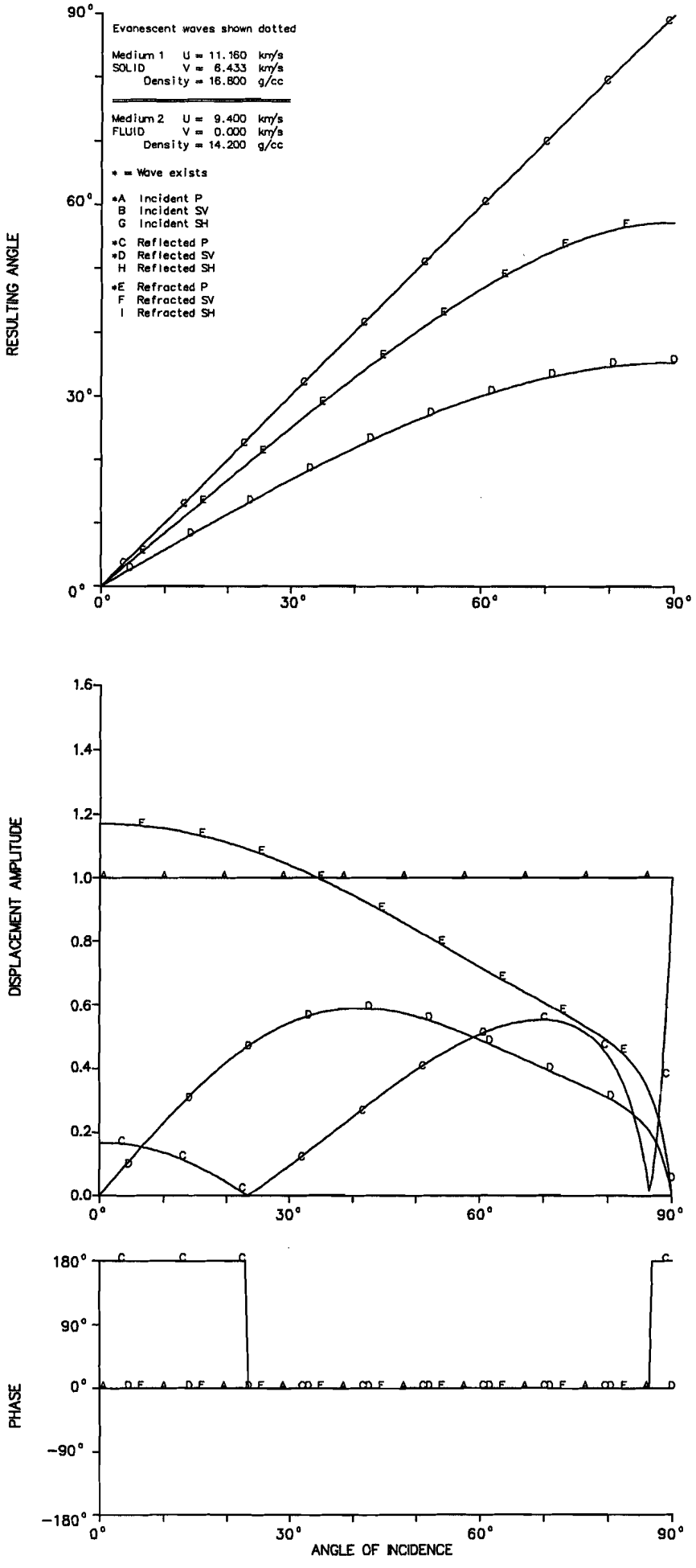

Figure 32. Solid–fluid interface (ICB–JB). Incident P from below.

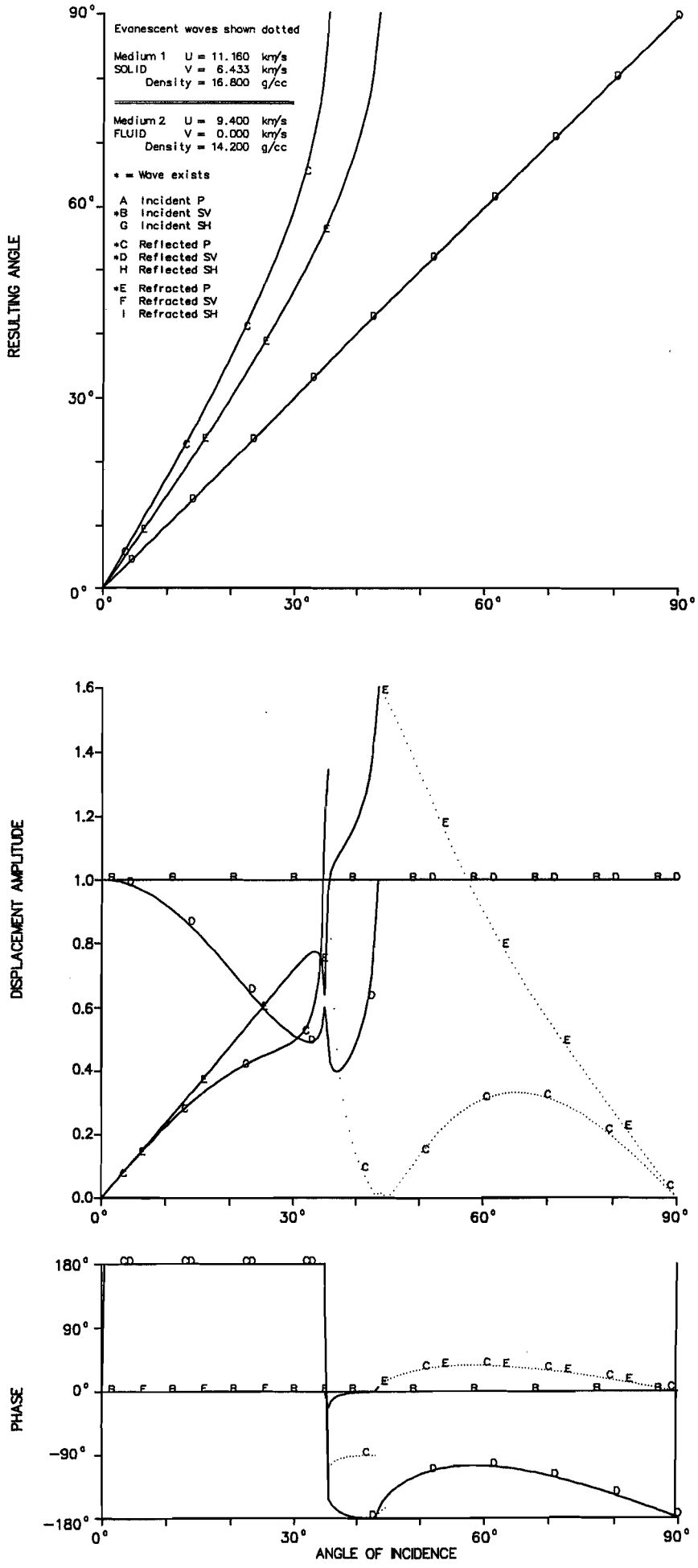

Figure 33. Solid–fluid interface (ICB–JB). Incident SV from below.

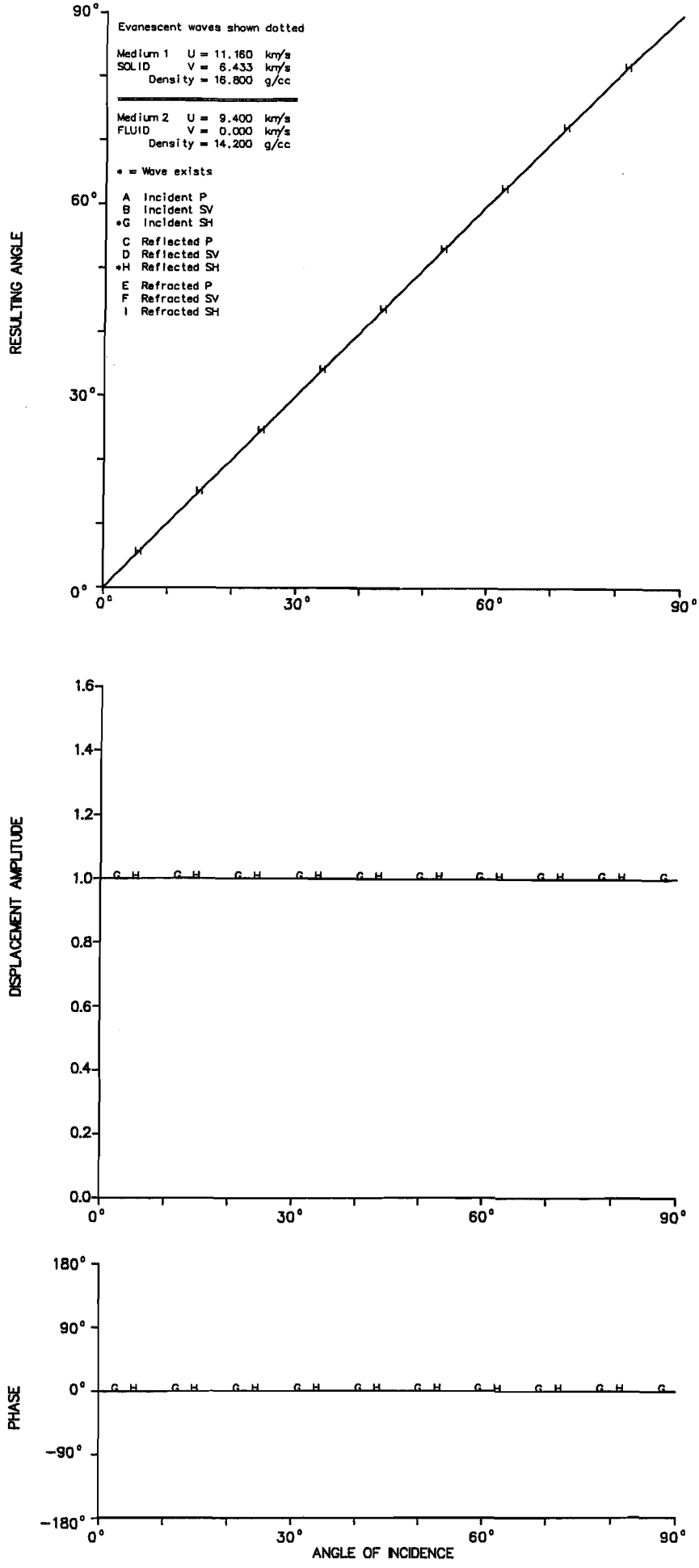

Figure 34. Solid–fluid interface (ICB–JB). Incident SH from below.

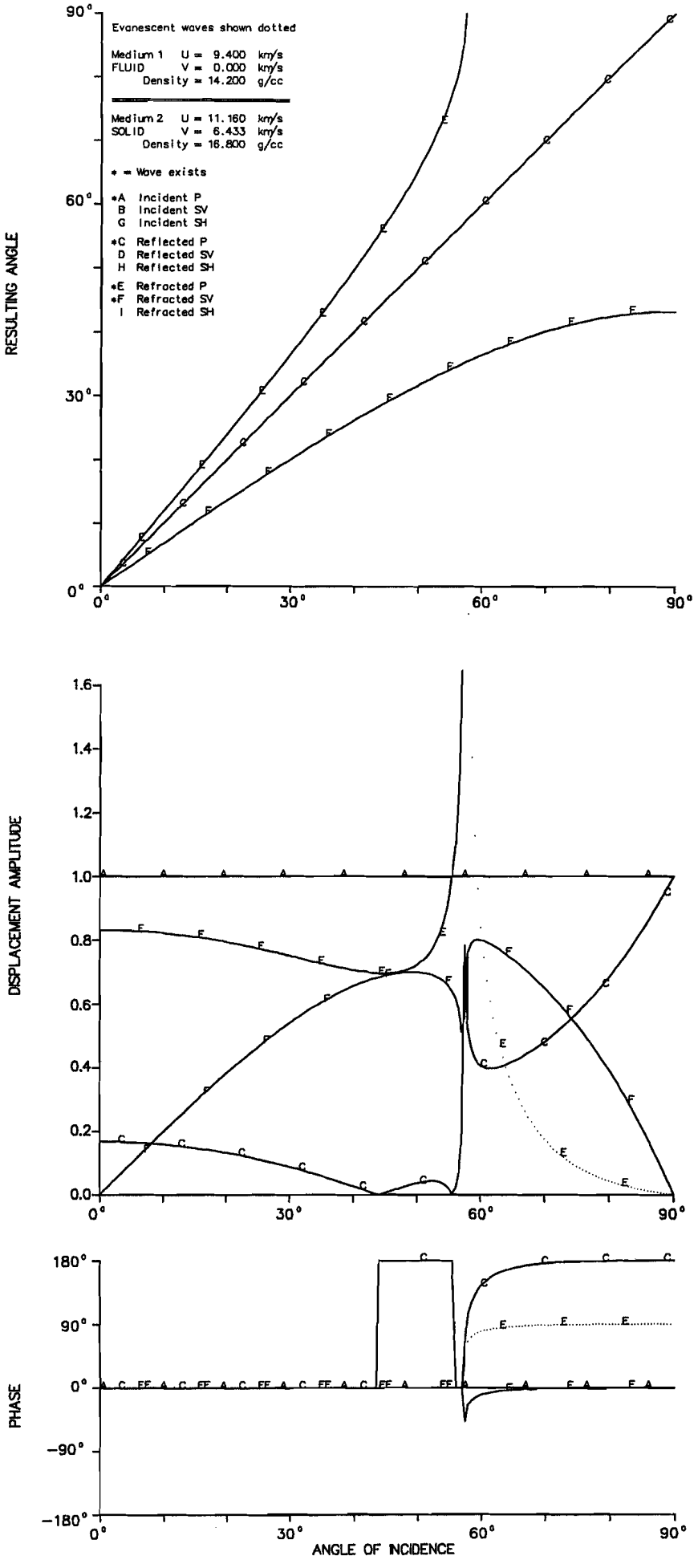

Figure 35. Solid–fluid interface (ICB–JB). Incident P from above.

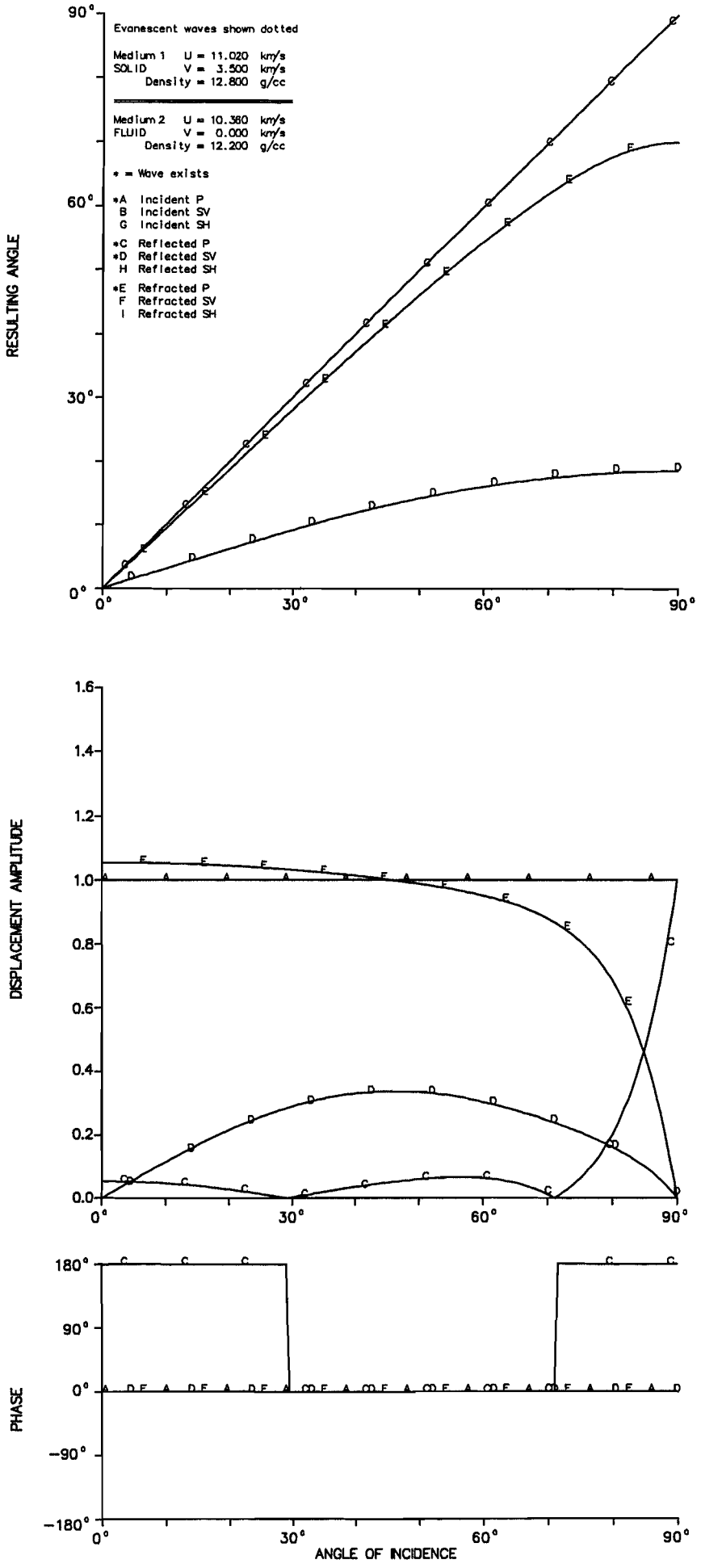

Figure 36. Solid–fluid interface (ICB–PREM). Incident P from below.

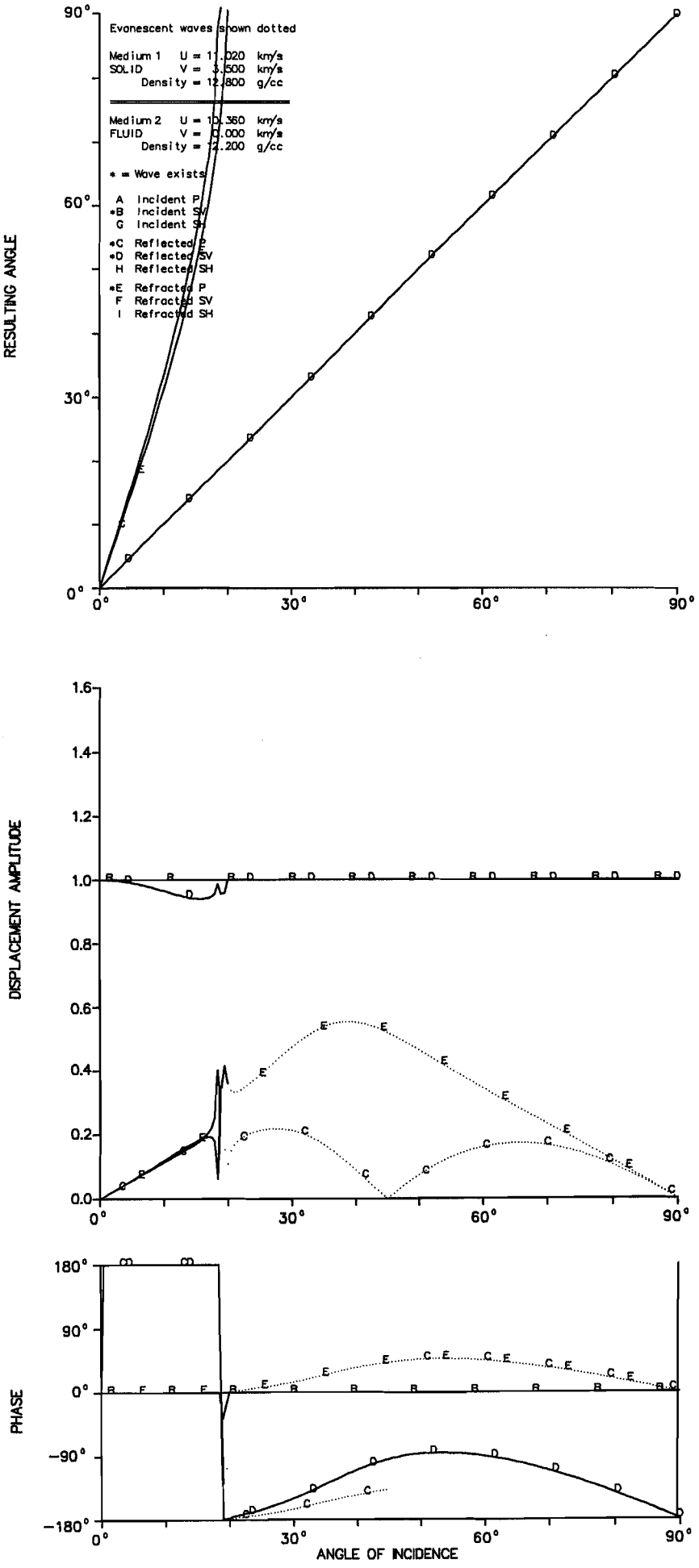

Figure 37. Solid–fluid interface (ICB–PREM). Incident SV from below.

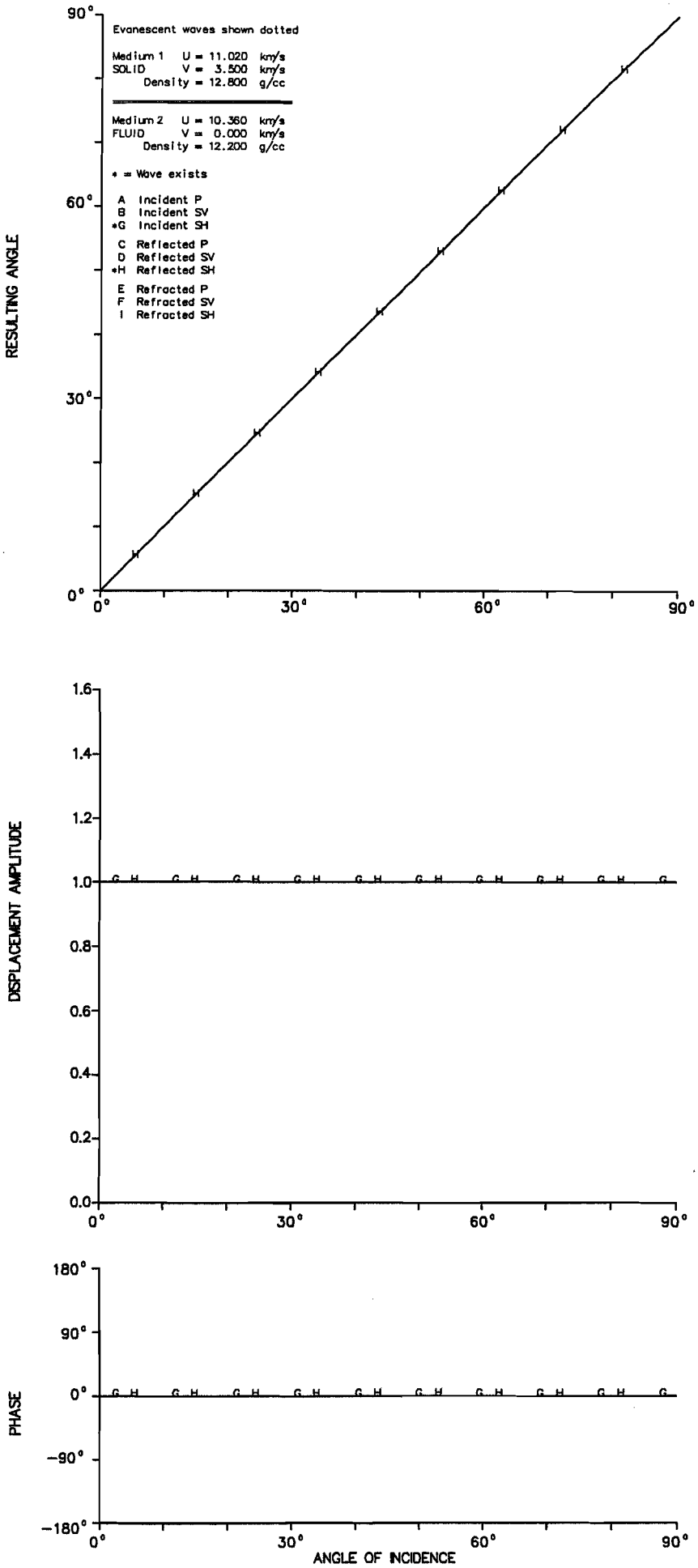

Figure 38. Solid–fluid interface (ICB–PREM). Incident SH from below.

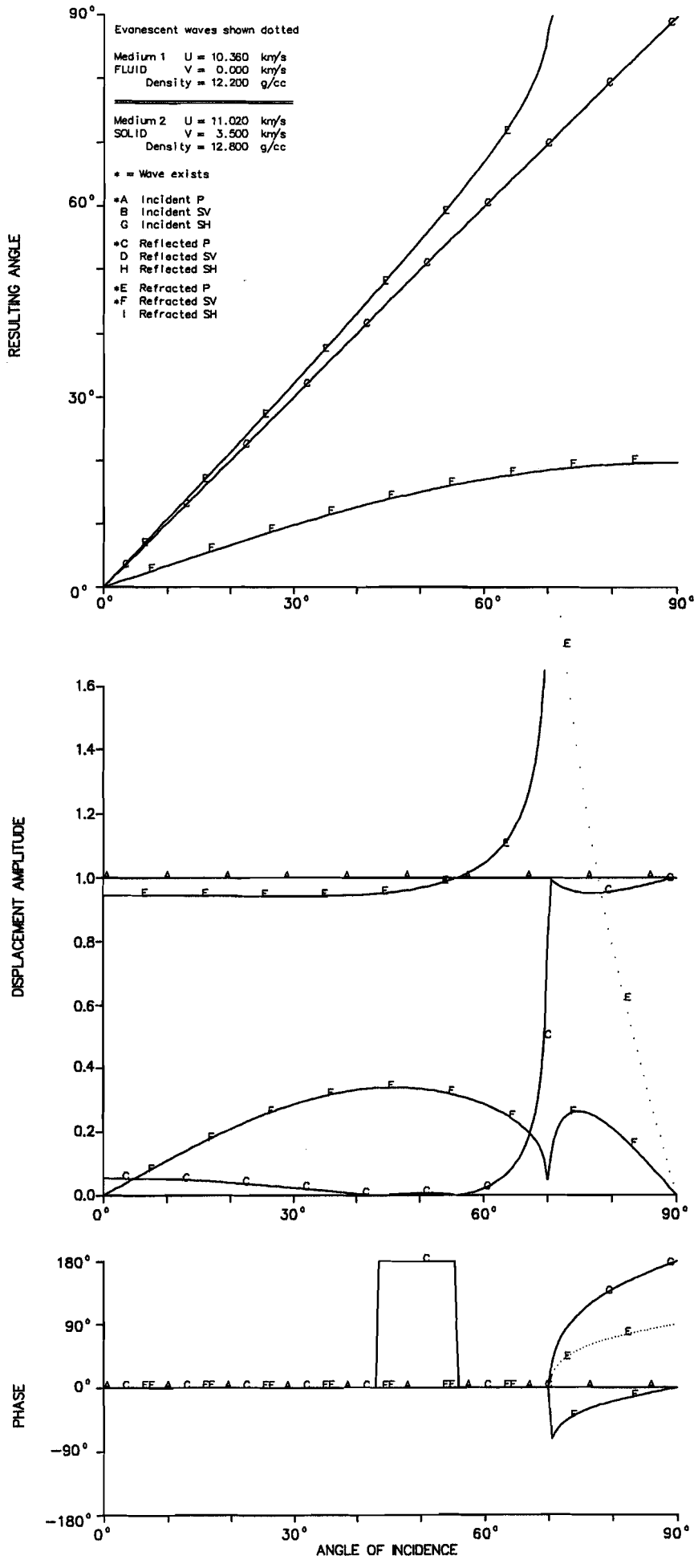

Figure 39. Solid–fluid interface (ICB–PREM). Incident P from above.

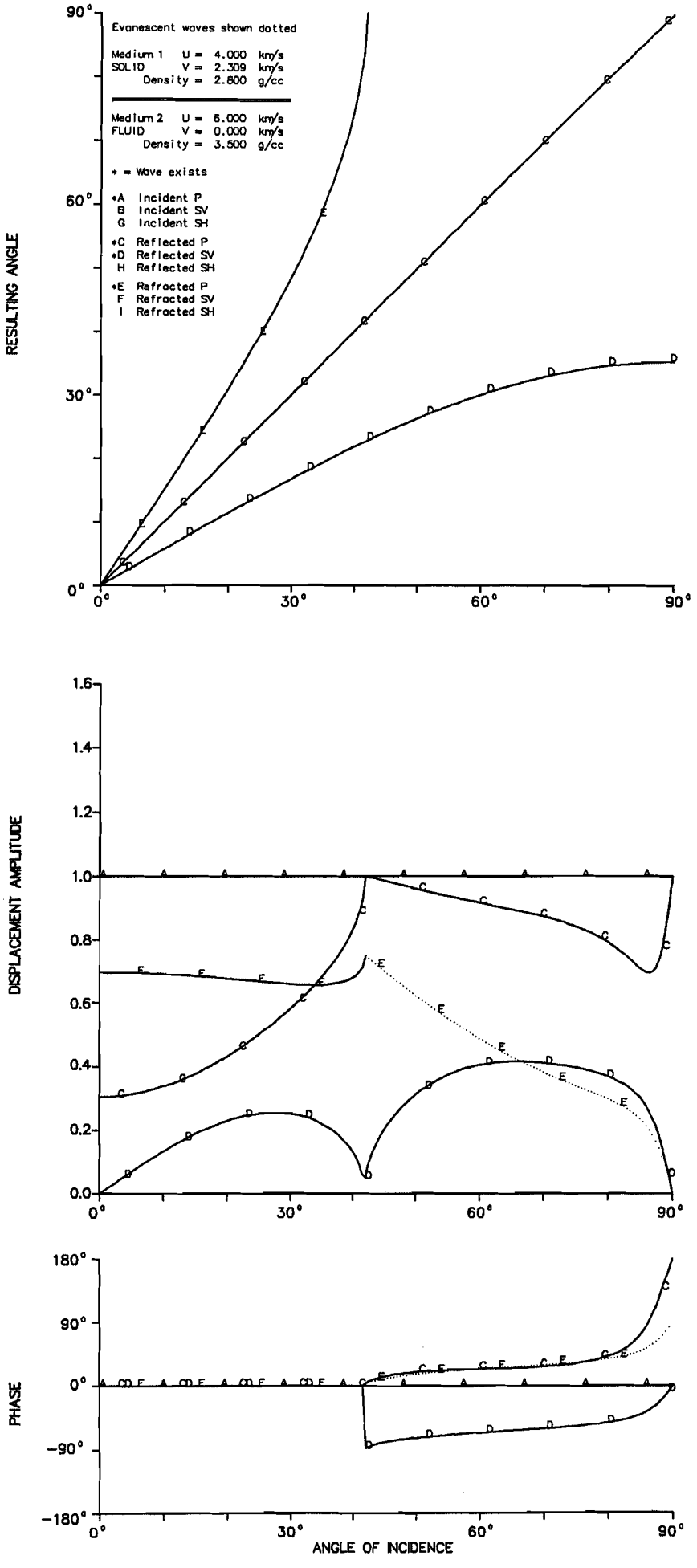

Figure 40. Solid–fluid interface (high U fluid). Incident P in the solid.

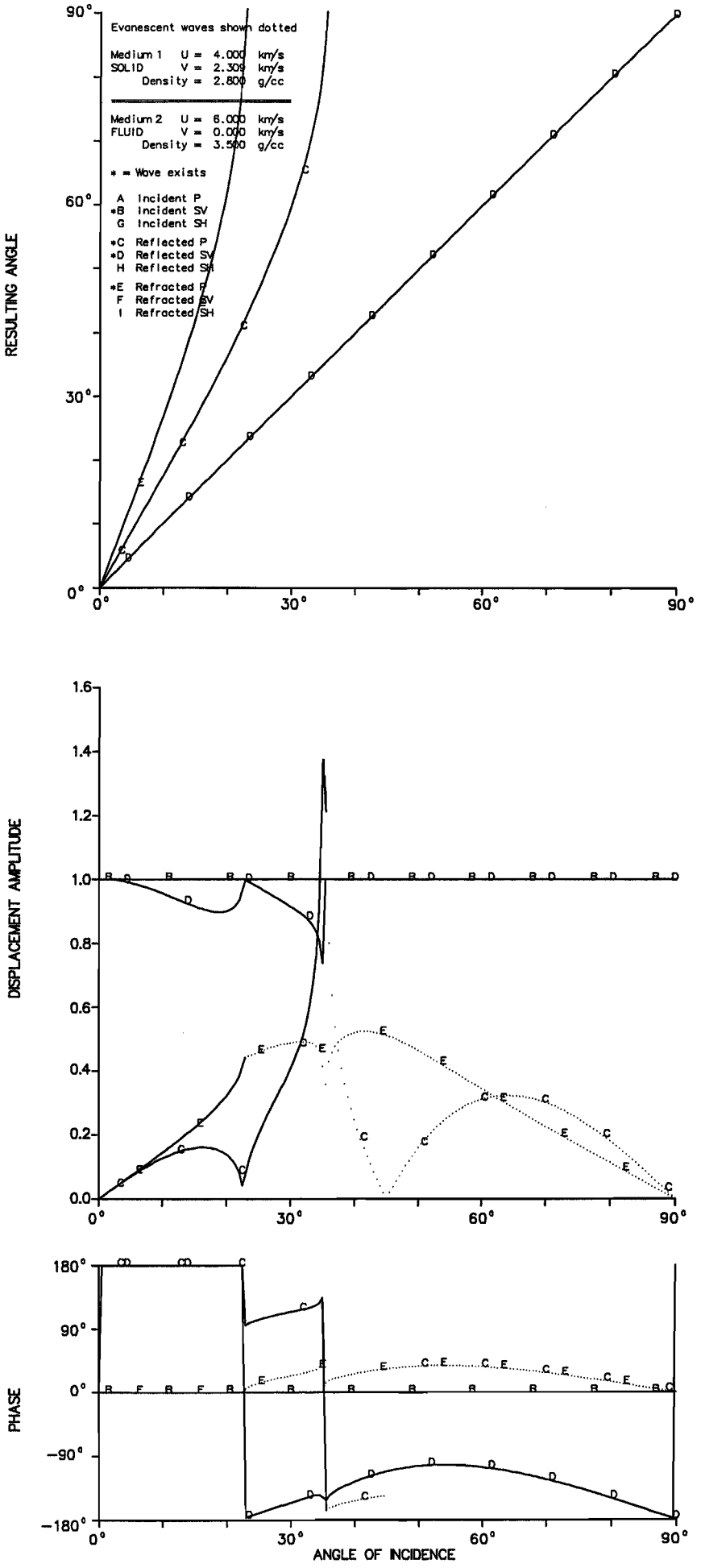

Figure 41. Solid–fluid interface (high U fluid). Incident SV in the solid.

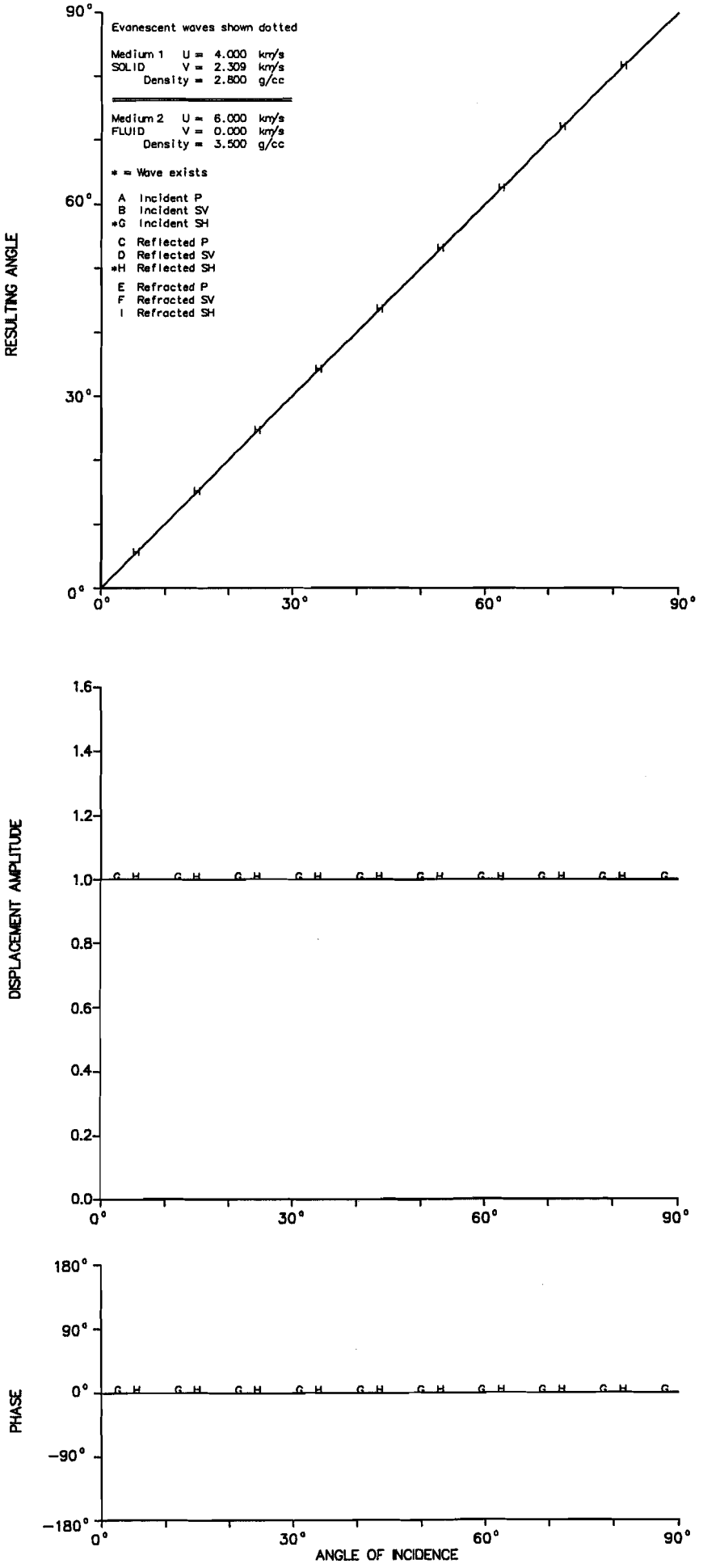

Figure 42. Solid–fluid interface (high U fluid). Incident SH in the solid.

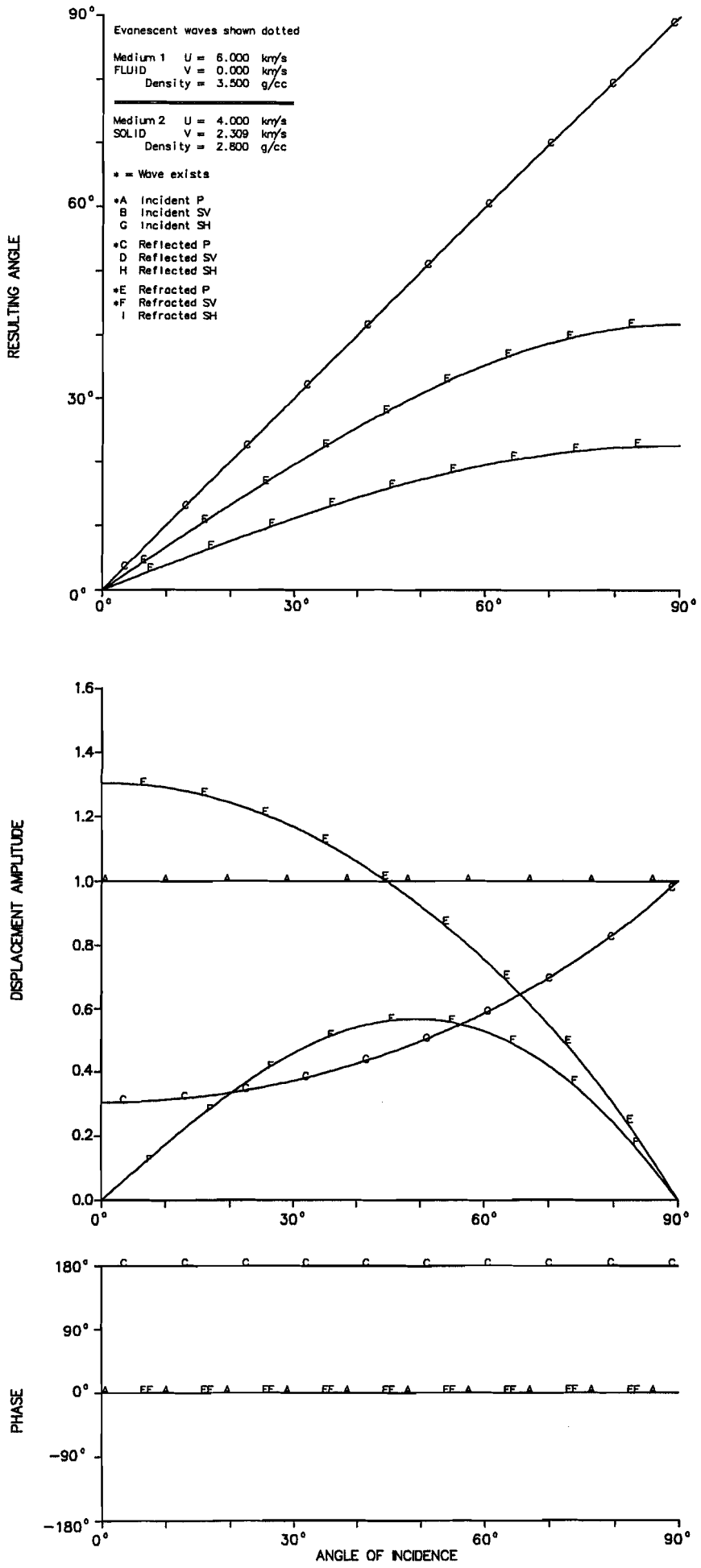

Figure 43. Solid–fluid interface (high U fluid). Incident P in the fluid.

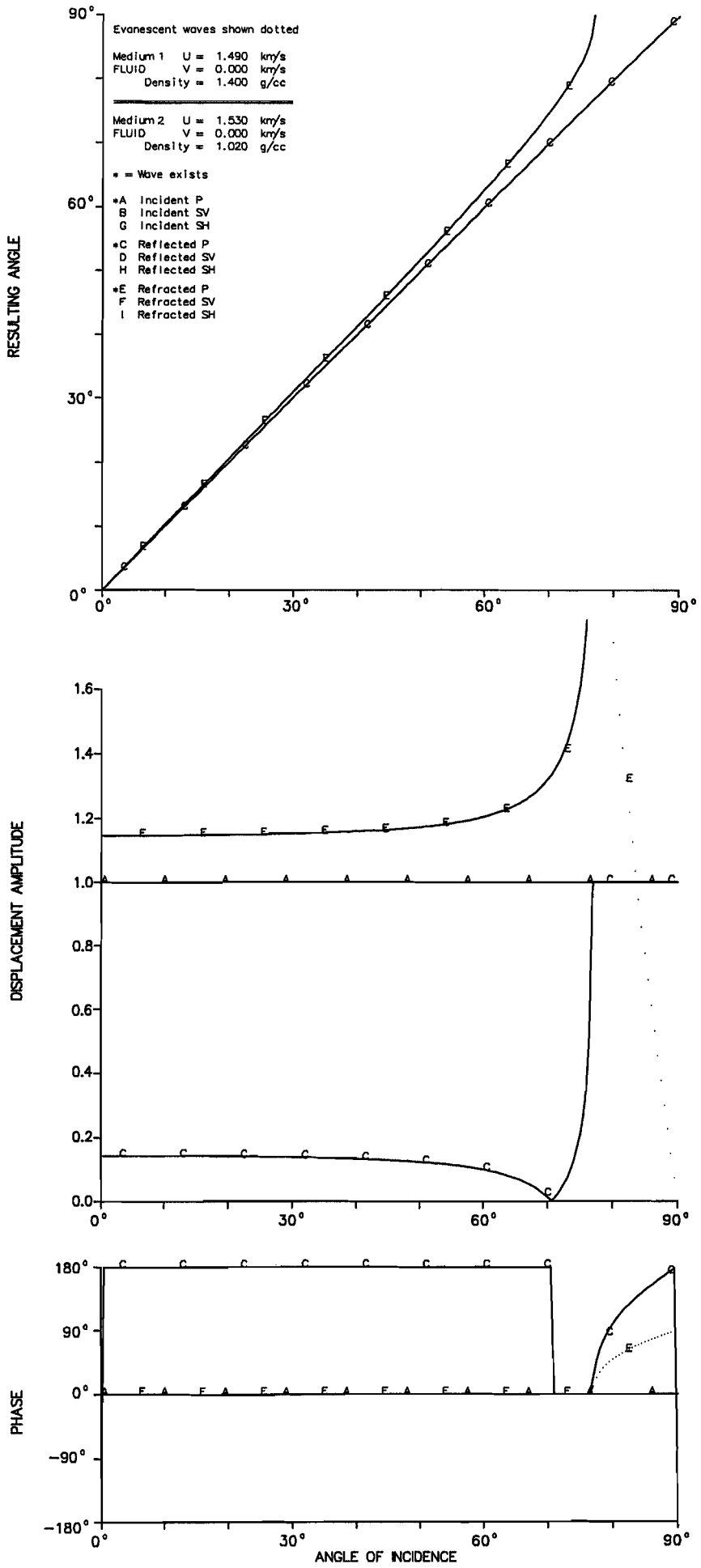

Figure 44. Fluid–fluid interface (seawater/sediment). Incident P from below.

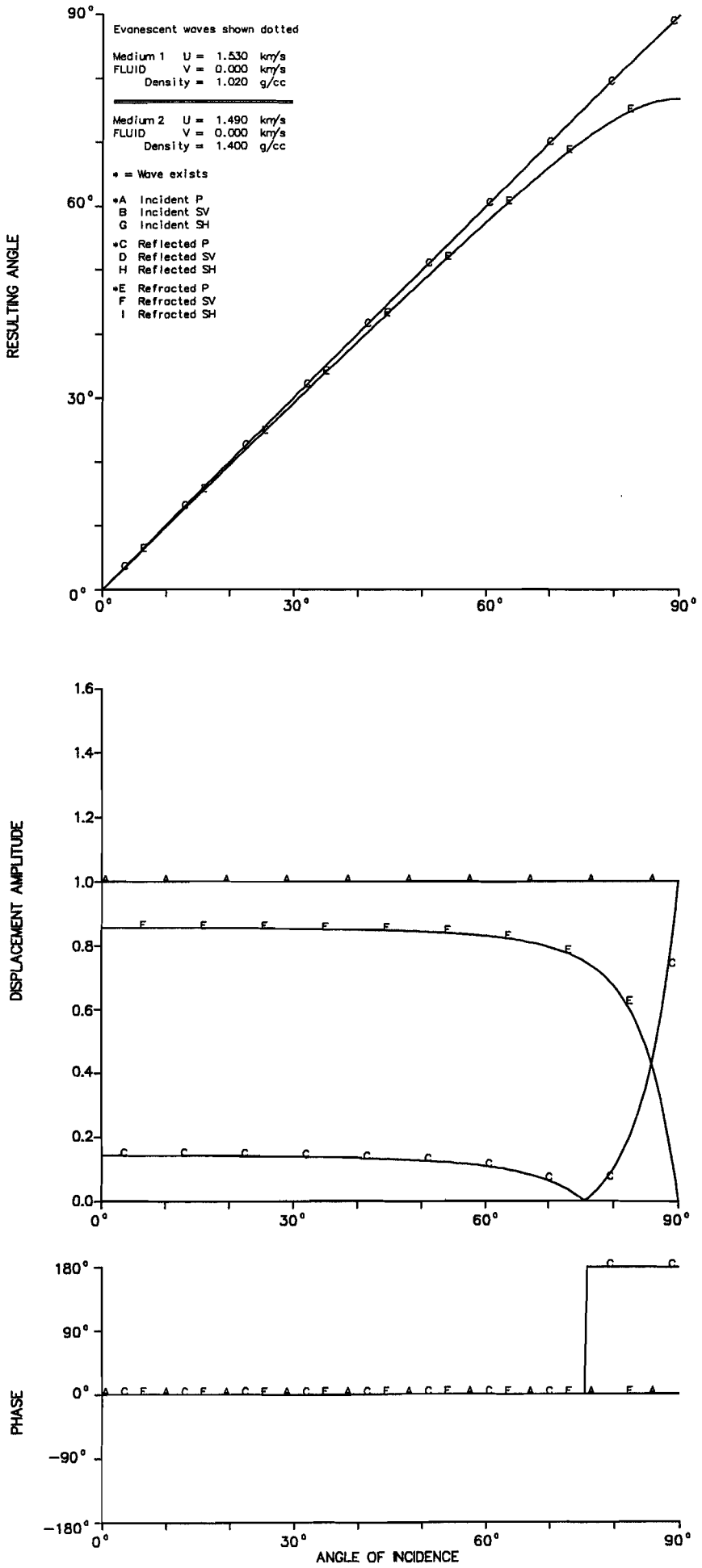

Figure 45. Fluid–fluid interface (seawater/sediment). Incident P from above.

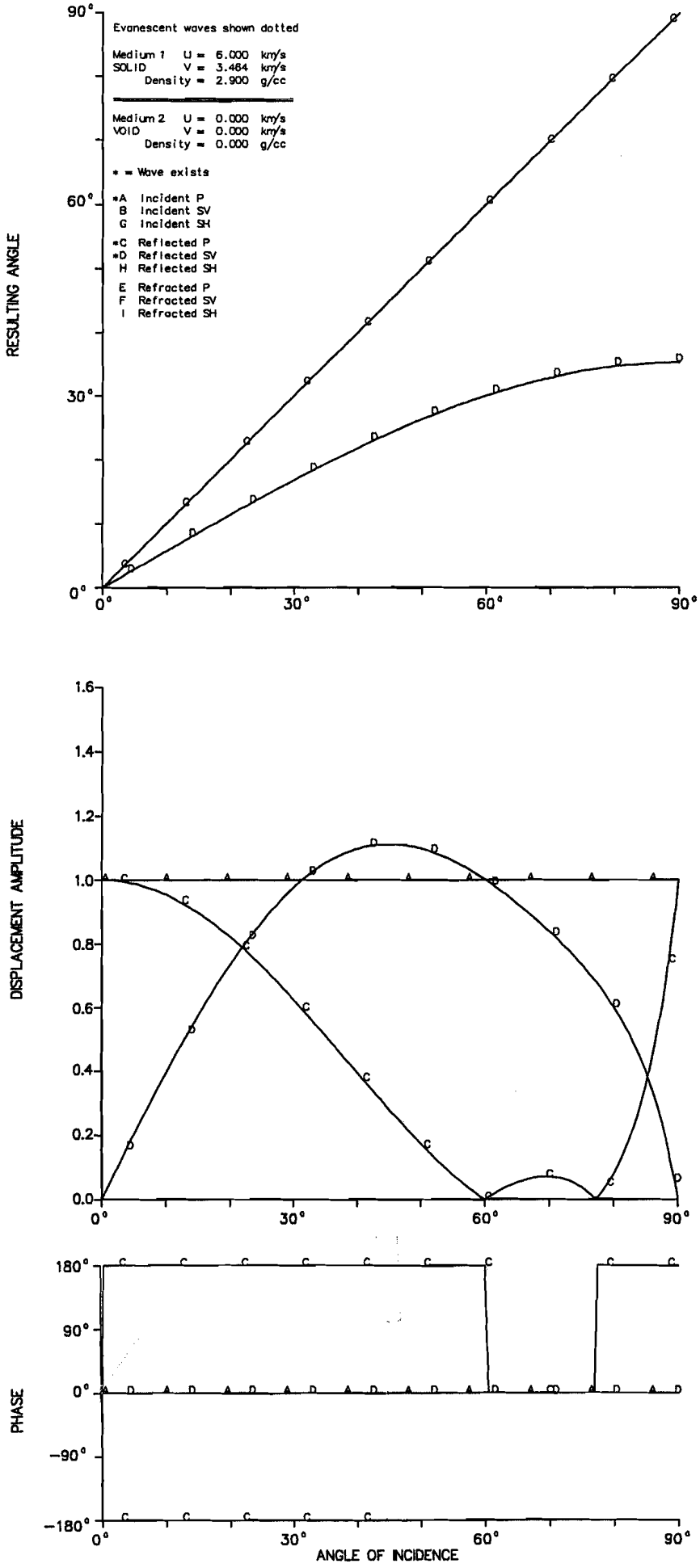

Figure 46. Solid free surface (Earth's surface). Incident P.

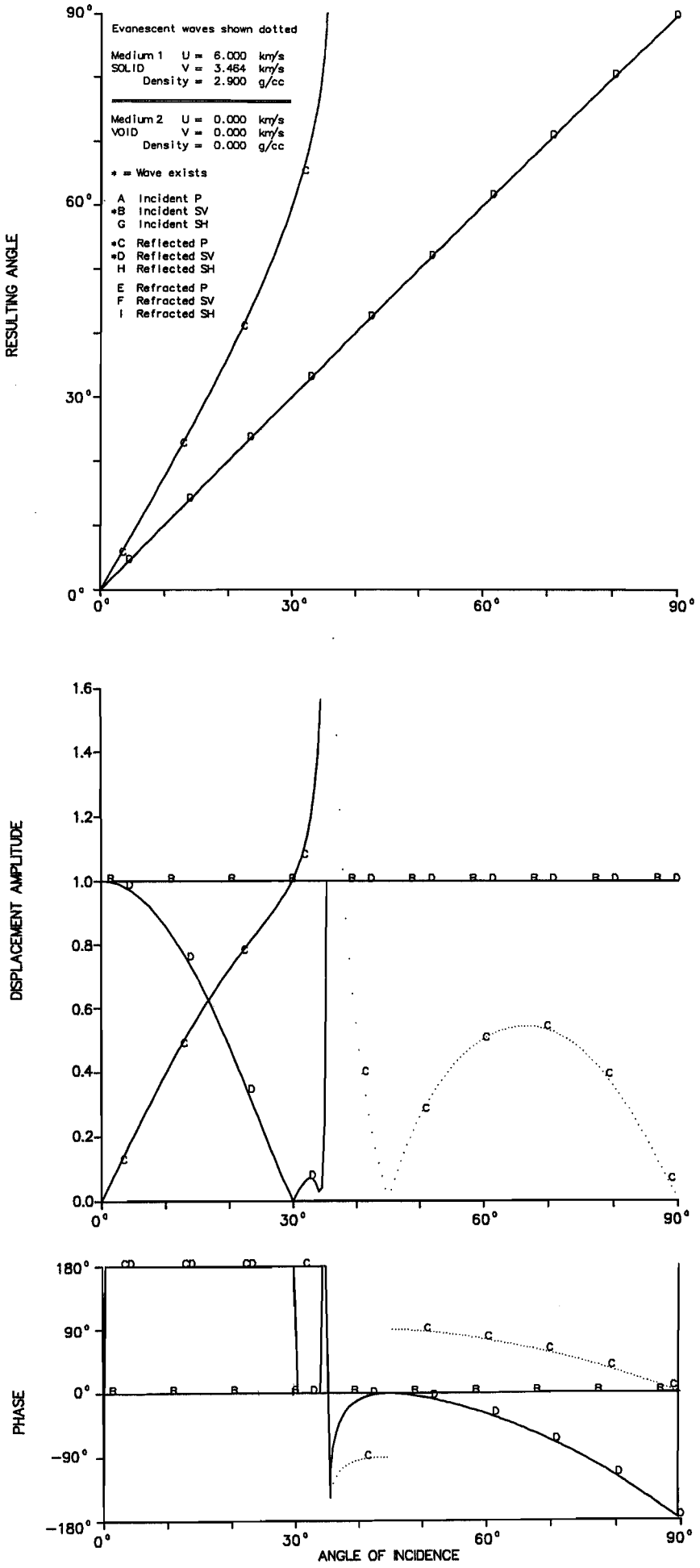

Figure 47. Solid free surface (Earth's surface). Incident SV.

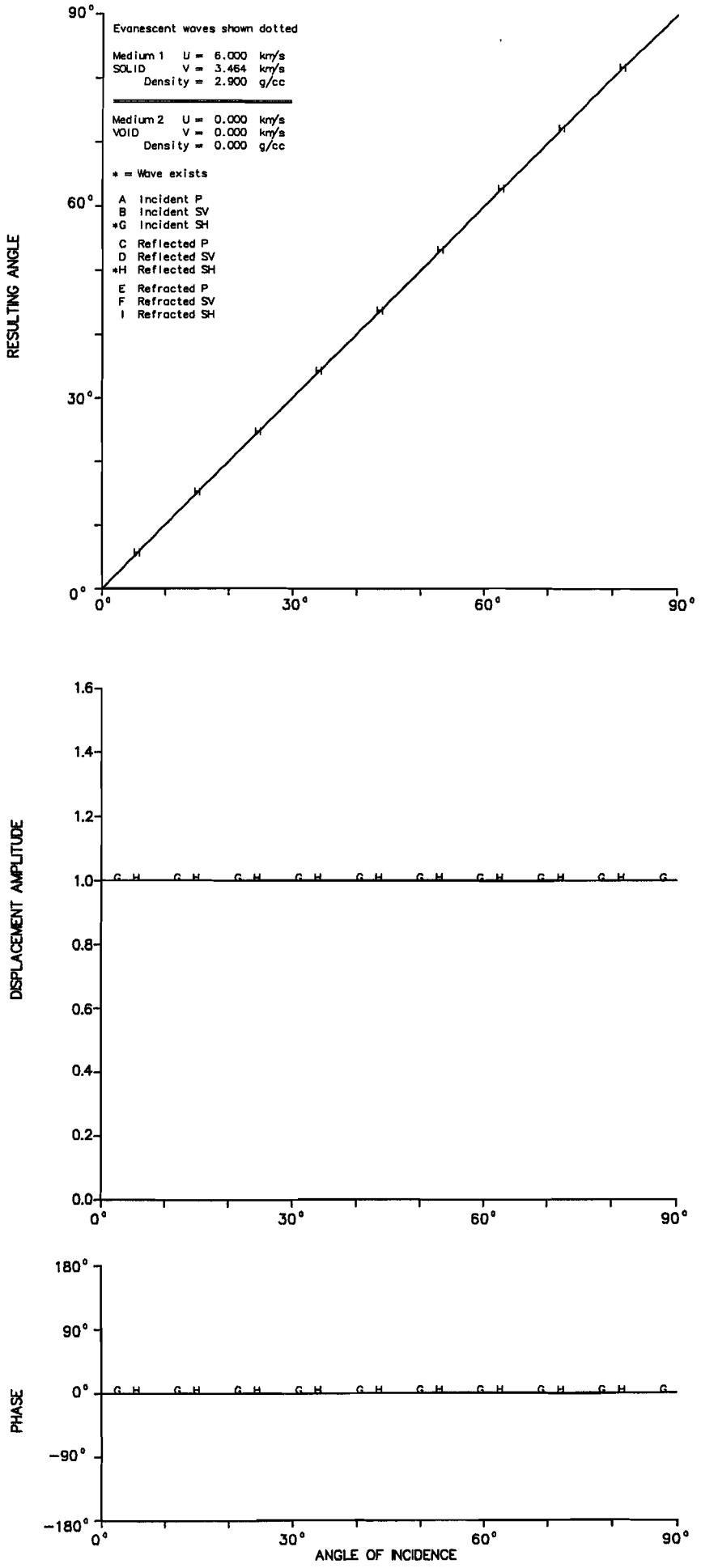

Figure 48. Solid free surface (Earth's surface). Incident SH.

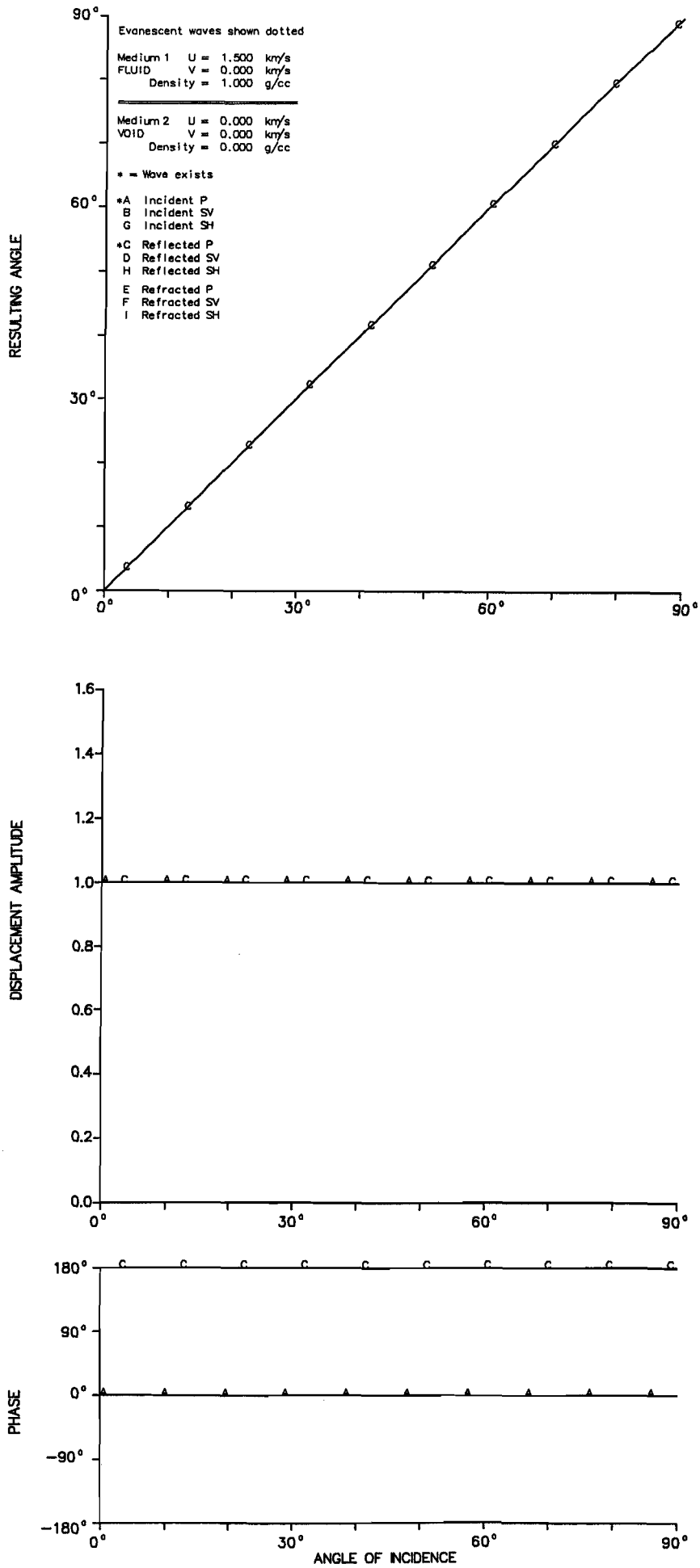

Figure 49. Fluid free surface (sea surface). Incident P.

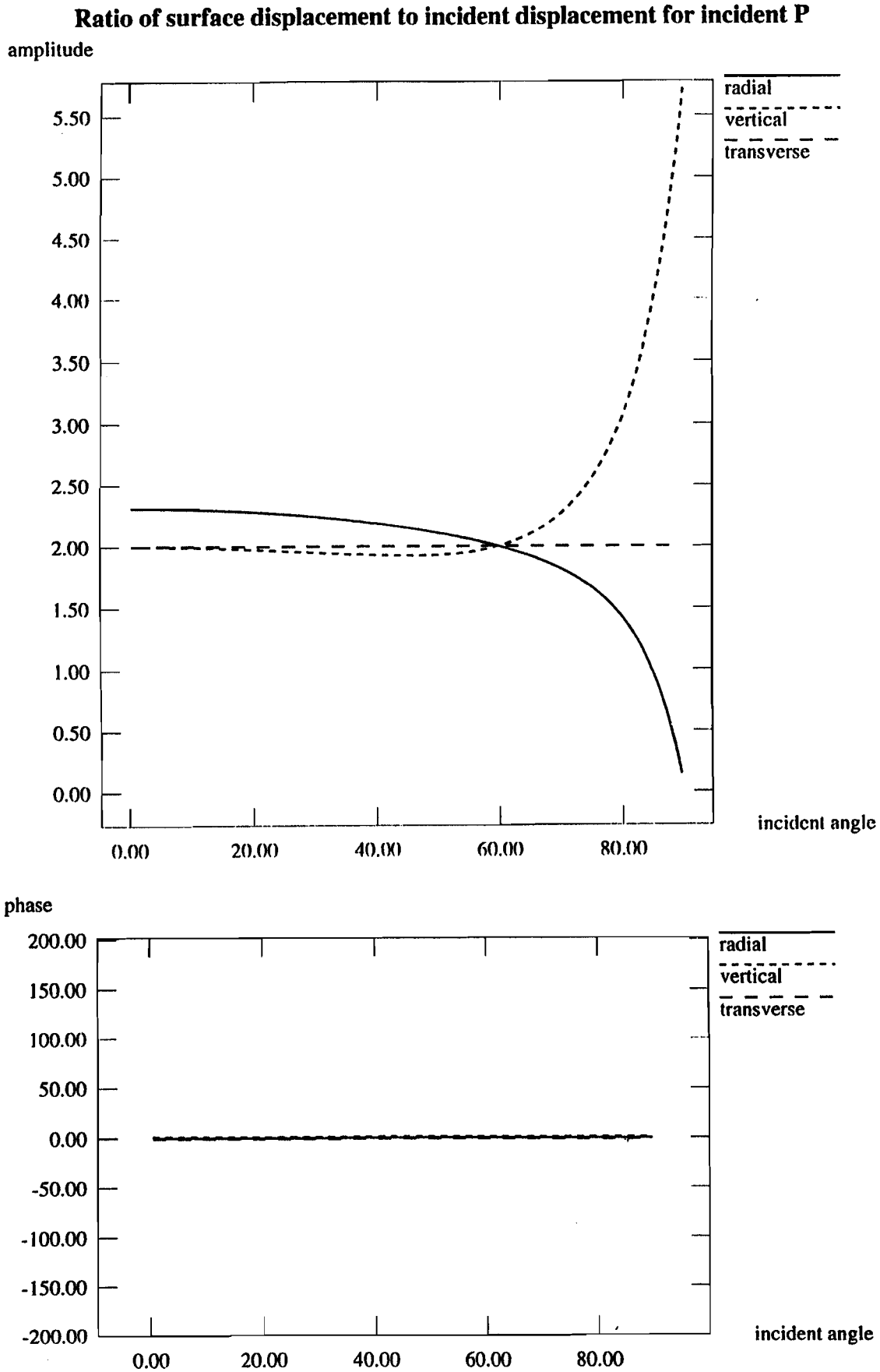

Figure 50 Ratio of displacement amplitude at the free surface to displacement amplitude of the incident wave, for an incident P wave, plotted against angle of incidence a. Ratios of the components in the radial, transverse and vertical direction (corresponding to the X_1, X_2 and X_3 directions respectively in figure 1) are shown as separate curves. In (a) the modulus of the ratio is shown, and in (b) the phase of the ratio. A Poisson solid is assumed.

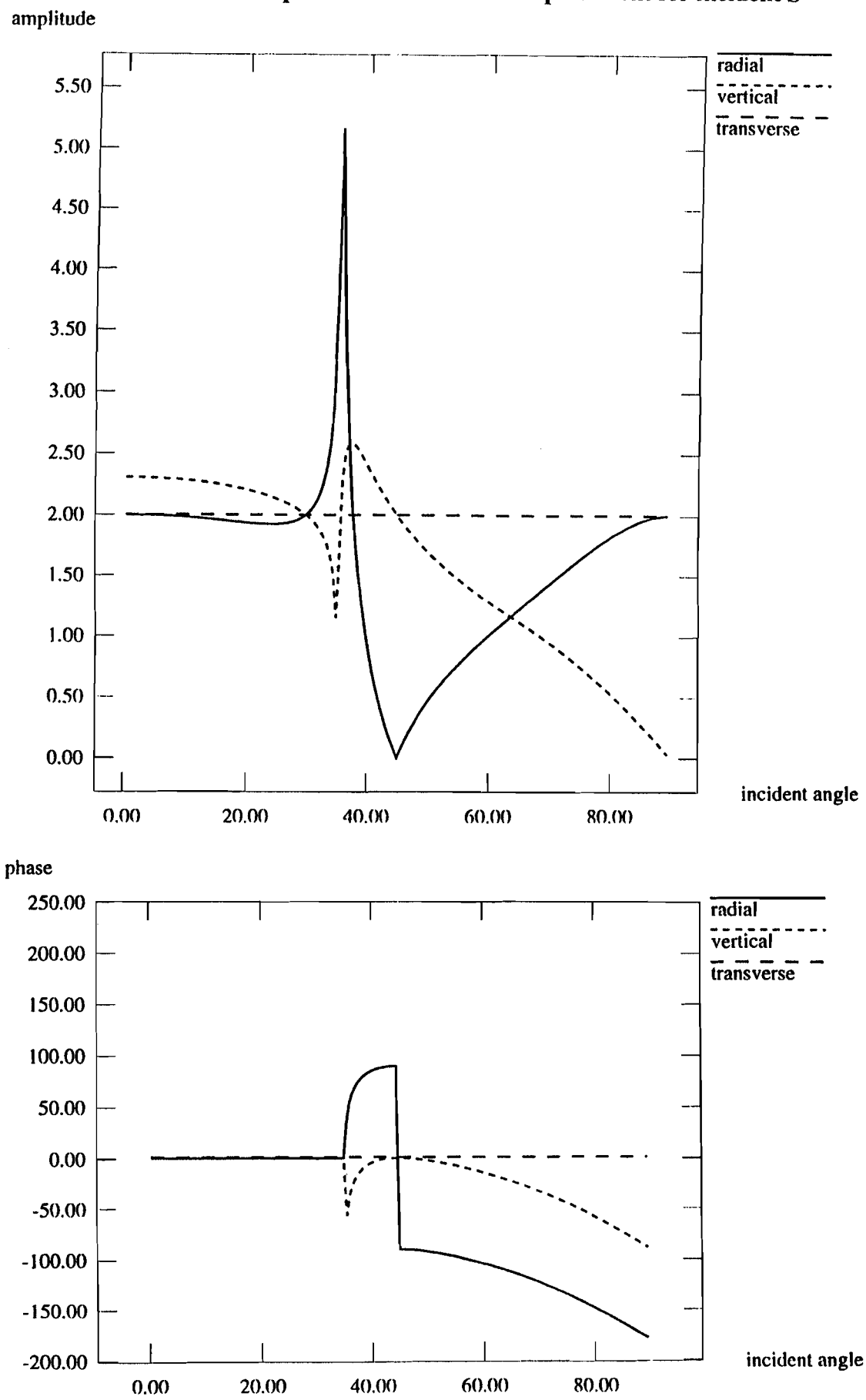

Figure 51 Ratio of displacement amplitude at the free surface to displacement amplitude of the incident wave, for an incident S wave, plotted against angle of incidence b. Ratios of the components in the radial, transverse and vertical direction (corresponding to the X_1, X_2 and X_3 directions respectively in figure 1) are shown separately. In (a) the modulus of the ratio is shown, and in (b) the phase of the ratio. A Poisson solid is assumed.

Available from

HER MAJESTY'S STATIONERY OFFICE

49 High Holborn, London W.C.1
71 Lothian Road, Edinburgh EH3 9AZ
9-12 Princess Street, Manchester M60 8AS
Southey House, Wine Street, Bristol BS1 2BQ
258 Broad Street, Birmingham B1 2HE
80 Chichester Street, Belfast BT1 4JY
or through a bookseller.

ISBN-0-85518209-1

Printed in England

UK UNLIMITED